

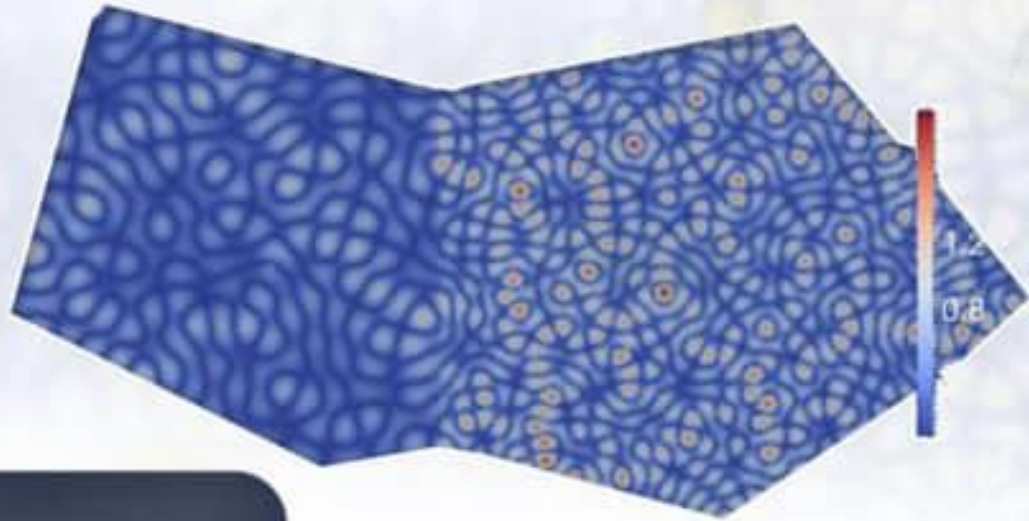


ISSN: 2789-858X

Scientific Journal for the faculty of Science - Sirte University



DOI: 10.37375/issn.2789-858X - Indexed by Crossref, USA




Volume2 Issue2 October 2022

Bi-annual Peer-Reviewed, Indexed, and Open
Accessed e-Journal

SJFSSU

Legal Deposit Number@National Library(Benghazi): 990/2021

 sjsfsu@su.edu.ly

 journal.su.edu.ly/index.php/JSFSSU



**Bi-annual, Peer-Reviewed, Indexed, and Open Accessed
e-Journal**

DOI: 10.37375/issn.2789-858X (Indexed by Crossref, USA)

Volume 2, Issue 2, October 2022

Editor in chief

Prof. Dr. Abdalla S. Radwan

Editorial Manager

Assoc.Prof. Dr. Haniyah A. Saed Ben Hamdin

Editorial Board

Assis. Prof. Dr. Gazala M. Alhdad.	Co-editor.
Assis. Prof. Dr. Fathia A. Mosa.	Co-editor.
Assis. Prof. Dr. Fatima .M. Mohamed.	Co-editor.
Assis. Prof. Aziza E. Eshtiwi.	Co-editor.
Assis. Prof. Dr. Mohammed O. Ramadan.	Proof-Reader in English.
Eng. Mohamed T. Alsriti.	Production Editor.

Advisory Scientific Committee of the SJFSSU

No	Name	Specialisation	Organisation	Country
1	Prof. Dr. Ahmad F. Mahgoub	Zoology	Science Faculty, Sirte University	Libya
2	Prof. Dr. Salem A. Abuhassia	Statistics	Science Faculty, Omar Al-Mukhtar University	Libya
3	Prof. Dr. Marei M. El-Ajaily	Chemistry	Science Faculty, Benghazi University	Libya
4	Prof. Dr. Huda Shaaban Elgubbi	Botany	Science Faculty, Misurata University	Libya
5	Prof. Dr. Nasser H. Sweilam	Applied Maths	Science Faculty, Cairo University	Egypt
6	Prof. Dr. Osama Ahmed Hlal	Geology	Science Faculty, Tripoli University	Libya
7	Prof. Dr. Mohamed A. Elssaidi	Environment Sciences	Environment & Natural Resources Faculty, Wadi Al-Shatti University	Libya
8	Prof. Dr. Ebrahim M. Daghman	Microbiology	Science Faculty, Misurata University	Libya
9	Prof. Dr. Ali Mohamed Awin	Mathematics	Science Faculty, Tripoli University	Libya
10	Prof. Dr. Ebrahim A. Elmerhaq	Information Technology	Information Technology Faculty, Tripoli University	Libya
11	Prof. Dr. Rafa A. Azzarroug	Physics	Science Faculty, Benghazi University	Libya
12	Prof. Dr. Osams M. Shalabiea	Astronomy	Science Faculty, Cairo University	Egypt
13	Prof. Dr. Abdualhamid S. Alhaddad	Environment Sciences & Natural Resources	Science Faculty, Misurata University	Libya

Editor in-Chief's Word

In the name of ALLAH, the Most Gracious, the Most Merciful.

All praise is due to ALLAH, Lord of the worlds, and prayers and peace be upon the prophet Muhammad, and upon his followers and his companions.

At the outset, we are delighted to congratulate all members of the editorial board of the journal and all the teaching fraternity of the faculty of science at Sirte University on the launch of the first scientific journal of our faculty. Moreover, we would like to commend the efforts made by the Dean of the faculty, which bore fruit in establishing this scientific platform. Furthermore, we hope that this journal will be a scientific platform that musters academics from inside and outside the university in the field of basic sciences and their applications to share and exchange their experiences and scientific research. The editorial board of the journal will be keen to adhere to the common quality standards for scientific publications by following certain rules for writing scientific research, investigating honesty and scientific accuracy. We ask ALLAH to grant us success so that this journal contributes to raising the university's classification and progress at both the local and regional levels.



This journal will provide its services to the academic community in the vital sectors and will contribute effectively to the process of building the society.

This journal aims to enrich the culture of scientific research and encourages academics to engage in scientific research. We also aspire that this journal puts its unique mark to distinguish among other local and non-local scientific journals. With ALLAH's help, we will strive to ensure that the journal obtains the recognized quality standards, whether at the local or regional level.

My deep appreciation to the editorial board, reviewers and researchers who make our journal a vehicle for their research works.

Peace, mercy and blessings of Allah are upon you.

Prof. Dr. Abdalla Salem Radwan

Editor in chief

Editorial Manager's Word

Dear Readers and Researchers,

In the name of ALLAH, the Most Gracious, the Most Merciful.

All praise is due to ALLAH, Lord of the worlds, and prayers and peace be upon the prophet Muhammad, and upon his followers and his companions.

First and Foremost, I would like to congratulate my colleagues in the editorial board, the faculty members and all the administrative and technical staff in the faculty of science on the release of the second volume of the SJFSSU. The SJFSSU publishes an original scientific research that fulfils the academic integrity requirements and meets the common scientific standards.

The SJFSSU aims to consolidate scientific research and encourages everyone in the academic community to engage in the field of scientific research. The SJFSSU editorial board is keen to abide to the common quality standards by adhering to the ethics of scientific research and the investigation of accuracy and scientific integrity.

Our ultimate goal, as SJFSSU editorial board, is to become one of the well-known journals in the world. With Allah's help, we will strive to ensure that the SJFSSU reaches the standards that are recognized local, and regionally.



Soon after the publication of the first Volume back in October 2021, the SJFSSU was registered in the Arab Impact Factor (AIF) database to obtain AIF=0.32. Moreover, the journal is indexed in the Crossref global platform and has an international Digital Object Identifier (DOI) for the whole journal and for the individual papers.

Finally, I would like to reiterate my gratitude and sincere thanks to all people who were involved, directly or indirectly, in the release of this issue. My special thanks go to my colleagues in the, editorial board, the peer reviewers and researchers who chose to publish their work in our journal. It is needless to say that any human work is not free of mistakes. This work is not exception despite the hard work that has been excreted in order to present it the best way possible. Therefore, should you have any comments /suggestions/ feedback, please feel free to contact us via email.

Peace, mercy and blessings of Allah are upon you.

Assoc.Prof. Haniyah A. S. Ben Hamdin

Editorial Manager

27-October-2022

About the Scientific Journal for the Faculty of Science-Sirte University (SJFSSU)

DOI: <http://www.doi.org/10.37375/issn.2789-858X>

The Scientific Journal for the Faculty of Science-Sirte University (SJFSSU, henceforth) is a bi-annual peer-reviewed and open accessed journal issued electronically by the faculty of science at Sirte University. The SJFSSU aims to encourage research in the scientific community and publish papers reporting original work that are of high standards and contribute to the development of knowledge in all fields of applied and pure (theoretical) science, namely mathematics, statistics, physics, chemistry, zoology, botany, microbiology, astronomy, computer science, information technology, geology, environment science and oceanography.

The SJFSSU accepts all types of articles such as research articles, review articles, topical review, case study/case reports, monograph, short communication, letters, conference/symposium special issues, editorials research articles and methodology articles.

Any opinions or views expressed in this journal do not reflect the opinions or views of the SJFSSU or its members. Moreover, the designation and the presentation of materials do not reflect any opinion whatsoever of the SJFSSU in terms of legal status of any country, territory...etc.

Policy and Publication Ethics of the Scientific Journal for the Faculty of Science-Sirte University (SJFSSU)

Publishing Cycle

The Scientific Journal of the faculty of science at Sirte University is published electronically on a semi-annual basis during the months of April and October.

Open Access Policy

The Scientific Journal of the faculty of science at Sirte University is an open-access journal that allows readers, authors and their institutions to obtain the full text of the articles published in it for free.

Copyright License Terms

All articles published in the Scientific Journal of the faculty of science at Sirte University are subject to the International Creative Commons License (CC BY 4.0 Creative Common Licence) and the author(s) retain copyright for the articles published by the journal with the guarantee of the following:

- 1- Making the article available on the magazine's website.
- 2- Granting any third party the right to use the article without any restrictions provided that its contents and original authors are preserved and the original source of publication is cited.

Intellectual Property Rights Copyrights

The Scientific Journal of the faculty of science at Sirte University allows authors to keep the copyright of their research without restrictions. The author retains all rights upon publication without prejudice to the open access policy of the journal, meaning:

- 1- Making the article available on the magazine's website.
- 2- Granting any third party the right to use the article without any restrictions provided that its contents and original authors are preserved and the original source of publication is cited.

Plagiarism Policy

2. To fulfil the academic integrity requirements, manuscripts submitted to the SJFSSU must adhere to ethical standards and refrain from plagiarism in any way. Thus all manuscripts submitted to the SJFSSU must be initially screened by plagiarism checker software.
3. If any plagiarism or scientific theft is detected before publication then the SJFSSU will contact the author/s in regard to this matter. If the editorial board of the SJFSSU is not satisfied with the justifications presented by the author, then the following strict actions will be taken against the author:
 - i. Such manuscript(s) will be immediately rejected.
 - ii. The editorial board forever will not consider any request for publication submitted by such author/s in the future.
 - iii. An announcement will be placed in this regard in the journal website and in the author's institution.
4. If any plagiarism or scientific theft is detected after publication then:
 - a. Immediately this article will be withdrawn from publication and republished on the journal's website and in the next issue of the journal with a watermark (RETRACTED).
 - b. An appropriate announcement will be placed in this regard through the journal website and in the author's institution.
 - c. d. An official letter to the author's institution regarding taking legal measures in this regard.
 - d. We can also consider more strict actions against authors based on seriousness of the incident.

Complaints and appeals

Anyone can submit his/her complaints/appeal to the Editor-in-Chief of the journal by email.

Publication fees

Publication in the journal is completely free and there are no fees either for submission, or for article processing APC, or for publication, or fees for the number of papers, or fees for coloured figures.

General Rules:

1. Any manuscript submitted to the SJFSSU must contain an original work which has been neither previously published, nor it is under consideration by another journal, conference, workshop or symposium.
2. The submitted manuscript must fulfil the common requirements of the scientific research, including presenting the problem, reviewing the relevant literature, analysing data, discussing results and draw the conclusion and the recommendations.
3. The SJFSSU accepts all types of articles such as research articles, review articles, topical review, case study/case reports, monograph, short communication, letters, conference/symposium special issues, editorials, research articles and methodology articles.
4. An author is required to write his or her manuscript carefully according to the basic and technical rules of the SJFSSU.
5. The SJFSSU only accepts manuscripts written in English language.
6. The subject of the submitted manuscript must be in the specified categories of the SJFSSU.
7. All individuals involved in the publishing process: from authors, editorial board, reviewers, must comply with standards of ethical behaviour.
8. All submitted manuscripts are subject to double-blind and peer-review process that is the author will be unaware of the reviewer's identity, and also the reviewer is unaware of the author's identity.
9. The SJFSSU follows the Code of Conduct of the Committee on Publication Ethics (COPE) and follows COPE Flowcharts for resolving cases of suspected misconduct. The Journal is particularly committed to the COPE Code of Conduct for Journal Publishers. Journal editors follow COPE's Code of Conduct and best practice guidelines for journal editors.

Author/s Responsibility:

1. The author is alone responsible for the proofreading and spelling check of his or her submitted manuscript.
2. The SJFSSU editorial committee has the right to make any editorial changes on the manuscript which is accepted for publication.
3. The author/ authors are prohibited from publishing in the journal for a period of three consecutive years if it appears that they have sent the manuscript to another journal at the same time that it was sent to the journal.
4. The author is not entitled to withdraw the manuscript during the evaluation process, unless the peer-review process exceeds six months. Thus the author could withdraw the manuscript provided that he informs the journal of his desire.
5. An author is kindly requested to disclose any affiliations, including financial, consultant or institutional associations that might lead to bias or a conflict of interest.
6. Any author is required to understand, complete and sign the 'Authorship, Copyright Transfer, Conflicts of Interest and Acknowledgments statement' which can be downloaded from the link: https://drive.google.com/file/d/1jvan4NOS_CFegJzOw8LR6RwH0vXoiA29/view?usp=sharing

The signed form should be scanned and attached electronically along with the submitted manuscript.

7. An author has to submit his or her manuscript electronically as a MS-Word file through the journal website via the link: <https://journal.su.edu.ly/index.php/SJFSSU/information/authors>
8. Without the need to contact the editorial committee with regard to submitted manuscript, an author can easily track his or her submitted manuscript electronically through the journal website via the link: <https://journal.su.edu.ly/index.php/SJFSSU/information/authors>

Author's Rights:

1. The Author retains the following rights:
 - i. All proprietary rights, such as patent rights.

- ii. Using all or part of the material published in his or her article in further research of his or her own filling, provided that permission is granted from the SJFSSU and an adequate acknowledgment should be appropriately credited and referenced for the SJFSSU.

Disclaimer

The author(s) of each article appearing in this Journal is/are solely responsible for the views, ideas expressed and the accuracy of the data in his or her manuscript. Thus the published papers do not reflect the opinions or views of the SJFSSU or its members. Furthermore, the designation and the presentation of materials do not reflect any opinion whatsoever of the SJFSSU in terms of legal status of any country, territory...etc.

Editors Responsibilities:

1. The editorial committee must ensure a fair double-blind peer-review of the submitted manuscript.
2. The editorial committee will strive to make sure there are no potential conflicts of interests between the author and the editorial and review personnel.
3. The editorial committee will ensure that all the information related to submitted manuscripts is sustained as confidential.

Reviewers Responsibilities:

1. The reviewers must ensure that all the information related to submitted manuscripts is kept as confidential.
2. Reviewer who is unable to review the submitted manuscript for any reason should notify the editorial director to excuse himself or herself from the review process.
3. Reviewers must review the submitted manuscripts objectively according to the journal's evaluation forms and adhere to the specified evaluation period of three months at max.

Review Process

1. If the submitted manuscript initially meets the specified requirements of the SJFSSU and successfully passes the plagiarism check, then directly it should go through the double blind and peer-review process.
2. The submitted manuscript is subject to double blind review by specialized referees suggested by the editorial committee in an undisclosed manner to evaluate the submitted manuscript.
4. The editorial board of the journal informs the author of the opinions of the referees and forwards its assessment report if the manuscript needs any corrections.
5. Any PhD-degree holder with a scientific degree (assistant professor or higher) who would like to be a referee in the SJFSSU should register and send his or her CV through the SJFSSU website.
6. An author is required to make any minor or major corrections that are suggested by the referees within a stipulated date.

Publishing Process

1. Once the decision is made of accepting the manuscript for publication at the SJFSSU, the author will be notified and facilitated with an acceptance letter to confirm that his or her manuscript is accepted for publication in the upcoming issue of the SJFSSU.
2. Once the issue of the journal has been realised, a soft-copy of each published paper will be sent to the author via his or her email address.

Author guidelines for preparing the manuscript

All submissions should strictly be prepared according to the following typing guideline:

1. The submitted manuscript should be approximately up to a maximum of 20 pages and a minimum of 5 pages (including tables, figures, references list, appendixes and supplements).

2. The submitted manuscript of types (review articles, topical review) should be approximately up to 45 pages maximum (including tables, figures, references list, appendixes and supplements).

Rules for the Paper Structure

3. The first page should contain the full title of the manuscript (the title should be concise and informative), then the name(s) of the author(s).
4. Affiliation with contact information including the (The affiliation(s) of the author(s), i.e. institution, (department), city, (state), country). A clear indication and an active, official university email address of the corresponding author.
5. This is followed by the abstract except for review article types which start with the introduction.
6. The abstract length should be of (250) words at the maximum and (150) words at the minimum.
7. In the abstract of the submitted manuscript, the following main points must be available: -
 - i. An introductory sentence related to the research topic to attract readers.
 - ii. Presentation of the research main point (purpose).
 - iii. Description of the method used in the research.
 - iv. Presentation of the achieved results.
 - v. A concluding sentence that includes a recommendation.
8. The keywords should be 4 to 6, which can be used for indexing purposes.
9. In the introduction of the submitted manuscript, the following main points must be available: -
 - i. Introductory sentences related to the research topic to attract readers.
 - ii. An adequate background, then the relevant literature review.
 - iii. Clearly state the object of the research.
 - iv. The limitation of the research.
 - v. The structure of the manuscript.
10. In the Material and methods section of the submitted manuscript, the author should provide sufficient details to allow the work to be

reproduced by an independent researcher. Methods that are already published should be summarized and indicated by a reference. If quoting directly from a previously published method, use quotation marks and also cite the source. Any modifications to existing methods should also be described.

11. Results should be clear and concise and presented separately from the discussion.
12. The discussion should explore the significance of the results of the work, not repeat them.
13. The main conclusions of the study may be presented in a short Conclusions section, which may stand alone or form a subsection of the Discussion section.
14. Collate acknowledgements in a separate section at the end of the article before the reference list and do not, therefore, include them on the title page, as a footnote to the title or otherwise. List contributions that need acknowledging (e.g., acknowledgments of technical help; acknowledgments of financial and material support, writing assistance or proof reading the article, financial arrangement, specifying the nature of the support).
15. Within the acknowledgments section, a conflict of interest statement must be included for all manuscripts even if there are no conflicts of interest.
16. If there is more than one appendix, they should be identified as A, B, etc. Formulae and equations in appendices should be given separate numbering: Eq. (A.1), Eq. (A.2), etc.; in a subsequent appendix, Eq. (B.1) and so on. Similarly for tables and figures: Table A.1; Fig. A.1, etc.
17. The author is asked to switch off the 'Track Changes' option in Microsoft Office files as these will appear in the published version.

Text Formatting Rules:

18. Use a normal, plain font (e.g., 10-point Times New Roman) for text.
19. Use italics for emphasis.
20. Use the equation editor or Math Type for equations.
21. Save your file in docx format (Word 2007 or higher).

Headings: Please use no more than three levels of displayed headings.

22. The manuscript (in two columns) should be single line space and the font type (Times New Roman) and the size should be as specified in this table:

Paper title	14 Bold
Authors names	10
Abstract	9
Address	10 Italic
Main headings	12 Bold
subheadings	10 Bold
Text	10
Figure and table captions	9

23. The metric system should be used, and the Arabic numbers should be used for page numbers and throughout the running text.

24. Abbreviations, if used should be defined at their first mention in the text and used consistently thereafter, and the non-standard ones should be avoided.

25. Mathematical equations should appear in a sequential order and should be numbered between the brackets ().

Tables

26. All tables are to be numbered using Arabic numerals.

27. Tables should always be cited in text in consecutive numerical order. For each table, please supply a table caption (title) explaining the components of the table and an explanatory legend.

28. Identify any previously published material by giving the original source in the form of a reference at the end of the table caption.

29. Footnotes to tables should be indicated by superscript lower-case letters (or asterisks for significance values and other statistical data) and included beneath the table body.

Figures

30. High resolution is required in preparing the figures in the manuscript, the file formats JPEG, PNG are preferred for the figures, images, etc.

31. If the figure, photo... etc. has been published elsewhere, then the original source must be acknowledged and a written permission from

the copyright holder must be obtained and submitted with the manuscript.

32. If photographs of people are used, then the photos must be obscured by clouds or a written permission by the concerned person must be obtained.
33. All figures are to be numbered using Arabic numerals.
34. Figure parts should be denoted by lowercase letters (a, b, c, etc)
35. References to figures and tables should be made in a sequential order as they appear in the running text, and should be numbered between the parentheses (), e.g. (Fig. 1) and (Tab. 1).
36. Ensure all figure and table citations in the text match the files provided.
37. When preparing your figures, pay attention to the size figures to fit in the column width.
38. Figures should have a short label.

References Style:

39. Enclose the references list at the end of the manuscript accordingly to the APA (American Psychological Association) style (5th to 7th) edition. A guide containing examples of common citation formats in APA can be found at the below link:

<https://guides.libraries.psu.edu/apaquickguide/>

40. How to create an APA cited paper in Microsoft Word:

<https://support.microsoft.com/en-us/office/apa-mla-chicago-%E2%80%93-automatically-format-bibliographies-405c207c-7070-42fa-91e7-eaf064b14dbb>

Page margins: The Page margins should be adjusted as,

Top	Bottom	left	Right
2	2	2.5	2

41. To prepare the manuscript, it is highly recommended to use the ready –template that is prepared by the editorial committee which is available electronically on the journal website at the ink:

<https://docs.google.com/document/d/1Q7JFml7kjZAw0qXLzv6L9nOoOdeRLtK/mobilebasic>

Scientific Journal for Faculty of Science-Sirte University (SJFSSU)

DOI: 10.37375/issn.2789-858X (Indexed by Crossref, USA)

Volume 2, Issue 2, October 2022

DOI: <https://doi.org/10.37375/sjfssu.v2i2>

Contents	page
Biochemical Study on the Kinetic Properties of the Invertase Produced by Saccharomyces Cerevisiae <i>Khaled S. Al salhen, Mafath A. Alhorer and Hala M. Imraja</i> DOI: https://doi.org/10.37375/sjfssu.v2i2.368	1-11
Statistical Study of Extract Keratin Protein from Waste Chicken Feather Based on Response Surface Methodology <i>Dalal M. Ibrahim, Hanan F. Emraged, Sumayyah M. Albarani, and Bushra Alnaji Abdalrazig</i> DOI: https://doi.org/10.37375/sjfssu.v2i2.297	12-18
Anticancer Screening of Quercetin as a Natural Treatment <i>Wedad A. A. Ahmed</i> DOI: https://doi.org/10.37375/sjfssu.v2i2.439	19-27
Measuring the Content of 16 PAH in Plant (potato) from Bradford in the UK <i>Heiam Hamed</i> DOI: https://doi.org/10.37375/sjfssu.v2i2.461	28-32
Mode of Formation of the Coastal Sabkha Sediments in the Coastal Plain of Al-Dafna Plateau <i>Ahmed A. Mohammed, Tarek I. Anan and Amin M. Gheith</i> DOI: https://doi.org/10.37375/sjfssu.v2i2.516	33-37
Muco-adhesion Evaluation of Polysaccharides in Simulated Physiological Fluids <i>Hana A. S. Binhamad and Ramadan Diryak</i> DOI: https://doi.org/10.37375/sjfssu.v2i2.510	38-45
Petrophysical Charaterizations of Some Reservoir Formations in Ghani Oilfield, Libya <i>Ibrahim M. Abou El Leil, Farag Adam and Ahmed Mohammed</i> DOI: https://doi.org/10.37375/sjfssu.v2i2.515	46-61

<p>Effect of Active Compounds for <i>Quercus</i> Fruit on Some Biochemical Parameters and Tissue Aorta in Induced Atherosclerosis Rats</p> <p><i>Intisar G. Taha and Nashwan I. AL-Lehebe</i></p> <p>DOI: https://doi.org/10.37375/sjfssu.v2i2.511</p>	<p>62-72</p>
<p>Micropropagation of <i>Paulownia elongata</i> tree through Plant Tissue Culture Technology</p> <p><i>Ahmed Shaaban, Salem Hammud, Mohammed Abo Sneena, Elmundr Abughnia</i></p> <p>DOI: https://doi.org/10.37375/sjfssu.v2i2.512</p>	<p>73-79</p>
<p>Mycoflora Associated with Barely Grains (<i>Hordeum vulgare</i> L.) in the Eastern Parts of Libya</p> <p><i>Marei M. Abdullah</i></p> <p>DOI: https://doi.org/10.37375/sjfssu.v2i2.295</p>	<p>80-85</p>
<p>Generating Matrices of Rotations in Minkowski Spaces using the Lie Derivative</p> <p><i>Anis I. Saad, Muneera Muhmoud and Attia A. Mostafa</i></p> <p>DOI: https://doi.org/10.37375/sjfssu.v2i2.317</p>	<p>86-90</p>
<p>The Fundamental Role of Neuroinflammation at the Beginning and Progression of Alzheimer's Disease</p> <p><i>Yousef Sawikr, Youssef F. Lawgali, Abdelkarem Elgazali and Ibrahim S. Ibrahim</i></p> <p>DOI: https://doi.org/10.37375/sjfssu.v2i2.557</p>	<p>91-98</p>



Biochemical Study on the Kinetic Properties of the Invertase Produced by *Saccharomyces Cerevisiae*

Khaled S. Al salhen¹, Mafath A. Alhorer² and Hala M. Imraja³

¹Biochemistry Department, Medicine Faculty, Derna University, Derna, Libya.

²Microbiology Department, Science Faculty, Omar El-Mokhtar University, El-beida, Libya.

³Chemistry Department, Science Faculty, Omar El-Mokhtar University, El-beida, Libya.

DOI: <https://doi.org/10.37375/sjfsu.v2i2.368>

A B S T R A C T

ARTICLE INFO:

Received 30 June 2022.

Accepted 24 September 2022.

Published 27 October 2022.

Keywords: *Invertase, Kinetic parameters, Optimum factors, Inhibition parameters.*

Invertases are enzymes that hydrolyze sucrose to produce an equimolar mixture of glucose and fructose, which is of interest for various industrial applications. The present study aimed to produce invertase by *Saccharomyces cerevisiae* isolated from Baker's yeast and grape samples using the standardize technique. The enzyme activity was characterized with some parameters like pH, temperature, metal ions, kinetic parameters and inhibitors (fructose, glucose and copper (II) sulfate). Spectrophotometric methods were used to study enzyme kinetics and to determine the factors affecting enzyme activity. The optimum activity was recorded at 55°C for both invertases. The optimum activity was at pH 6.0 for Baker's yeast invertase and at pH 10 for grape invertase. From Lineweaver-Burk Plot, V_{max} was found to be 24.39 ± 2.44 nmol/min/mg protein and the K_m approximately 0.860 ± 0.04 mM for Baker's yeast invertase but in case of grape invertase, V_{max} was 23.25 ± 3.14 nmol/min/mg protein and the K_m approximately 1.243 ± 0.07 mM. Enzyme activity was increased in the presence of 5 mM Ca^{+2} ions for Baker's yeast, whereas showed the maximum activity at 5 mM Mg^{+2} ions in case of grape fruit invertase. Using sucrose as substrate, the K_{cat} , K_{cat}/K_m and K_s values were 0.28 ± 0.02 min⁻¹, 0.325 ± 0.03 mM⁻¹ min⁻¹ and 27.03 ± 5.24 ml/min/mg protein for Baker's yeast invertase activity, whereas were 0.56 ± 0.008 min⁻¹, 0.045 ± 0.003 mM⁻¹ min⁻¹ and 24.39 ± 7.11 ml/min/mg protein for grape invertase values. In conclusion, the *S. cerevisiae* isolated from grape fruits was more potent for invertase production in comparable with that isolated from Baker's yeast.

1 Introduction

Enzymes are proteins that produced by all living cells as catalysts for specific chemical reactions. In enzymatic reactions, the molecule at beginning is called substrates, and then they convert into different molecules called products. Almost all biological cells need enzymes to increase the rate of chemical reactions in order to occur at rates sufficient for life. Enzymes are very important part in some food processes, such as making of cheese,

bread, wine and beer, for thousands of years (Dewdney, 1973). Invertase (EC 3.2.1.26) is one of the most widely used enzymes in confectionery industry for preparation of jams and candies (Klein *et al.*, 1989). Invertase, also known as -fructofuranosidase, catalyzes the conversion of sucrose, a non-reducing disaccharide, to fructose and glucose, which are reducing monosaccharides (Arise *et al.*, 2020). Inverted sugar syrup is the result of combining

glucose and fructose (Mobini-Dehkordi *et al.*, 2008). Invertases are found in nature in various isoforms that are distinguished by their subcellular locations. For example, in yeast cells, it can be found in two forms: extracellular or intracellular invertase, while in plants, there are three isoforms that differ in biochemical properties and subcellular locations (Acosta *et al.*, 2000). Invert sugar is a sugar composed of an equimolar mixture of fructose and glucose that is sweeter and has less crystallinity than sucrose (Goosen *et al.*, 2007). Invertases are known to be used in a variety of industrial food applications, including the production of non-crystallizing creams, artificial honey, lactic acid, ethanol, confectionary (food), digestive aid tablets, powder milk for infants, and other infant foods (Phadtare *et al.*, 2004; Sikander, 2007). Despite invertase wide range of applications in numerous industries, commercially available invertase is quite expensive, restricting the enzyme's usefulness. Microorganisms are primarily used in the synthesis of invertase, which requires very precise control of production conditions and a high level of purification for taste and health reasons, making the enzyme pricey (Laluce, 1991). It occurs widely in microorganisms and was first isolated in 1860 by Berthelot using alcohol precipitation (Neumann, & Lampen, 1967).

Saccharomyces cerevisiae is particularly interesting microorganism, it synthesizes two invertase isoenzymes biosynthesized by yeast strains, *Aureobasidium* sp. *Rhodotorulaglutinis*, *Saccharomyces cerevisiae* (Mona, & Mohamed, 2009), *Saccharomyces carlsbergensis* (Shankar *et al.*, 2010). *Saccharomyces cerevisiae* is the organism of choice for invertase production because of its characteristic high sucrose ferment ability. The aim of this study was carried out to produce extracellular invertase enzyme of *Saccharomyces cerevisiae* newly isolated and partial purification from Baker's yeast and grape samples to determine the kinetic factors and conditions that will maximize the activity of the enzyme which will help boost its suitability for industrial prospects.

2 Materials and Methods

Yeast, sucrose, glacial acetic acid, sodium acetate, sodium potassium tartrate, sodium hydroxide, silver nitrate, glucose, fructose, Bovine serum albumin (BSA), Coomassie brilliant blue (G-250) and 3,5-dinitrobenzoic Acid (DNS) were obtained from Sigma/Aldrich Chemical Company Ltd, Poole, UK.

2.1 Isolation of Microorganisms

In this study, *Saccharomyces cerevisiae* strains were isolated from Baker's yeast and fruit samples such as grape and used to produce invertase. Grape samples were gathered from El-beida city's local market and utilized to isolate invertase-producing yeast. Each cotton wool plugged Erlenmeyer flask was filled with YPS agar medium containing: (sucrose 30.0 g/l, peptone 5.0 g/l, and yeast extract 3.0 g/l). The flasks were sterilized in an autoclave for 15 minutes at 15 lbs pressure (121°C) and then cooled to room temperature (Dworschock & Wickerham, 1961). For 2-3 days, the Petri plates were incubated at 30°C in an incubator (Model: MIR-153, Sanyo Japan). YPS agar slants were used to transfer the colonies. Cultural and physical traits were used to identify the isolates (Barnett *et al.*, 1979).

2.1.1 Isolation of Efficient Invertase Producer

By inoculating a culture into sucrose broth, an efficient invertase producer (*Saccharomyces cerevisiae*) was isolated. The broth was tested for invertase activity after three days of incubation by boiling it with Benedict's reagent (green to brick red color indicates positive result) (Arumugam *et al.*, 2014).

2.1.2 Identification of *Saccharomyces Cerevisiae* Gram's Staining

Gram's staining was applied to a loopful broth culture and viewed microscopically under an oil immersion microscope. Budding yeast cells that were Grams positive were observed (Arumugam *et al.*, 2014).

2.1.3 Lacto Phenol Cotton Blue Staining

Lacto phenol Cotton Blue Staining producer was used to stain a loop of broth culture, which was observed under high power objectives. The presence of budding yeast cells was observed (Arumugam *et al.*, 2014).

2.1.4 Extracellular Invertase Production

The culture medium was centrifuged at 10000 rpm for 10 minutes at 4°C. The supernatant was used as crude enzyme source for invertase assay.

2.2 Measurement of Invertase Activity

The activity of the enzyme was determined using sucrose as substrate. A suitable amount (100µl) of the enzyme solution was mixed with buffered (acetate buffer pH 6.0 for invertase from Baker's yeast and sodium phosphate buffer pH 10.0 for invertase from grape sample) 30 mM aqueous sucrose solution. The reaction was carried out at

55°C for 30 min and the volume was made up to 3 ml by adding distilled water. To stop the reaction, 3 ml of dinitrosalicylic acid reagent (DNS) was added and the mixture was heated for five minutes in a boiling water bath. After cooling, the intensity of the color was read at 540 nm in UV-Vis spectrophotometers (Miller, 1959).

The invertase units in each sample were determined by using the following formula:

Units of invertase activity in each assay

$$\text{Tube} = \frac{\Delta\text{ABS}/30.0\text{min} \cdot \text{Final volume}}{a \cdot 1.0\text{cm}}$$

Where, ΔABS = absorbance change

a = mill-molar absorptivity constant

Total units = Number of units / Final volume * Final volume / ml of dilute enzyme added * total ml of dilute enzyme / ml of stock added * ml of stock fraction/ 1. Protein concentration was estimated according to the method described by Bradford depending on bovine serum albumin (BSA) standard curve (Bradford, 1976).

The specific activity was determination by using following equation:

$$= \frac{U}{\text{mg}} = \frac{\text{Enzyme activity } \frac{U}{\text{ml}}}{\text{Protein concentration } \frac{\text{mg}}{\text{ml}}}$$

2.3 Protein Estimation

The protein concentration of enzyme solutions was measured by Bradford method (Bradford, 1976). Bradford reagent (5ml) was added to a test-tube containing 0.1 ml of the diluted enzyme. A blank was run parallel. The tubes were vortexed. The absorbance was noted at 595 nm on a spectrophotometer. The bovine serum albumin (BSA) standard curve was used to calculate the amount of protein in each sample.

2.4 Effect of pH and Temperature on Invertase Activity

The effect of pH on invertase activity was determined by assaying the enzyme as mentioned before with the difference that the activity was determined at different pH ranging from 3-13 (50mM acetate and 50mM sodium phosphate buffer) at 55°C as described earlier (Amin et al., 2010). The optimal temperature for invertase activity was determined by measuring the activity at various temperatures (25-70°C), as described by Amin et al (2010).

2.5 Effect of Various Metal Ions on Invertase Activity

The crude invertase was mixed with 5 mM concentration of various salts such as CaCl_2 , CuCl_2 , MgCl_2 , SnCl_2 , NiCl_2 , CuCl_2 and NaCl for 30min at 55°C pH 6 and 10 for invertase from Baker's yeast and grape sample respectively before adding the substrate and subsequently invertase activity was determined (Shankar et al., 2010).

2.6 Determination of The Mode of Inhibition and Inhibitor Constant (Ki)

For crude invertase of *S. cerevisiae*, the effect of different chemical inhibitors on invertase activity was studied individually. Before adding the substrate, the crude invertase was mixed with 0.5, 1, 2, and 5mM concentrations of different chemical inhibitors such as fructose, CuSO_4 , and glucose for 30 minutes at 55°C, pH 6.0 and 10 for invertase from Baker's yeast and grape sample, respectively (Aziz et al., 2011).

2.7 Determination of Kinetic Parameters for Crude Invertase

The kinetic parameters (Michaelis-Menton constant) K_m and maximal velocity V_{max} of invertase activity of *S. cerevisiae* were determined individually from Lineweaver Burk plot optimal assay conditions, 55°C, pH 6.0 and 10 for invertase from Baker's yeast and grape sample respectively at 30 min for sucrose concentrations ranging from 0.25, 0.5, 1, 2, 5, 10 and 20 mM. The evaluation of these graph yielded the kinetic parameters for the invertase activity (Sivakumar et al., 2012).

2.8 Statistical Analysis

Results were expressed as means \pm standard division of the mean ($n = 6$). Statistical significance was set at $P < 0.05$ by using a t-test. Microsoft Excel has calculated kinetic parameters for invertase activity.

3 Results

3.1 Isolation and Identification of Yeast Cultures

Different strains of *Saccharomyces cerevisiae* were isolated from Baker's yeast and grape fruit samples. On the basis of morphology and sporulation, they were identified using conventional yeast identification procedures.

3.2 Effect of pH on *S. cerevisiae* Invertase Activity

In the present study, the effect of pH for invertase activity by *S. cerevisiae* of Baker's yeast and grape fruit were

assessed. The effect of pH on the activity of crude invertase was determined in the pH range of 3.0-13. Maximum invertase activity of was recorded at pH 6.0 and pH 10 for both extracellular invertases (*S. cerevisiae*) were isolated from Baker's yeast and grape fruit respectively. The enzyme activity was decreased at pH 13 for both enzymes. The pH stability of enzyme was measured by the standard assay method with sucrose. An average of retaining activity was observed between pH 5.0 and 8.0 for Baker's yeast invertase and between pH 8.0 and 11 for invertase from grape sample (Fig. 1 and 2).

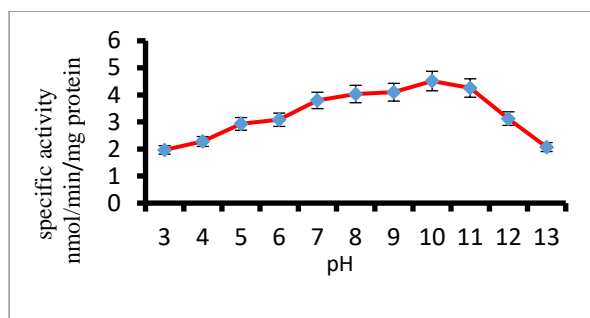


Figure (1). Effect of pH on invertase activity by *S. cerevisiae* (grape fruit).

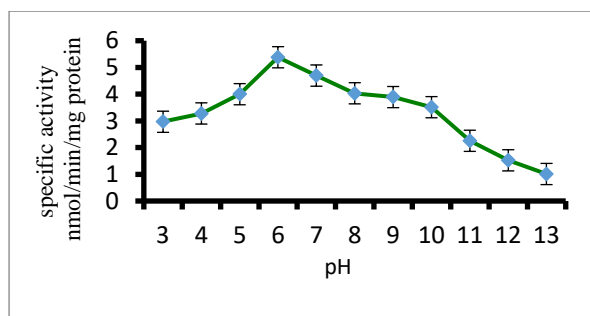


Figure (2). Effect of pH on invertase activity by *S. cerevisiae* (Baker's yeast).

3.3 Effect of Temperature on *S. cerevisiae* Invertase Activity

In the study of effect of temperature on invertase, it was observed that invertase was sensitive to temperature; the higher the temperature, the higher the rate of reaction. The increase in the rate of reaction is due to an increase in the number of molecules that have sufficient energy to enter into the transition state. From (Fig. 3), the reaction rate of invertase for both, extracellular invertases increased from 35°C to 55°C.

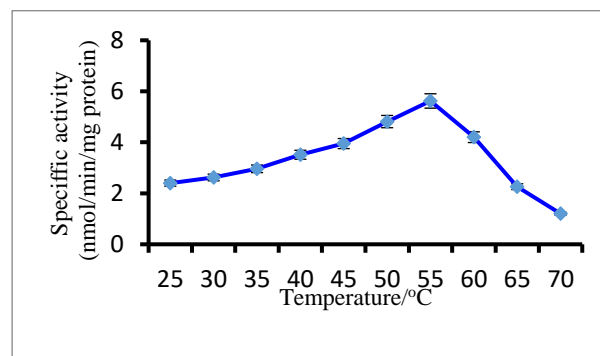


Figure (3). Effect of temperature on invertase activity by *S. cerevisiae* (Baker's yeast and grape fruit).

3.4 Effect of Various Metal ions on *S. cerevisiae* Invertase Activity

The effect of different metals ions (CaCl₂, CuCl₂, MgCl₂, SnCl₂, NiCl₂, CuCl₂ and NaCl) on invertase activity for both, extracellular invertases of *S. cerevisiae* was examined by incubating various metal ions with extract at 55°C for 30 minutes (Fig. 4 and 5). Maximum amount of invertase activity of 2.69 ± 0.03 nmol/min/mg protein was recorded in calcium chloride and minimum invertase production of 0.34 ± 0.005 nmol/min/mg protein was recorded in tin (II) chloride by *S. cerevisiae* of Baker's yeast (Fig. 4). Among the tested metal ions, the maximum amount of extracellular invertases for grape fruit was recorded in magnesium chloride (1.25 ± 0.02 nmol/min/mg protein), whereas the minimum amount of invertase production was observed in sodium chloride (0.09 ± 0.001 nmol/min/mg protein) (Fig. 5).

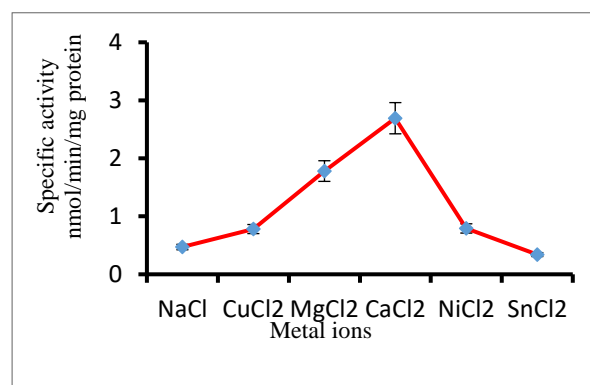


Figure (4). Effect of metal ions on invertase activity by *S. cerevisiae* from Baker's yeast.

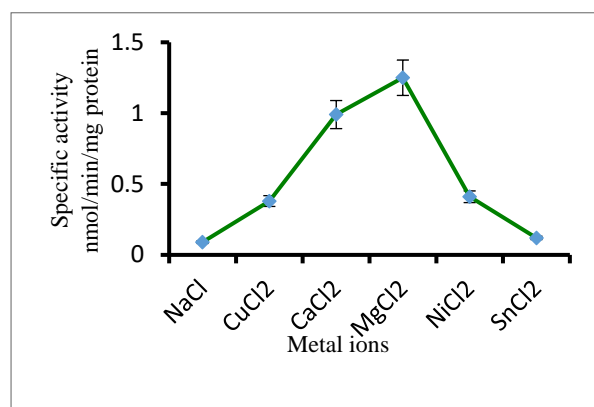


Figure (5). Effect of metal ions on invertase activity by *S. cerevisiae* from grape sample.

3.5 Determination of Kinetic Parameters for *S. cerevisiae* Invertase

The kinetic parameters of enzymatic reaction were calculated by the Lineweaver-Burk linearization using the Michaelis-Menton kinetic model. The kinetic parameters (K_m and V_{max}) were determined at 55°C and pH 6 and 10 for both, extracellular invertases (*S. cerevisiae*) for concentrations ranging between 0.25 to 5 mM of sucrose as substrate. The K_m and V_{max} of *S. cerevisiae* for Baker's yeast is 0.860 ± 0.04 mM and 24.39 ± 2.44 nmol/min/mg protein (Fig. 6). The K_m and V_{max} of *S. cerevisiae* for grape fruit is 1.243 ± 0.07 mM and 23.25 ± 3.14 nmol/min/mg protein (Fig. 7). The results of this study indicated that sucrose is a better substrate of extracellular invertases (Baker's yeast) than extracellular invertases (grape fruit) with a K_m value 1.5-fold higher (1.243 ± 0.07 mM) and the lower V_{max} (23.25 ± 3.14 nmol/min/mg protein).

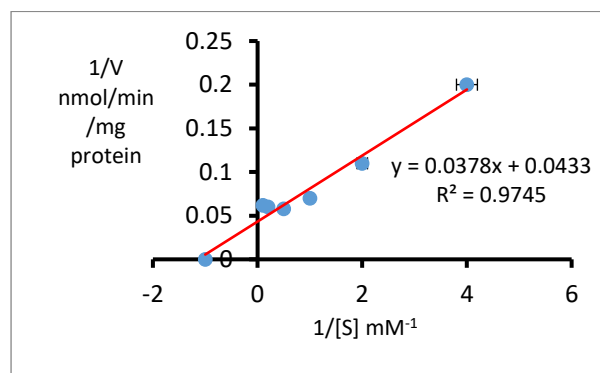


Figure (6). Determination of K_m and V_{max} of *S. cerevisiae* of Baker's yeast invertase (Lineweaver Burk plot; 50 mM citrate pH 6, 55°C, 30 min, substrate concentration ranging from 0.25-5 mM; Mean and standard deviation were determined from three replicates). The intercept on the y-axis corresponding to $1/V_{max} = 0.0433$, slope corresponding to $K_m/V_{max} = 0.0378$.

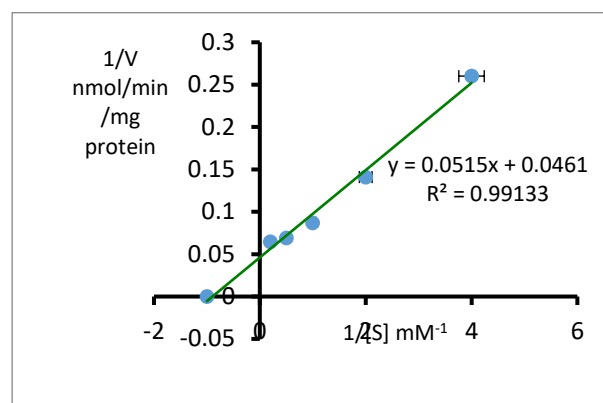


Figure (7). Determination of K_m and V_{max} of *S. cerevisiae* of grape fruit invertase (Lineweaver Burk plot; 50 mM sodium phosphate pH 10, 55°C, 30 min, substrate concentration ranging from 0.25-5 mM; Mean and standard deviation were determined from three replicates). The intercept on the y-axis corresponding to $1/V_{max} = 0.0461$, slope corresponding to $K_m/V_{max} = 0.0515$.

3.6 Kinetics of Sucrose Hydrolysis by *S. cerevisiae* Invertases

Extracellular invertases (*S. cerevisiae*) for Baker's yeast and grape fruit were assayed at 55°C in the reaction mixtures (pH = 6.0 and 10, respectively) containing different amounts of sucrose (0.25-5.0 mM). The data were plotted according to the Lineweaver-Burk plot to determine the values of kinetic constants (V_{max} and K_m , K_{cat} , and K_{cat}/K_m , Fig. 6 and 7) as described previously. A Lineweaver-Burk plot was applied to determine the kinetic constants (K_m and V_{max}). The catalytic center activity for both, extracellular invertases (*S. cerevisiae*) (K_{cat}) and specificity constant (K_{cat}/K_m) of sucrose was determined (Tab. 1).

Table (1). The catalytic properties of invertase from *S. cerevisiae*.

Invertases types		
Catalytic properties	Baker's yeast	Grape fruit
K_m (mM)	0.860 ± 0.04	1.243 ± 0.07
V_{max} (nmol/min/mg protein)	24.39 ± 2.44	23.25 ± 3.14
$^aK_{cat}$ (min^{-1})	0.28 ± 0.02	0.56 ± 0.008
K_{cat}/K_m ($\text{mM}^{-1} \text{min}^{-1}$)	0.325 ± 0.03	0.045 ± 0.003
K_s (V_{max}/K_m) (ml/min/mg protein)	27.03 ± 5.24	24.39 ± 7.11

The substrate efficiency ($K_s = V_{max}/K_m$).

The turnover number ($K_{cat} = V_{max}/[E]$).

^a Calculated estimating a molecular mass of 270 kDa for the active enzyme.

The kinetic constants (K_m & V_{max}).

The specificity constant (K_{cat}/K_m).

3.7 Determination of Inhibition constants (K_i) for *S. cerevisiae* Invertases

In order to determine the K_i for *S. cerevisiae* invertase inhibitors with a series of experiments were conducted with different chemical inhibitors. The crude invertase was mixed with 0.5, 1, 2 and 5 mM concentration of different chemical inhibitors such as fructose, CuSO_4 and glucose for 30 min at 55°C, pH 6.0 for invertase from Baker's yeast before adding the sucrose as substrate and subsequently invertase activity was determined. Lineweaver-Burk plots from this data were used to determine the inhibitor constant (K_i). (Fig. 8 to 13) show the effect of these inhibitors on extracellular invertase. (Tab. 2) summarizes the K_i and mode of inhibition of different inhibitors with invertase activity.

Table (2). Summary of inhibition constant (K_i) and mode of inhibition of different inhibitors with Baker's yeast extracellular invertase

Invertase inhibitor	K_i (mM)	Mode of inhibition
Fructose	0.45 ± 0.09	Competitive
CuSO_4	0.066 ± 0.003	Uncompetitive
Glucose	0.014 ± 0.001	Non-competitive

The values shown are the (Mean \pm S.D), obtained from three separate the crude invertase for Baker's yeast.

It was found that all extracellular invertase inhibitors had a K_i values between 0.01 mM to 0.4 mM with the lowest K_i value with glucose. The weakest extracellular invertase inhibitors found was fructose. Lineweaver-Burk plot analysis revealed that the inhibitors had different modes of inhibition. Glucose was a non-competitive inhibitor (Fig. 8 and 9), while CuSO_4 was uncompetitive inhibitors (Fig. 10 and 11). Fructose was found to be a competitive inhibitor (Fig. 12 and 13).

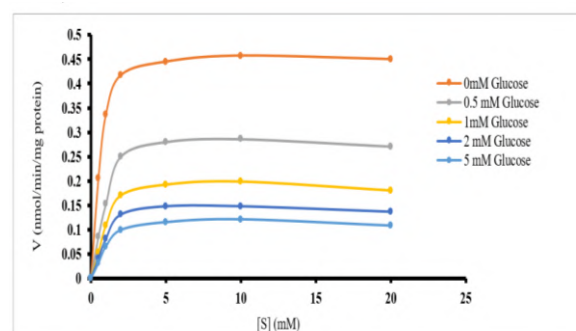


Figure (8). Saturation kinetics plot for glucose inhibition with sucrose as an invertase substrate in extracellular invertase for Baker's yeast.

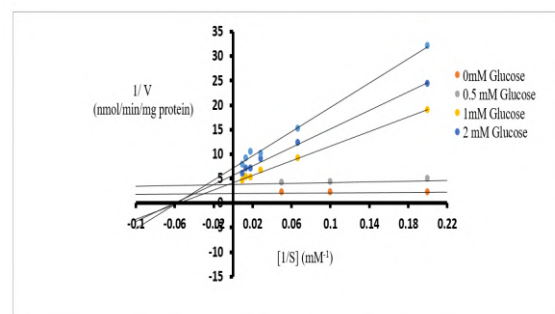


Figure (9). Lineweaver-Burk plot for glucose inhibition (non-competitive) with sucrose as an invertase substrate in extracellular invertase for Baker's yeast.

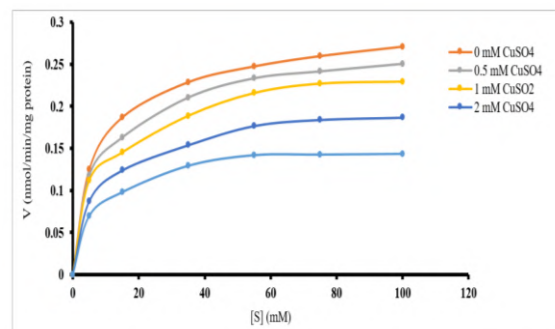


Figure (10). Saturation kinetics plot for CuSO_4 inhibition with sucrose as an invertase substrate in extracellular invertase for Baker's yeast.

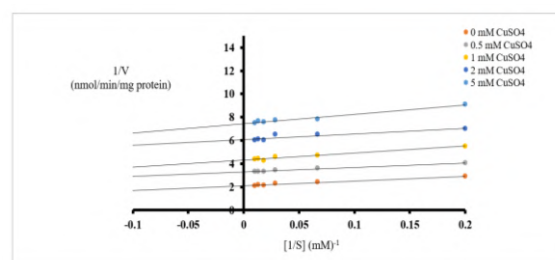


Figure (11). Lineweaver-Burk plot for CuSO_4 inhibition (uncompetitive) with sucrose as an invertase substrate in extracellular invertase for Baker's yeast.

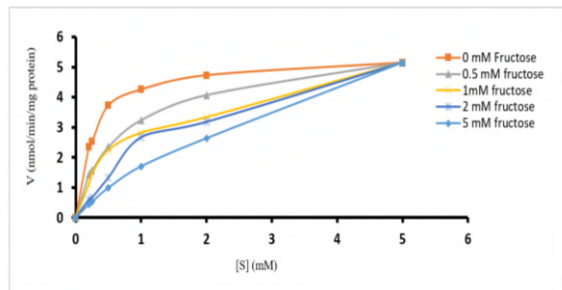


Figure (12). Saturation kinetics plot for fructose inhibition with sucrose as an invertase substrate in extracellular invertase for Baker's yeast.

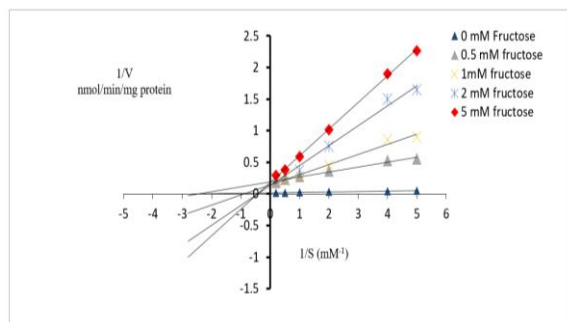


Figure (13). Lineweaver-Burk plot for fructose inhibition (competitive) with sucrose as an invertase substrate in extracellular invertase for Baker's yeast.

4 Discussion

The identification of *S. cerevisiae* was carried out (Barnett *et al.*, 1979; Gustavo *et al.*, 2022). Colonies were flat, smooth, moist, glistening, and creamy in color. They appeared on YPS agar plates after 24 h, rapidly grew and fully matured within 3 days. Microscopic studies showed that *S. cerevisiae* is one of the budding yeast. Cells in the sediment of YPS broth were unicellular and globose. The bud raised on different parts of the cell surface on a narrow base as said to be multilateral (multipolar) budding was typical. The spores formed by *S. cerevisiae* were 1-4 spores per ascus. They were rounded and slightly oval in shape. Screening of *S. cerevisiae* isolates was carried out in shake flask by submerged fermentation for invertase production. The effect of pH on the activity of crude invertase was determined in the pH range of 3.0-13. A change in pH affects the ionization of essential active site amino acid residues that are involved in substrate binding and catalysis. The ionization of these residues may cause distortion of the active site cleft and hence may indirectly affect enzyme activity. The effect of pH is related to the growth and metabolic activities of the organism (Bodade *et al.*, 2010). This result was supported by the finding of Shankar *et al.* (2014) who

showed that the maximum invertase activity was at pH 6.0 by *Saccharomyces cerevisiae* MK. Uma *et al.* (2010) reported that the maximum invertase activity was found at pH 6 by *Aspergillus flavus*. Patil *et al.* (2012) evaluated the *Aspergillus* sp. invertase; it gave the good invertase activity for pH 6. Yamamoto *et al.* (1986) showed that maximum invertase activity was recorded at pH 6.8 for invertase from *Brevibacterium divaircatum*. Invertase exhibits marked stability towards pH changes and denaturants. Unlike other enzymes, invertase exhibits relatively high activity over a broad range of pH (3.5-5.5), with the optimum near pH of 4.5. (Essel & Osei, 2014). Invertases from *Saccharomyces cerevisiae* are usually active in slightly acidic to neutral pH (3.0-7.0), to close to neutral pH (6.5-7.0) (Belcarz *et al.*, 2000). However, optimum activity was highly active at pH 3.6 to 5.0 with optimum pH 4.5. Nguyen *et al.*, (2000) found that *Aspergillus niger* invertase was stable at pH range from 5.0 to 6.5. However, Benattouche *et al.* (2016) was noted that the invertase by *Streptococcus* sp. isolated from the date increased in pH from pH 7.0 to pH 8.0. Result also, showed that the invertase activity maxima observed at pH 10 (Fig. 1) by *S. cerevisiae* (grape fruit). These results are in line with Lee & Strum, (1996) results who reported that the maximum invertase increased above pH 9.0 by alkaline invertase isolated from carrot. On the other hand, the pH of a soluble invertase present in Semillon grape berry juice has been determined to be acidic not alkaline (Nakanishi *et al.*, 1991). Thus, further basic research is still needed. For instance, it remains unclear whether or not differences exist in gene expression patterns and regulation of sugar metabolism between grape species (Pan *et al.*, 2009). The activity of the invertase declined from 60°C to 70°C. This implies that the enzyme was denatured which led to the loss of activity of the invertase. Since enzymes, like invertase, were proteins with tertiary structure, they can be denatured when exposed to high temperatures. Denatured proteins do not react as much as the newly extracted proteins, thus resulting into a drastic drop of the rate of reaction (Campbell & Farrell, 2012). The temperature optimum was found 55°C in the present study (Fig. 3). These results agree with the findings by L'Hocine *et al.* (2000) who reported that the 55°C gave good invertase activity for invertase from *Aspergillus Niger* strain. On the other hand, Shankar *et al.* (2014) reported that the 30°C gave good invertase activity for invertase by an *S. cerevisiae* strain. In addition, Gine *et al.* (2010) found that 37°C gave good invertase by *Lactobacillus reuteri* CRL 100. Moreover, Benattouche *et al.* (2016) also

reported that the maximum invertase activity was recorded at 50°C for invertase by *Sterptococcus sp.* The similar results, Amin *et al.* (2010) reported that a slight increase in the activity of acid invertase was observed with Ca^{+2} , Mn^{+2} and Mg^{+2} ions. Shankar *et al.* (2014) showed that maximum invertase of 89.11% was recorded at CaCl_2 . However, Nakanishi *et al.*, (1991) reported that effect of 0.01 M of KCl, NaCl, MgCl_2 and CaCl_2 on the activity of both wine and grape juice invertases were negligible. Voster & Botha (1998) reported similar effects of Hg^{2+} on the activity of sugarcane neutral invertase. It was also reported that 0.005 M FeCl_2 , CuCl_2 , ZnCl_2 , CdCl_2 and AlCl_3 reduced the activity of invertase approximately 80, 73, 32, 45 and 22% respectively (Mahbubur-Rahman, 2004). (Dahot & Noomrio 1996) reported increase in invertase activities in the presence of MgCl_2 and CaCl_2 ions. They suggested that thiol groups at the catalytic site are important for the invertase activity. Metal ions play important roles in the biological function of many enzymes. The various modes of metal-protein interaction include metal-, ligand-, and enzyme-bridge complexes. Metals can serve as electron donors or acceptors. Chang *et al.* (1994) reported that purified enzyme had an optimal pH (5-6), temperature (50°C) and a K_m value of 0.53 mM for catalyzing self-transfer reaction from sucrose. Gine *et al.* (2010) reported that for invertase in *Lactobacillus reuteri* (CRL 1100), the K_m (6.66 mM) and V_{max} (0.028 $\mu\text{mol}/\text{min}$) values for sucrose were obtained. Uma *et al.* (2010) reported the result for invertase by *Aspergillus flavus* in Lineweaver-Burk plot of the enzyme affinity for sucrose gave a straight line plot from which the K_m as 0.23 mg/ml and V_{max} was 15.8 U/mg. Ribeiro and Vitolo, (2005) stated the result for conventional Lineweaver-Burk plot, the kinetic constants for soluble invertase ($K_m = 18.3$ mM and $V_{max} = 0.084$ U/mgE) and insoluble invertase ($K_m = 29.1$ mM and $V_{max} = 0.075$ U/mgE) invertase were calculated. Almeida *et al.* (2005) investigated the kinetic parameters of enzymatic reaction were calculated by the Lineweaver-Burk linearization using the Michaelis-Menton kinetic model. For the auto-immobilized enzyme it was obtained a K_m of 447 mM and V_{max} of 2,805 mmol/min. Uma *et al.* (2012) also stated the Michaelis-Menton kinetics for and constants were determined from a Lineweaver-Burk plot. The kinetic constant of invertase was V_{max} 28.57U/mg and K_m of 0.26 mg/ml. Whereas, Mona *et al.* (2009) evaluated the invertase from *Saccharomyces cerevisiae* NRRL Y-12632 in K_m value of the pure enzyme was found to be 60 mM while its V_{max} was 35.5 min mg protein as calculated by Hanes-Woolf plot. The rate of

sucrose hydrolysis; decreased by increasing substrate concentration, which may be due to substrate inhibition. However, Talekar *et al.* (2010) reported the kinetic constants for soluble invertase ($K_m = 10.80$ mM and $V_{max} = 21.59$ $\mu\text{mol}/\text{minutes}$) were calculated from nonlinear regression. Whereas, Guimaraes *et al.* (2007) stated that invertase from *Aspergillus niveus* had K_m value of 5.78 mM and V_{max} of 28.46 U per mg of protein per min and Chavez *et al.* (1997) investigated that invertase from *Candida utilis* and *Saccharomyces cerevisiae* exhibited K_m values of 11 and 25 mM, respectively. In a summary, a kinetic constant of invertase isolated from many organisms is affected by many factors such as enzyme sources, optimum pH, optimum temperature, thermal stability and molecular mass. This means that the good affinity of the extracellular invertases (Baker's yeast) for sucrose substrate. This was due to the lower accessibility of the substrate to the active site of the invertase enzyme (Bayramolu *et al.*, 2003). The kinetic parameters of both, extracellular invertase shown in Table 1 shows the most dramatic change, with about a 22.5% reduction in K_{cat} for grape invertase. There was big change in the K_{cat}/K_m of Baker's yeast invertase. The K_{cat}/K_m value of Baker's yeast invertase was about ≈ 8 -fold increase in the catalytic process. The key advantages revealed here are the low K_m (0.860 ± 0.04 mM), the high V_{max} , (23.25 ± 3.14 nmol/min/mg protein) and the high K_{cat}/K_m (0.28 $\text{mM}^{-1} \text{min}^{-1}$). This could be due to the ionized state of the Baker's yeast invertase whose charges have been reserved and that the sucrose binds more strongly to the active site than transition state of the substrate substantiating with the study of Myers *et al.*, (1997). This indicated that the Baker's yeast had higher affinity towards binding sucrose to the active site. The turnover number (K_{cat}) and specificity constant (K_{cat}/K_m) values of both enzymes (Tab. 1) showed that the activity of the Baker's yeast was better compared to grape invertase. Furthermore, specificity constant K_s (27.03 ml/min/mg protein) again confirmed that the Baker's yeast invertase was higher and more specific for sucrose as compared to grape invertase K_s (24.39 ml/min/mg protein) (Tab. 1). There are a few reports investigating the kinetic parameters of *S. cerevisiae* invertases. Partially purified invertases from *S. cerevisiae* K_{cat} and K_{cat}/K_m for sucrose substrate was 5.66 min^{-1} and $2.16 \times 10^7 \text{ M}^{-1}\text{Min}^{-1}$ (Reddy & Maley, 1996). Invertase production by *Saccharomyces cerevisiae* on from the wild-culture had K_{cat} and K_{cat}/K_m for sucrose equal to 122 min^{-1} and $19.51 \text{ M}^{-1}\text{min}^{-1}$ (Ul-Haq & Ali, 2005). In this study preliminary experiments were performed with three well-documented inhibitors of

extracellular invertase for Baker's yeast. Lee and Sturm (1996) support this finding who reported that invertase enzyme of carrot root was inhibited by their reaction products glucose and fructose. Fructose was a competitive inhibitor of neutral (Ki, 13.4 mM) and alkaline (Ki 16.3 mM) invertase. In contrast, glucose inhibited neutral (Ki, 28 mM) and alkaline (Ki, 33 mM) invertase noncompetitively. Fructose and glucose were competitive and noncompetitive inhibitors, with Ki values of 38 mM and 72 mM, respectively of rice alkaline invertase (Lin *et al.*, 1999). Fructose acts as a competitive inhibitor for the invertases, which implies that there is tighter binding of fructose to the active site in these enzymes (although the binding is still weaker than that of glucose) (Wu & Birch, 2005). These results indicated that the enzyme activity could be modulated by its end products.

5 Conclusions

The current study established the presence of invertase activity in *S. cerevisiae* which was isolated from both Baker's yeast and grape samples using the standardize techniques. Invertase isolated from *S. cerevisiae* was found to have maximum activities at pH 6 and 10 and maximum temperature of 50°C. The activity of the enzyme was affected by the presence of metal ions in various degrees. A comparison of a number of kinetic parameters of Baker's yeast and grape fruit invertase showed marked differences. The inhibition of hydrolysis of sucrose by invertase was characterized for three different inhibitor compounds. Inhibition studies showed that fructose, glucose and CuSO₄ inhibited invertase competitively, non-competitively and un-competitively respectively. Hence, *S. cerevisiae* may be recommended as a local source for the production of invertase enzyme, thus reducing the cost of production significantly.

Acknowledgements

The authors express their gratitude to Department of Chemistry, Faculty of Science, Omar Al-Mukhtar University, El-beida, Libya for their cooperation in carrying out this study.

Conflict of Interest: There are no financial, personal, or professional conflicts of interest to declare.

References

Acosta N, Beldarrain AI, Rodriguez Y, Alonso Y (2000) Characterization of recombinant invertase expressed in methylotrophic yeasts. *Biotechnology and Applied*

- Biochemistry.* 32:179-178. DOI: 10.1042/ba20000064
- Almeida AC, Araujo LC, Costa AM, Abreu CA, Lima GD, Palha MD (2005) Sucrose hydrolysis catalyzed by auto-immobilized invertase into intact cells of *Cladosporium cladosporioides*. *Electronic Journal of Biotechnology.* 1:717-725.
- Amin F, Bhatti H, Asgher M (2010) Partial purification and characterization of an acid invertase from *saccharum officinarum* l. *Pak. J. Bot.* 42:2531-2540.
- Arise RO, Olawoye DO, Acho MA, Olufemi O, Adewale AA, Alejlowo O, Nwonuma C (2020) Kinetic characteristics of partially purified invertase from *Citrullus lanatus* Rind. *Ceylon Journal of Science.* 49:61-69. DOI: <http://doi.org/10.4038/cjs.v49i1.7706>
- Arumugam G, Mohamed A, Sadiq, M, Nagalingam M, Panneerselvam A (2014) Production of invertase enzymes from *Saccharomyces cerevisiae* strain isolated from sugarcane and grape juices. *European Journal of Experimental Biology.* 4:29-32.
- Aziz S, Jalal F, Nawaz M, Niaz B, Shah FA, Memon M, Latif F, Nadeem S, Rajoka MI (2011) Hyperproduction and thermal characterization of a novel invertase from a double mutant derivative of *Kluyveromyces marxianus*. *Food Technol Biotechnol.* 49:465- 473.
- Barnett JA, Payne RW, Yarrow D (1979) A guide to identifying and classifying yeasts, Cambridge University Press, Cambridge. pp 25-78.
- Bayramolu G, Akgol S, Bulut A, Denizli A, Yakup AM (2003) Covalent immobilization of invertase onto a reactive film composed of 2-hydroxyethyl methacrylate and glycidyl methacrylate: properties and application in a continuous flow system. *Biochemical Engineering Journal.* 14:117-126. DOI:10.1016/S1369-703X(02)00170-5
- Belcarz A, Ginalska G, Lobarzewski J, Penel G (2002) The novel non-glycosylated invertase from *Candida utilis* (the properties and the conditions of production and purification). *Biochim. Biophys. Acta.* 1594:40-53. DOI: 10.1016/s0167-4838(01)00279-5
- Benattouche Z, Bachir Raho G, Bouhadi D, Sahnouni F (2016) Characterization of partially purified extracellular thermostable invertase by *Streptococcus sp* Isolated from the Date. *Bull. Env. Pharmacol. Life Sci.* 5:65-72. DOI: 10.1016/0003-9969(79)90006-2
- Bodade GR, Chandarahas N, Arfeen SA (2010) Optimization of culture conditions for glucose oxidase production by a *Penicillium chrysogenum SRT 19* strain. *Engineering and Life Science.* 10:35-39. DOI:10.1002/elsc.200900030
- Bradford, NM (1976) A rapid and sensitive method for quantitation of microorganism qualities of protein utilizing the principle of protein dye binding analysis. *Biochem.* 72:248-254.

- Campbell M, Farrell S (2012) Biochemistry (7th Ed.) China, China Translation & Printing Services Limited.
- Chang YY, Yjuang RH, Su JC, Sung HY (1994) Partial purification and characterization of invertase isozymes from rice grains. *Biochem. Mol. Biol.* 33: 607-15.
- Chavez FP, Rodriguez L, Diaz J, Delgado JM, Cremata JA (1997) Purification and characterization of an invertase from *Candida utilis*: Comparison with natural and recombinant yeast invertases. *J. Biotechnol.* 53:67-74. DOI: 10.1016/s0168-1656(97)01663-5
- Dahot MU, Noomrio MH (1996) Purification and some properties of invertases from *Achras sapota* fruit. *J. Islamic. Acad. Sci.* 2:31-36.
- Dewdney PA (1973) Enzymes in food processing. *Nutrition & Food Science.* 73:20-22.
- Dworschack RG, Wickerham LJ (1961) Production of extracellular and total invertase by *Candida utilis*, *Saccharomyces cerevisiae*, and other yeasts. *Appl. Microbiol.* 9:291-294. DOI: 10.1128/am.9.4.291-294.1961
- Essel K, Osei Y, (2014) Investigation of some kinetic properties of commercial invertase from yeast. *Nat. Prod. Chem. Res.* 2:6. DOI: 10.4172/2329-6836.1000152
- Gine, S.C.; Maldonado, M.C. and Valdez, F.G.D. (2010): "Purification and characterization of invertase from *Lactobacillus reuteri* CRL 1100", *Curr Microbiol.*, 40(3):181-184. DOI: 10.1007/s002849910036
- Goosen C, Yuan, XL, Van Munster JM, Ram AF, Van der Maarel MJ, Dijkhuizen L (2007) Molecular and biochemical characterization of a novel intracellular invertase from *Aspergillus niger* with transfructosylating activity. *Eukaryot. Cell.* 6:674-681. DOI: 10.1128/EC.00361-06
- Guimaraes LH, Terenzi HF, Lourdes MD, Jorge JA (2007) Production and characterization of thermo stable extracellular β -fructofuranosidase produced by *Aspergillus ochraceus* with agro industrial residues as carbon sources. *J. Enz. Microbial. Technol.* 42:52-57. DOI 10.1016/j.enzmictec.2007.07.021
- Mandujano GP, Lorca HC, Alves CD, Prado GO, Martins HR, Novaes HR, Alves IC, Anderson F (2022) Identification and selection of a new *Saccharomyces cerevisiae* strain isolated from Brazilian ethanol fermentation process for application in beer production. *Food Microbiology.* 103:103-958. doi.org/10.1016/j.fm.2021.103958
- Klein RD, Poorman RA, Favreau MA, Shea MH, Hatzembuhler NT, Nulf S (1989) Cloning and sequence analysis of the gene encoding invertase from the yeast *Schwanniomyces occidentalis*. *Curr. Genet.* 16:145-152. DOI: 10.1007/BF00391470
- L'Hocine Z, Wang B, Jiang B, Xu S (2000) Purification and partial characterization of fructosyltransferase and invertase from *Aspergillus niger* AS0023. *J. Biotechnol.* 81:73-84. DOI: 10.1016/s0168-1656(00)00277-7
- Laluce C (1991) Current aspects of fuel ethanol production in Brazil. *Critical Reviews in Biotechnology.* 11:149-161. doi.org/10.3109/07388559109040620
- Lee H, Sturm A (1996) Purification and characterization of neutral and alkaline invertase from carrot. *Plant physiol.* 112:1513-1522. doi: 10.1104/pp.112.4.1513
- Lin C, Lin H, Wang A, Yisung H (1999) Purification and characterization of an alkaline invertase from shoots of etiolated rice seedlings. *New Phytol.* 142: 427-434.
- Mahbubur-Rahman SMM, Sen PK, Hasan MF, Mian MAS, Habibur-Rehman M (2004) Purification and characterization of invertase enzyme from sugarcane. *Pak. J. Biol. Sci.* 7:340-345. DOI: 10.3923/pjbs.2004.340.345
- Miller GL (1959) Use of dinitrosalicylic reagent for determination of reducing sugars. *Anal. Chem.* 3: 426-428. doi.org/10.1021/ac60147a030
- Mobini-Dehkordi M, Nahvi I, Zarkesh-Esfahani, H, Ghaedi K, Tavassoli R, Akada R (2008) Isolation of a novel mutant strain of *Saccharomyces cerevisiae* by an ethyl methane sulfonate-induced mutagenesis approach as a high producer of bioethanol. *Journal of Bioscience and Bioengineering.* 105:403-408. DOI: 10.1263/jbb.105.403
- Mona MR, Mohamed UN (2009) Production, purification and characterization of extracellular invertase from *Saccharomyces cerevisiae* NRRL Y-12632 by Solid-State Fermentation of red carrot residue. *Aust. J. Basic. Appl. Sci.* 3:1910-1919.
- Myers DK, Lawlor DT, Attfield PV (1997) Influence of invertase activity and glycerol synthesis and retention on fermentation of media with a high sugar concentration by *Saccharomyces cerevisiae*. *Appl. Environ. Microbiol.* 63:145-150. doi: 10.1128/aem.63.1.145-150.1997
- Nakanishi K, Wu W, Yokotsuka K (1991) Purification and some properties of thermostable invertase from wine. *J. Ferment. Bioeng.* 71:66-68. doi.org/10.3136/fstr.12.131
- Neumann NP, Lampen JO (1967) Purification and properties of yeast invertase. *Biochemistry.* 6:468-75. DOI: 10.1021/bi00854a015
- Nguyen QD, Rezessy-Szabo JM, Bhat MK, Hoschke A (2005) Purification and some properties of β -fructofuranosidase from *Aspergillus niger* IMI303386. *Process Biochemistry.* 40:2461-2466. DOI:10.1016/j.procbio.2004.09.012
- Pan QH, Cao P, Duan CQ (2009) Comparison of enzymes involved in sugar metabolism from *Shang-24* (*Vitis quinquangularis*) and *Cabernet Sauvignon* (*Vinifera vinifera*) at veraison. *Aust. J. Grape Wine Res.* 15:9-17.

- Patil M, Bhamre R, Patil U (2012) Invertase production from *Aspergillus* sp. M1 isolated from Honeycomb. Int. J. Appl. Biores. 15:1-5.
- Phadtare SD, Britto V, Pundle A, Prabhune A, Sastry M (2004) Invertase lipid biocomposite films: preparation, characterization and enzymatic activity. Biotechnology Progress. 20:156-161. DOI: 10.1021/bp034236t
- Reddy A, Maley F (1996) Studies on identifying the catalytic role of Glu-204 in the active site of yeast invertase. The journal of biological chemistry. 271: 13953-13958. DOI: 10.1074/jbc.271.24.13953
- Ribeiro RR, Vitolo M (2005) Anion exchange resin as support for invertase immobilization. Journal of Basic and Applied Pharmaceutical Sciences. 26:175-179.
- Shankar S, Madhan R, Sathyavani R, Niket B (2010) Production and partial purification of invertase using *Cynpogon caecius* leaf powder as substrate. Indian J. Microbiol. 50:318-324. doi: 10.1007/s12088-010-0011-3
- Shankar T, Thangamathi R, Sivakumar T (2014) Characterization of invertase from *Saccharomyces cerevisiae* MTCC. African journal microbiology research. 8:1385-1393. DOI:10.5897/AJMR2014.6612
- Sikander A (2007) Kinetics of invertase production in batch culture. Pakistan Journal of Botany. 39:907- 912.
- Sivakumar T, Shankar T, Vijayabaskar P, Ramasubramanian V (2012) Optimization for keratinase enzyme production using *Bacillus thuringiensis* TS2. Academic Journal of Plant Sciences. 5:102-109. DOI: 10.5829/idosi.ajps.2012.5.3.6279
- Talekar S, Kate VGA, Samant N, Kumar C, Gadagkar S (2010) Preparation and characterization of cross-linked enzyme aggregates of *Saccharomyces cerevisiae* invertase. Australian Journal of Basic and Applied Sciences. 4:4760-4765.
- Ul-Haq I, Ali S (2005) Invertase production from a hyper producing *Saccharomyces cerevisiae* strain isolated from dates. Pak. J. Bot. 37:749-759.
- Uma C, Gomathi D, Muthulakshmi C, Gopalakrishnan VK (2010) Production, purification and characterization of invertase by *Aspergillus flavus* using fruit peel waste as substrate. Adv. Biol. Res. 4: 31-36.
- Uma C, Gomathi D, Ravikumar G, Kalaiselvi M, Palaniswamy M (2012) Production and properties of invertase from a *Cladosporium cladosporioides* in SmF using pomegranate peel waste as substrate. Asian Pacific Journal of Tropical Biomedicine. 2: S605-S611. doi.org/10.1016/S2221-1691(12)60282-2
- Vorster DJ, Botha FC (1998) Partial purification and characterization of sugarcane neutral invertase", Phytochemistry. 49:651-655. doi.org/10.1016/S0031-9422(98)00204-0
- Wu L, Birch R (2005) Characterization of the highly efficient sucrose isomerase from *Pantoea dispersa* UQ68J and cloning of the sucrose isomerase gene. Applied and environmental microbiology. 71:1581-1590. doi: 10.1128/AEM.71.3.1581-1590.2005
- Yamamoto K, Kitamoto Y, Ohata N, Isshiki S, Ichikawa Y (1986) Purification and properties of invertase from a glutamate-producing bacterium. J. Ferment. Tech. 64:285-292. DOI:10.5897/AJMR2014.6612N



Statistical Study of Extract Keratin Protein from Waste Chicken Feather Based on Response Surface Methodology

Dalal M. Ibrahim¹, Hanan F. Emrayed², Sumayyah M. Albarani¹, and Bushra Alnaji Abdalrazig¹

¹Chemistry Department, Science Faculty, Omar Al-Mukhtar University, Libya.

²Chemical Engineering Department, Engineering Faculty, Omar Al-Mukhtar University, Libya.

DOI: <https://doi.org/10.37375/sjfsu.v2i2.297>

A B S T R A C T

ARTICLE INFO:

Received 01 July 2022.

Accepted 12 September 2022.

Published 27 October 2022.

Keywords:

Chicken feather waste, reducing agent, keratin protein, UV-Vis analysis, RSM:

The feathers contain a significant amount of keratin protein, which is used in cosmetics, shampoos, hair treatment creams, and skin creams. Dissolving chicken feathers with reducing agent and then separating the protein from chemicals are the key steps involved. However, in order to enhance the amount of recovered keratin as much as possible, the best conditions for extracting keratin from chicken feathers are required. In this study, Response Surface Methodology (RSM) was used in order to simulate and optimize the operating parameters for extracting keratin from waste chicken feathers in order to increase the amount of keratin protein compared to previous studies. Dissolving chicken feathers using sodium sulphide as a reducing agent at various periods, temperatures, and concentrations is the first step in the fundamental technique. After the feathers have been dissolved with a reducing agent, the fluid is treated with an ammonium sulfate solution to precipitate the protein. As determined by a biuret test and UV-Vis analysis, the keratin protein had a maximum wavelength of 290 nm. Finally, the statistical optimization of the extraction conditions provided a better understanding of the reaction parameters. The optimum yield of keratin was achieved at 3.7 hours at 30.07°C with 0.05 M sodium sulfide.

1 Introduction

Many countries had a large poultry slaughterhouse sector that discarded about four million tones of chicken feathers each year, and they took advantage of the circumstance to conduct research and find ways to monetize the waste. There is a growing interest in the creation of environmentally friendly, renewable-resource-based materials. The current research is the first in Libya to recycle chicken feather waste, and it focuses on extracting natural keratin protein from chicken feathers with the help of a reducing agent. Reducing substances aid in lowering the stability of keratin fibers in their solid state, which is present in feathers. In order to dissolve keratin fibers into protein solutions, these chemicals will break down disulfide bonds, hydrogen bonds, and salt linkages. Feathers make up over 90% of the keratin protein in waste biomass, as previously stated (Fakhfakh-

Zouari, Haddar, Hmidet, Frikha, & Nasri, 2010; Gessesse, Hatti-Kaul, Gashe, & Mattiasson, 2003; Grazziotin, Pimentel, De Jong, & Brandelli, 2006; Saucedo-Rivalcoba, Martínez-Hernández, Martínez-Barrera, Velasco-Santos, & Castaño, 2011).

A-keratins and b-keratins are the two most common types of keratins (Barone, Schmidt, & Gregoire, 2006; Sharma & Gupta, 2016). In mammals, a-keratins are found in abundance, while b-keratins are found in abundance in birds and reptiles. A-keratins may be found in mammals' hair, wool, horns, nails, claws, and hooves, while b-keratins can be found in reptiles' nails, scales, claws, shells, feathers, beaks, and quills (Ng et al., 2012). The reductants function quickly and without creating any chemical changes or a reduction in protein yield. The

solutions' by-products act like true proteins, not hydrolysis by-products. Sulfosalicylic acid and ammonium sulfate, two common protein precipitants, are employed to precipitate their solutions. Keratin is well-known for its ability to stretch in a variety of directions without breaking and for forming a strong, fibrous matrix in tissues (Yamauchi & Yamauchi, 2002).

According to Leichner. (2019), chicken feather keratins can be converted to natural protein that is soluble in alkali or acid and digestible by trypsin and pepsin. To achieve this, the disulfide bonds in keratin were broken. Keratins in feathers are made up of twisted, pleated sheets that are then stabilized and toughened by disulfide bonds. The strength of the keratin in chicken feathers can be reduced by disrupting these disulfide connections, allowing the keratin to become soluble and convert to natural protein (Leichner et al., 2019).

In the case of Schrooyen et al, oxidizing chemicals like bromine, permanganate, and hydrogen oxide break disulfide bonds very slowly, slowing down the protein extraction process. On the other hand, the reducing agents operate swiftly and dissolve keratin only in alkaline reactions (pH 10 to 13), but their activity is not solely due to alkali. The results of these processes behave like real proteins, not hydrolysis byproducts. Schrooyen et al explored the effect of adding varying amounts of SDS on the rate of aggregation of polypeptide chains and the rate of oxidation of cysteine residues during dialysis, as have a few other researchers (Schrooyen, Dijkstra, Oberthür, Bantjes, & Feijen, 2001). Yamauchi et al. studied urea, 2-mercaptoethanol, (Kamarudin et al., 2017) solution (sodium dodecyl sulphate). They discovered that using SDS as a surfactant sped up the extraction process and boosted the yield. It also stabilized the aqueous protein solution following urea removal via dialysis against 2-mercaptoethanol-containing water (0.08 wt percent). The surfactant binds to keratin and is eliminated by dialysis significantly more slowly than other low-molecular-mass substances (Yamauchi & Yamauchi, 2002).

Many countries had a large poultry slaughterhouse sector that disposed of approximately four million tonnes of chicken feathers per year, and they took advantage of the circumstance to conduct research and find ways to monetize the waste. Currently, there is a growing interest in the production of environmentally friendly materials derived from renewable resources. The current study is the first in Libya to recycle chicken feather waste, and it focuses on extracting natural keratin protein from chicken feathers using a reducing agent and methodically optimizing extraction conditions. The present research was undertaken to extract natural keratin protein from chicken feathers by using different reducing agents. The reducing agent helps in decreasing the stability of keratin fibers in the solid form found in feathers. These reagents will break down disulfide bonds, hydrogen bonds, and salt linkages of the keratin fibers in order to dissolve them into protein solution. In this study, keratin is extracted on

a lab scale using sodium sulfide as a reducing agent. RSM is used to optimize the keratin extraction process to determine the best parameters to increase the amount of keratin.

2 Response Surface Methodology

RSM is a set of statistical and mathematical approaches used in the chemical field to investigate the impacts of a variety of variables and how their interactions affect the desired response (Kamarudin et al., 2017). Used central composite design (CCD) to build the input parameters in this study because it produces more precise prediction findings than other methods. Figure (1) shows the estimating procedure for this method

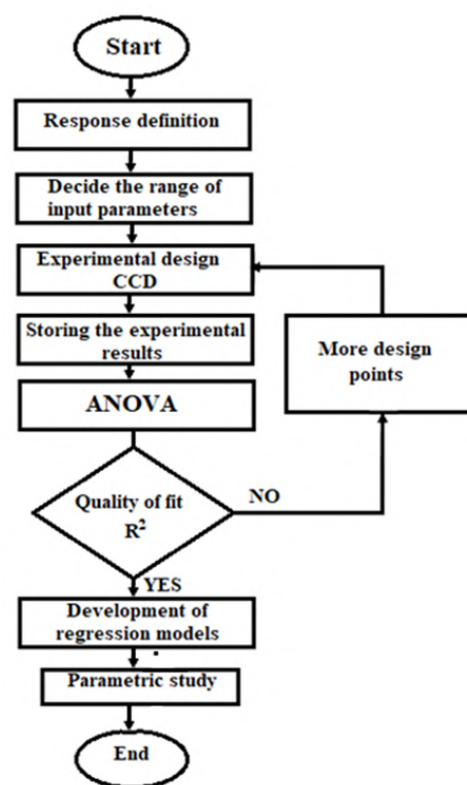


Figure (1). Response Surface Methodology (RSM) Flow Chart.

An ANOVA is used to examine the relationship between the factors and the responses. The significant factor is represented by the "P-value" statistic in the analysis of variance (ANOVA) table of the model and its terms, which should be less than 0.05. The smaller the 'P-value,' the more significant the result (Welu, Beyan, Balakrishnan, & Admassu, 2020).

3 Materials and Methods.

3.1 Chemical Tools and Materials of the Experiment

The utilized glassware is conical flask, beakers 250ml - Filter paper, burette, graduated cylinder, weightier, and heater, while the materials that are used in the extraction are shown in Table (1).

Table (1). The Experiment Materials

Chemicals	Molecular Formula
Sodium sulphide	Na ₂ S
Ammonium sulphate	(NH ₄) ₂ SO ₃
Sodium hydroxide	NaOH
Copper sulphate	CuSO ₄
Potassium hydroxide	KOH

3.2 Feathers before treatment

Feathers from poultry processing are collected and steeped in ether for 24 hours. The major goal is to remove stains, oil, and grease from the feathers before processing them. After that, the feathers are cleaned in soapy water and dried in the sun. After that, the dried feathers are mixed and properly stored in a sealed plastic bag.

3.3 Chicken Feathers Dissolving

According to RSM, the sodium sulfide solutions are changed in a range of 0.5-1M, the temperature range is 30° to 80°C, and the heating and spinning time is changed in a range of 2-6 hours. Sodium sulfide solutions are prepared in molarity in a 1 liter conical flask. Weigh and add 10 g of mixed chicken feathers to the sodium sulfide solution. The solution is heated while the PH is kept at about 10–13, and the solution is swirled continuously. The solution is then filtered and centrifuged for 5 minutes at 10,000 rpm. To remove particles, the supernatant liquid was carefully collected and filtered using filter paper. In 0.5 L of deionized water, 20 g of ammonium sulfate is dissolved. Stir the solution until all of the ammonium sulfate particles have been dissolved. The solution is subsequently filtered to remove any remaining particles.

3.4 Precipitation of proteins

The feather filtrate solution had been collected and mixed in a beaker previously. Ammonium sulfate solution is added drop by drop. Feather filtrate and ammonium sulfate solution are used in a 1:1 ratio. The solid particles are carefully recovered after centrifuging the solution for 5 minutes at 20,000 rpm. The supernatant liquids are collected.

3.5 Protein Purification

100 mL deionized water is added to the recovered solid particles (washing). The solution is centrifuged at 20,000 rpm for 5 minutes, and the solids are carefully collected. The solid particles are then dissolved in a 100 mL sodium hydroxide solution at a concentration of 2 M. All of the liquids are carefully collected and kept after centrifuging the solution at 20,000 rpm for 5 minutes, while the solids are discarded. The precipitating, washing, and dissolving steps are repeated three times each.

3.6 Biuret Test

A copper sulphate solution of 1% and a potassium hydroxide solution of 1% are made. In a 1:1 ratio, 5 mL of the collected solution is combined with potassium hydroxide solution. To the mixed solution, three drops of copper sulphate solution are added. Observed and documented changes in the solution. The absorbance of the solution is measured using UV-Vis.

3.7 RSM Procedure Process

The Design-Expert software version 7.0 was applied to design the experiments based on the Central Composite Design (CCD) and then study the influence of the experimental parameters on the amount of produced protein. (Table 2) shows the selected input parameters and their levels that were used to identify the parameters of the production of the keratin protein. In Table (2) (-1), (0), and (+1) were chosen to indicate the lowest, central, and highest level, respectively. Three experimental parameters were investigated: design parameter A was the Na₂S, design parameter B was temperature, and design parameter C was time. Moreover, the responses in this study were the amount of keratin protein.

Table (2). Independent parameters considered in this study and their levels for central composite design

Parameter	-1	0	+1
Na ₂ S(M)	0.5	0.75	1
Temperature (Co)	30	55	80
Time (hr)	2	4	6

Optimization was applied using the desirability profile and its functions in the RSM. The input parameters with high desirability were chosen as the final experimental parameters for producing keratin protein. The target was to maximize the amount of keratin protein and minimize the experimental time, with the Na₂S, and temperature being set in a certain range for satisfactory results within the upper and lower limits. The solution with high desirability was preferred. Table (3) shows the target value and the upper value for all the parameters.

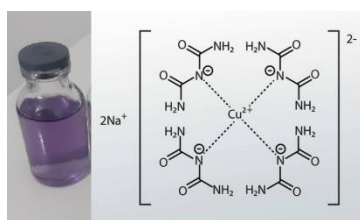
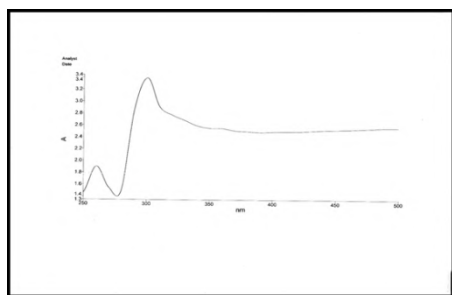
Table (3). Target value and limit for optimization of the Experimental parameter

Experimental parameter	Target	Lower limit	Upper limit
Na2S(M)	In a range	0.5	1
Temperature(Co)	In a range	30	80
Time	Minimize	2	6

4 Results and Discussion

4.1 Observation

In a sodium sulfide solution, chicken feathers totally dissolve. The biuret test confirms the presence of protein. After the reagent is added, the solution turns purple, which is only feasible if peptide bonds are present. The purple color increases as the amount of peptide bonds increases. Keratin had previously been removed, according to the results of a biuret test and a UV-visible spectrophotometer. The biuret test, as shown in Figure (2), showed the existence of protein, and the display of the absorption spectra on the keratin solution revealed a value of λ_{max} at 290 nm, as shown in Figure (3).

**Figure (2).** Biuret Test**Figure (3).** UV visible spectrum of extracted keratin

Absorbance is proportional to a solution's concentration. As the absorbance rises, the protein concentration rises as well. Because the solution is extremely alkaline, with a pH ranging from 10 to 13, the absorbance of feathers in sodium sulfide reactive solution is maximum, and the dissolving rate of feathers in sodium sulfide solution is high. The ionic bond formed by electrostatic attraction between the NH_3^+ group of di amino acids and the COO^- group of dicarboxylic acids can be disrupted in the

alkaline state because the proton is removed from the amino group. These ionic bonds must be disrupted first for some reason in order to diminish the disulfide bonds of the keratin and disintegrate the feathers. The sodium sulfide solution is readily alkaline, but it requires the addition of sodium hydroxide to make it alkaline with a pH of 10 to 13. Protons cannot be removed without an alkaline state, resulting in the ionic link being broken. As a result, sodium hydroxide plays a critical role in the dissolution of feathers.

4.2 Statistical Investigation of Extraction Parameters of Keratin Using RSM

The Na2S, temperature, and time were changed based on the central composite design (CCD). The responses in this study were to the amount of keratin protein. The arrangement of the central composite design, responses, and their values from the experimental results of different parameters. A total number of fifteen experimental were executed and the responses are listed in Table (4).

Table (4). Central composite design arrangement, responses and their values for experimental results of amount of Keratin protein.

Run	Independent factors			Response
	A: Na2S (M)	B: Temperature (C°)	C: Time (hr)	Amount of Keratin Protein
1	1	30	6	3.3
2	0.75	55	4	3.4
3	0.75	55	2	2.9
4	0.50	55	4	3.8
5	0.75	55	6	3.4
6	0.75	55	4	3.4
7	0.75	55	4	3.4
8	1	80	2	2.7
9	0.50	30	2	4.9
10	0.50	80	6	2.4
11	0.75	55	4	3.4
12	1	55	4	3.0
13	0.75	55	4	3.4
14	0.75	30	4	3.9
15	0.75	80	4	2.9

Experimental results reflected that the amount of keratin protein varied between (2.4-4.9) as seen in Table (4). The analysis of variance (ANOVA) can be seen in Table (5) which shows the independent variables, the Na2S, and the time that were significant ($p < 0.05$). Additionally, the interaction impact of the Na2S, and the temperature were significant as the p-value was equal to < 0.0001 , while, the temperature, the interaction impact of the Na2S, and the time, and the interaction impact of the temperature, and the time were insignificant as the p-values were equal to 0.1499, 0.024 and 0.47, respectively.

Table (5). ANOVA table for Amount of Keratin Protein response in surface quadratic model.

Source	Mean Square	F value	P-value Prob > F	Remarks
Model	0.78	59.43	<0.0001	Significant
A-Na2S	0.20	15.31	0.0045	Significant
B-Temperature	0.033	2.54	<0.1499	Not Significant
C-Time	0.22	16.67	0.0035	Significant
AB	0.70	53.48	<0.0001	Significant
AC	0.10	7.69	0.024	Not Significant
BC	0.0075	0.57	0.47	Not Significant

The impact of the independent parameters on the responses was illustrated graphically in terms of 3-D surface plots and can be seen clearly below. These graphs were drawn by fixing one independent parameter while the other two parameters being used to determine the response were left untouched. Figure (4) shows the amount of keratin protein against AB. The graph shows that any decrement in the Na2S would have some negative effects on the response, while temperature would have clear positive effects on the response. However, the decrement of both parameters would have clear negative effects on the response. That means the effect of the interaction of both parameters is very high.

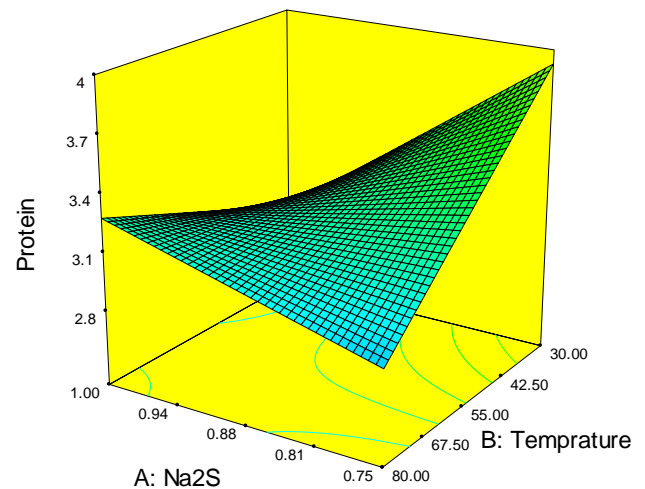


Figure (4). 3 D surface plot for Influence of Na2S and temperature in the amount of keratin protein

Figure (5) shows the amount of keratin protein against AC, and the graph shows that any decrement in the Na2S would have some positive effects on the response, while the increment in the time showed significant positive effects on the response. The decrement of Na2S and the increment of time would have clear positive effects on the response. That means the effect of the interaction of both parameters is low.

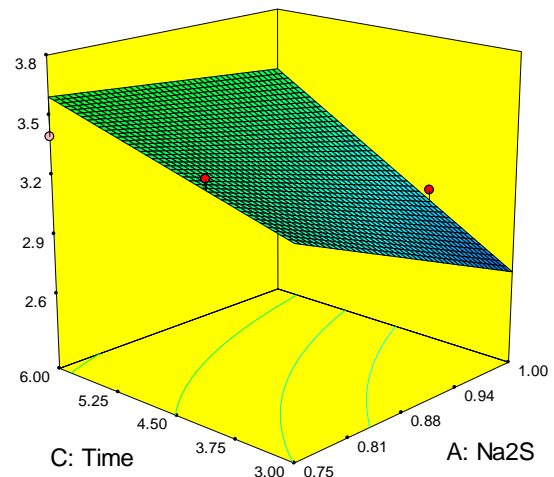


Figure (5). 3 D surface plot for Influence of Na2S and time in the amount of keratin protein

Figure (6) shows the amount of keratin protein against BC, and the graph shows that any decrement in the temperature would have some positive effects on the response, while the increment in the time showed significant positive effects on the response. The decrement of temperature and the increment of time would have clear positive effects on the response. That means the effect of the interaction of both parameters is low.

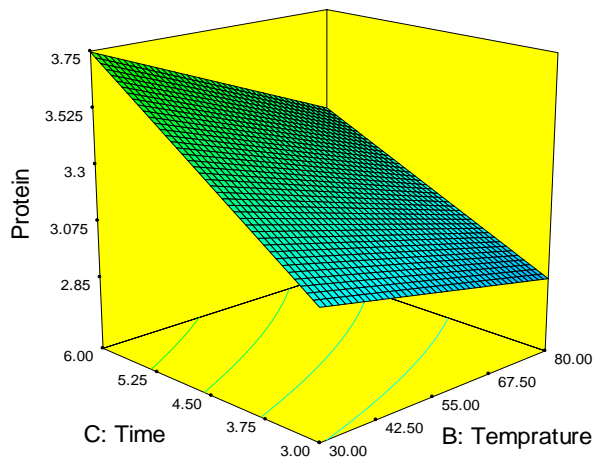


Figure (6). 3 D surface plot for Influence of time and temperature in the amount of keratin protein.

4.3 Optimization of the Experimental parameter

RSM was used in this work to optimize the independent parameters of producing keratin protein. The primary benefit of utilizing the response surface methodology (RSM) is that the amount of protein can be enhanced by regulating the input parameters. The optimization analysis was established by the desirability analysis in Equation (1) (Welu et al., 2020). It was not necessary that the desirability value should be 1.0 as the value was completely dependent on how closely the lower and upper limits were set relative to the actual optimum values.

$$D = (d_1 x d_2 x \dots x d_n)^{1/n} = (\prod_{i=1}^n d_i)^{1/n} \quad (1)$$

Where D was the overall desirability ranging from 0 to 1 and n was the number of responses. The extracted keratin protein with parameters that had the highest desirability was chosen as a ideal experimental that has high amount of protein. The optimum condition for all case studies were achieved when the amount of protein was maximized with the highest desirability value of 1. From Figure 7, it can be clearly seen that RSM calculated the amount of protein was at maximum when the parameters of the experimental were as follows: NS2A was 0.5 M, the temperature was 30 C°, and the time was 3.7 hr.

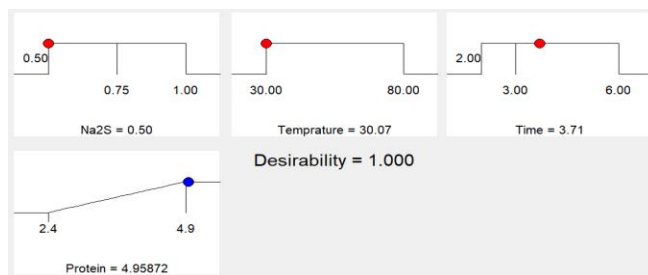


Figure (7). Ramp function graph of desirability for optimization solution for Amount of Keratin Protein

The bar graph and ramp function graph of Figure 7 show the desirability values for output responses. The dot on each ramp reflected the factor setting or response prediction for that particular response characteristic. The height of the dot shows how much desirable it was compared to the baseline. A linear ramp function was created between the low value and the goal or the high value and the goal, as the weight for each parameter was set equal to one.

5 Conclusions

The aim of this research was to locate a different source of keratin protein. Chicken feathers are a hazard for the environment since they contain crude protein and take a long time to decompose. The chicken feathers were first dissolved with reducing agents, and then protein was precipitated out of the solution with ammonium sulfate in this experiment. The presence of the protein was initially validated by the biuret test, in which the reagent turned purple in the presence of peptide bonds, while the absence of keratin protein was proven by the value of max. Finally, statistical adjustment of the extraction conditions resulted in a better understanding of the reaction parameters as well as a high keratin yield. The extraction process of keratin can be scaled up from the laboratory to the industrial level.

Acknowledgements

The authors are grateful to Omar Al-Mukhtar University especially, the Department of Chemistry.

Conflict of Interest: The authors declare that there are no conflicts of interests.

References

- Barone, J. R., Schmidt, W. F., & Gregoire, N. (2006). Extrusion of feather keratin. *Journal of applied polymer science*, 100(2), 1432-1442.
- Fakhfakh-Zouari, N., Haddar, A., Hmidet, N., Frikha, F., & Nasri, M. (2010). Application of statistical experimental design for optimization of keratinases production by *Bacillus pumilus* A1 grown on chicken feather and some biochemical properties. *Process Biochemistry*, 45(5), 617-626.
- Gessesse, A., Hatti-Kaul, R., Gashe, B. A., & Mattiasson, B. (2003). Novel alkaline proteases from alkaliphilic bacteria grown on chicken feather. *Enzyme and Microbial Technology*, 32(5), 519-524.
- Grazziotin, A., Pimentel, F., De Jong, E., & Brandelli, A. (2006). Nutritional improvement of feather protein by treatment with microbial keratinase. *Animal feed science and technology*, 126(1-2), 135-144.
- Kamarudin, N. B., Sharma, S., Gupta, A., Kee, C. G., Chik, S. M. S. B. T., & Gupta, R. (2017). Statistical investigation of extraction parameters of keratin from chicken feather using Design-Expert. *3 Biotech*, 7(2), 1-9.
- Leichner, C., Steinbring, C., Baus, R. A., Baecker, D., Gust, R., & Bernkop-Schnürch, A. (2019). Reactive keratin

- derivatives: A promising strategy for covalent binding to hair. *Journal of colloid and interface science*, 534, 533-541.
- Ng, C. S., Wu, P., Foley, J., Foley, A., McDonald, M.-L., Juan, W.-T., . . . Chen, C.-F. (2012). The chicken frizzle feather is due to an α -keratin (KRT75) mutation that causes a defective rachis. *PLoS genetics*, 8(7), e1002748.
- Saucedo-Rivalcoba, V., Martínez-Hernández, A., Martínez-Barrera, G., Velasco-Santos, C., & Castaño, V. (2011). (Chicken feathers keratin)/polyurethane membranes. *Applied Physics A*, 104(1), 219-228.
- Schrooyen, P. M., Dijkstra, P. J., Oberthür, R. C., Bantjes, A., & Feijen, J. (2001). Stabilization of solutions of feather keratins by sodium dodecyl sulfate. *Journal of colloid and interface science*, 240(1), 30-39.
- Sharma, S., & Gupta, A. (2016). Sustainable management of keratin waste biomass: applications and future perspectives. *Brazilian Archives of Biology and Technology*, 59.
- Welu, K. T., Beyan, S. M., Balakrishnan, S., & Admassu, H. (2020). Chicken feathers based Keratin extraction process data analysis using response surface-box-Behnken design method and characterization of keratin product. *Current Applied Science and Technology*, 163-177.
- Yamauchi, A., & Yamauchi, K. (2002). Formation and properties of wool keratin films and coatings. *Protein-based films and coatings*, 253-274.



Anticancer Screening of Quercetin as a Natural Treatment

Wedad A. A. Ahmed

Chemistry Department, Science Faculty, Sabratha University, Sorman, Libya.

DOI: <https://doi.org/10.37375/sjfsu.v2i2.439>

A B S T R A C T

ARTICLE INFO:

Received 14 June 2022.

Accepted 21 September 2022.

Published 27 October 2022.

Keywords:

Oxidation stress, Anticancer, Quercetin, Apoptosis, Antioxidant

Oxidation stress is a process that damages the cells of the body, and also leads to the happen of many diseases such as cancer. This disease is known among all ages in every part of the world. In cancer cells, increasing types of free radicals flaw the balance in the cell and thus increasing free radicals target all types of molecules, including proteins, lipids, and nucleic acids. If the body cannot produce enough antioxidants, increasing free radicals damage the cells of the body. The defect in apoptosis also prevents malignant cells from being damaged. This paper aims to study the effect and activity of quercetin as an antioxidant and anticancer drug in vitro. The mechanism of increasing free radical formation causing cell damage will be explained. This study also presents a discussion about the mechanism of apoptosis pathways using the MTT scale to measure the cell's ability to metabolic activity and whether the cells are still alive. The most significant shifts were for (Raji, MOLT-4 and CT-26 equal to 0.18 ± 0.09 , 2.1 ± 0.9 , and 5.5 ± 0.38 , respectively). Apoptosis was detected using the BD Annexin V FITC assay and apoptosis was measured at ($P < 0.001$). Also, in vivo, the positive effects of different doses of quercetin on affected models are discussed.

1 Introduction

Under normal circumstances, a person's life continues with health problems. Wrong practices such as smoking and environmental pollutants lead to the production of harmful things in the body called free radicals (Phaniendra et al., 2015). When these unstable free radicals attack the body, the body produces antioxidants to protect it. If the body cannot produce enough antioxidants (Shi et al., 2019), free radicals damage the cells of the body.

Atoms are stable by filling orbitals with electrons. When the orbital is filled with electrons, the additional number of electrons shift to the next path. If the electrons ends, and at the same time the outer orbit of the atom is not filled with the required number of electrons, then this atom is attached to another atom to complete the outer orbit of the atom's electrons. In this case, the atom with an incomplete outer shell is known as free radical (Phaniendra et al., 2015).

Free radicals are unstable atoms react quickly with other materials (Phaniendra et al., 2015), (Widowati et al., 2013) For example, when oxygen molecules split into single atoms that do not have double electrons, they become unstable free radicals intended to bind to other molecules (Tavsana and Kayalia, 2019), (Prieto-Bermejo and Hernández-Hernández, 2017). If these steps continue to occur, the process can be called oxidation stress (Pham-Huy et al., 2008). The process of oxidation stress damages the cells of the body, and also leads to many diseases, such as cancer. Free radicals target all types of molecules, including proteins, fats, and nucleic acids. When a person gets older, the body loses its ability to fight the effects of free radicals (Phaniendra et al., 2015), (Pham-Huy et al., 2008). This leads the body to more free radicals and more oxidation stress (Widowati et al., 2013), (Pham-Huy et al., 2008). The danger of "oxidation stress" is that free oxygen atoms reach the genetic material in DNA cells, affecting their structure

and causing a mutation in the cell, which turns into diseased cells or malignant cancer cells (Phaniendra et al., 2015), (Prieto-Bermejo and Hernández-Hernández, 2017).

Free radicals which call reactive spices are produced in the human body and are an internal source for the metabolism process (Tavsana and Kayalia, 2019), but there are many lifestyle factors that can accelerate the production of these free radicals, such as exposure to toxic chemicals, drugs, and pollutants. These factors are called external sources. These free radicals caused by accelerating agents are called hyperreactive spices (Prieto-Bermejo and Hernández-Hernández, 2017). The oxidation (pro- oxidation) reaction occurs when free radicals interact with any molecule that collides with them (Pham-Huy et al., 2008). This process disables free radicals, but turns the other molecule into new free radicals. This is how a free radical chain reaction starts, damaging all of the molecules it interacts with. When the molecules are damaged, cells stop working and die (Pham-Huy et al., 2008).

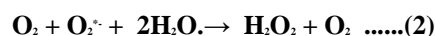
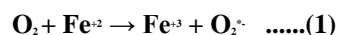
In cancer cells, oxidation stress occurs with the increase in oxidation processes (Phaniendra et al., 2015), (Pham-Huy et al., 2008). Normal, uninfected cells contain reactive types of oxygen that modulate cell function. Whereas in cancer cells, these types are increasing, and they facilitate imbalances in the cell (Pham-Huy et al., 2008).

The free radical oxidation process can be controlled by antioxidants (Shi et al., 2019), (Pham-Huy et al., 2008). Antioxidants are chemicals that work against free radicals. It also prevents free radical oxidation, and donates electrons to free radicals to become stable (Shi et al., 2019), (Pham-Huy et al., 2008). The benefit that makes antioxidants unique is to donate an electron without becoming free radicals. Different types of food act as antioxidants, and the body also produces some antioxidants, such as vitamins (Shi et al., 2019), (Pham-Huy et al., 2008).

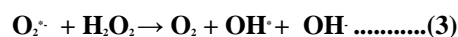
The main antioxidants found inside the cells of the body are enzymes, the non-enzymatic component called glutathione and various types of oxidase (Shi et al., 2019). These antioxidants eliminate reactive oxygen species (ROS). For example, (ROS) are eliminated by "superoxide dismutases (SOD) (Tavsana and Kayalia, 2019), (Prieto-Bermejo and Hernández-Hernández, 2017), glutathione peroxidase (GPx), (Phaniendra et al., 2015) peroxiredoxins (PRDXs), glutaredoxins, thioredoxins (TRXs), and catalases." Also, these enzymes and catalases are found within mitochondria. For example, enzymes convert the free-radical O_2^- anion into hydrogen peroxide and then discard it (Phaniendra et

al., 2015), (Prieto-Bermejo and Hernández-Hernández, 2017), (Pham-Huy et al., 2008).

Cells contain a number of components which are mitochondria, endoplasmic reticulum and peroxisomes. Each of these three components does its job. Within all these organs there are different types of enzymes that have oxidation activation (Pham-Huy et al., 2008). These enzymes react with oxygen molecules to produce radicals. In the body of an organism, during the process of metabolism, a number of reactive free radicals are produced using various reactions (Tavsana and Kayalia, 2019), such as the endogenous oxidation reaction and non-enzymatic reactions. These free radicals have one non-double electron, such as O_2^- , RO^\cdot , ROO^\cdot , OH^\cdot and ... etc. All of them are highly efficient, and their half-life is 10^{-6} s, 10^{-6} s, 10^{-7} s, 10^{-10} s respectively (Phaniendra et al., 2015). For example, in mitochondria, the radical of anions O_2^- and H_2O_2 can be formed by oxides enzymes under physiological conditions (Phaniendra et al., 2015), (Prieto-Bermejo and Hernández-Hernández, 2017).



Cells are more susceptible to damage due to the formation of new hydroxyl radicals resulting from the reaction of anions O_2^- and H_2O_2 as equivalent. (3) (Phaniendra et al., 2015).



While H_2O_2 damaged by "catalase, glutathione peroxidase and peroxiredoxins enzymes", glyceraldehyde-3-phosphate enzyme cannot function as intended, so it stops when H_2O_2 is in high concentrations (Phaniendra et al., 2015). This is because it produces OH^\cdot which damages DNA action. 8-Hydroxydeoxyguanosine is the product of many chemical reactions that take place between the hydroxyl radical and the components of DNA (Phaniendra et al., 2015). Due to the number of changes that occur in the immune system, 8-hydroxydeoxyguanosine is responsible for a number of abnormalities that cause cancer. High levels of 8-hydroxydeoxyguanosine is produced within mitochondrial DNA (Prieto-Bermejo and Hernández-Hernández, 2017), because increasing types of free radicals are produced inside mitochondria whereas in nucleic DNA, the levels are low (Phaniendra et al., 2015), (Shi et al., 2019), (Pham-Huy et al., 2008).

RNA is produced in the nucleus and secreted into the cytoplasm to stay there. As the RNA is demolished and then rebuilt, the DNA will be stable (Prieto-Bermejo and Hernández-Hernández, 2017). There is a great deal of

damage to RNA in the cytoplasm due to oxidation stress that results in increasing free radicals. Damage from oxidation stress to RNA is more than that from DNA. (Phaniendra et al., 2015), (Prieto-Bermejo and Hernández-Hernández, 2017). This damage is due to the fact that the RNA is close to the mitochondria, which is the right place for generating excess types of oxygen (Phaniendra et al., 2015).

The human body is prepared to deal with cancer cells (Nicholson, 2016). To create new cells, these cells are in a continuous state of reincarnation (Nicholson, 2016). Every second, more than ten million new cells are created by transcription, replacing others that have permanently terminated their activity. Hence, the cells have a mutation during transcription. Besides, cells are constantly exposed to substances that destroy and damage DNA. DNA is the main component of the cell's genetic map and is responsible for transcription (Prieto-Bermejo and Hernández-Hernández, 2017). This problem and damage is caused by unstable free radicals during the metabolism process. Cancer develops when there is an imbalance between antioxidants and oxidants. Major damage to the immune system, proteins and fats is caused by the accumulation of free radicals that are caused by metabolism (Pham-Huy et al., 2008).

The immune system damages the abnormal cells right before the cells can multiply (Pham-Huy et al., 2008), (Nicholson, 2016). It contains white cells that damage these abnormal cells before they take any chance to reproduce. Responsibility does not depend on the immune system alone, but there is a special program within each cell that identifies any abnormality or mutation that occurs during reproduction (Pham-Huy et al., 2008), (Nicholson, 2016). Most of the time, the protective mechanisms within the body are able to prevent the happen of cancer (Pham-Huy et al., 2008). However, the immune system sometimes loses its ability to recognize and damage cancer cells, and these cells begin to multiply uncontrollably. On the other hand, when there is a large number of abnormal cells, the immune system cannot do its job (Nicholson, 2016).

1.1 Mechanism of reaction to form (ROS): (Phaniendra et al., 2015) (Tavsana and Kayalia, 2019), (Prieto-Bermejo and Hernández-Hernández, 2017).

There are a number of pathways used to transfer electrons within mitochondria. Complex I and Complex II or III are the main paths (Phaniendra et al., 2015). As a result of this transfer of electrons shown in Figure (1), the rate of free radical production increases with the increase in the rate of metabolic processes, as some of these radicals turn into hydrogen peroxide which has high toxicity due to the activation of mitochondrial superoxide dismutase (Phaniendra et al., 2015). In the absence of

catalase or glutathione, hydrogen peroxide remains in the cells and causes damage to the tissues of the organism (Phaniendra et al., 2015).

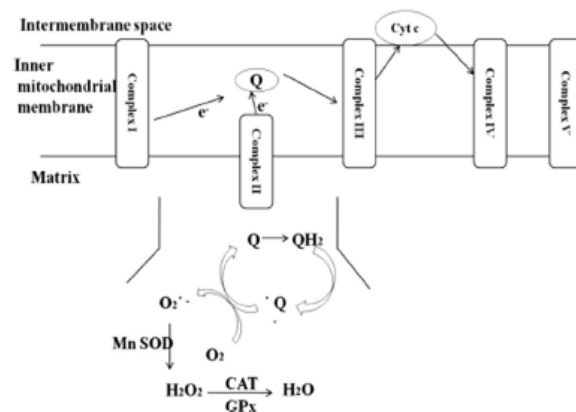


Figure (1): Production of (ROS) and their toxicity inside of mitochondria.

One of the main and natural things that happen in the tissues of the human body is that the cells of the body are in a state of constant renewal (Abcam, 2016). By dividing cells, new cells are formed. For example, skin cells are damaged over time and replaced with new cells. Also, the fragmented small particles are eliminated by neighboring cells. This ordered process is called apoptosis (Phaniendra et al., 2015), (Abcam, 2016), (Xiong, 2014), (<https://www.cancerquest.org/cancer-biology/apoptosis>, 2020). There are three important pathways that occur to initiate the apoptotic process of cell death, the death receptor pathway, the mitochondrial pathway, and the "Perforin / Granzyme" pathway. In the first pathway, death signals are sent inside the cell by a series of proteins. These proteins perform a number of tasks, the most important of which is caspase activation (Phaniendra et al., 2015), (Xiong, 2014), (<https://www.cancerquest.org/cancer-biology/apoptosis>, 2020).

In the second pathway: the proteins of the Bcl-2 family have various functions such as stimulating apoptosis and at the same time acting as an anti-apoptotic, and the proteins of the Bcl-2 family can tell which signal before apoptosis occurs (Xiong, 2014). For example, BH3 proteins are part of the most important proteins in the Bcl-2 family, and have a unique function that activates the "Bax or Bak" proteins. The "Bax or Bak" proteins are called pro-apoptotic proteins (<https://www.cancerquest.org/cancer-biology/apoptosis>, 2020). Also, BH3 proteins prevent "Bax or Bak" proteins from being anti-apoptotic proteins. As a result of the permeability of the outer mitochondrial membrane (Xiong, 2014), an apoptotic factor called Cytochrome c is excreted from the mitochondrial membrane into the cytosol. A number of compounds are produced, such as

"apoptosome" and "Apaf-1", which activate a series of caspases. These caspases are enzymes that damage required cells as shown below (Xiong, 2014).

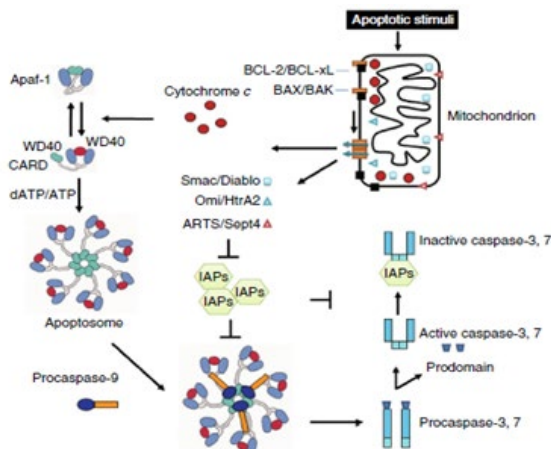


Figure (2). Activation of caspases by mitochondria pathway (Xiong, 2014).

In the last pathway: the purpurin protein is produced by lymphocytes. This protein can open small pores in the plasma membrane (Xiong, 2014). Lymphocytes also work to produce small molecules that can enable these particles to enter these pores and secrete a number of enzymes, such as Granzyme that complete the implementation process and activate chains of caspases (<https://www.cancerquest.org/cancer-biology/apoptosis>, 2020). The implementation stage is one of the last stages that cannot be stopped upon implementation. When the orders are damaged, the cells are damaged by a number of Caspases. Caspases damage desired cells. The surrounding cells are swallowed, digested, and permanently disposed of (Xiong, 2014).

Cells can decline and die in multiple ways. Most cells in vertebrates die by the mitochondrial pathway. The mitochondrial pathway begins with a wide range of signals such as DNA damage, growth factor deprivation, and more (<https://www.cancerquest.org/cancer-biology/apoptosis>, 2020). The changes that transform a normal cell into a malignant cell. It is simple. When cancer cells proliferate, cell death (apoptosis) decreases (<https://www.cancerquest.org/cancer-biology/apoptosis>, 2020). In fact, cancer cells inhibit the apoptotic response, as it is the defect in apoptosis that prevents malignant cells from being killed. Induction of apoptosis by inhibition of cell proliferation was determined by Widowati et al.. The defect in apoptosis can be treated with quercetin using the caspase-3 activation mechanism and regulation of a number of enzyme pathways (Xiong, 2014).

1.2 Quercetin

A healthy diet rich in antioxidants plays an important role in fighting free radical damage (Ramalalingam et al., 2015), (Niu et al., 2011), (Mukherjee et al., 2019). Polyphenolics have been isolated from many types of natural foods such as vegetables, fruits, nuts, peels, roots, etc. These compounds are called flavonoids. They have biological activities (Ramalalingam et al., 2015), (Niu et al., 2011). For example, quercetin as shown below in Figure 3 is one of the most abundant antioxidants in the human diet and can be a drug that prevents and treats different types of cancers (Niu et al., 2011), (Mukherjee et al., 2019). It is part of the flavonoids that can use a unique mechanism. Quercetin is metabolized within the gastrointestinal tract, and can be absorbed into the membrane of the small intestine without using the hydrolysis process (Mukherjee et al., 2019). Therefore, the focus of a number of previous studies was on extracting many natural substances that act as antioxidants and anti-cancers. For example, the results of the current studies conducted by Ramalalingam et al. were for the extraction of chloroform from the leaves of *Aristolochia indica* L, and quercetin was also extracted for its antioxidant and anti-cancer properties by Guomin et al. and Mukherjee et al.

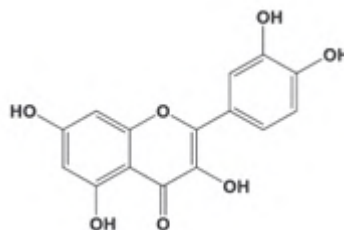


Figure (3). Chemical structure of Quercetin (Mukherjee et al., 2019).

Quercetin has a total antioxidant capacity, TAC, which inhibits the activity of excessive oxygen species caused by the presence of diethylnitrosamine, which is one of the components of cigarette smoke that causes hepatocellular carcinoma. Apoptosis has several pathways that quercetin can activate such as the pathway in MDA-MB-231 cells through the diffusion of the calcium signal to mitochondria. Also the activation of many caspases, the activation of the intrinsic pathway in HepG2 cells, thus "quercetin promotes translocation of Bax from cytosol into mitochondria membrane leading to depolarization of mitochondrial membrane" and the resulting response to the control of some signals as shown in Figure 4. The rest of the other mechanics are available in the study of Rather and Bhagat, 2020.

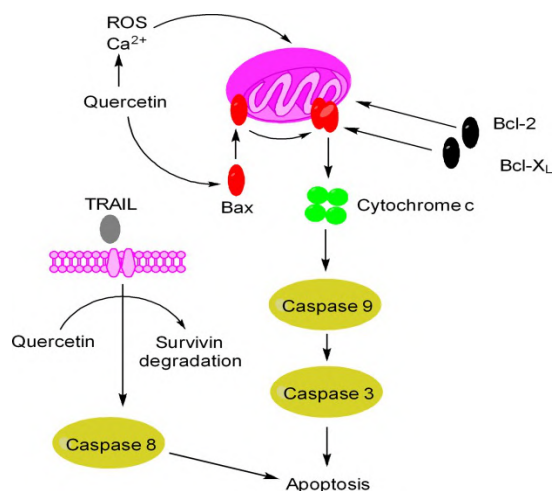


Figure (4): Mechanism of Quercetin as therapeutic medicine (Rather and Bhagat, 2020)

2. Methods

2.1 MTT Assay:

It is a test to measure cell viability and metabolic activity. In the cytosol inside the cell, this assay depends on the use of dimethylsulfoxide (DMSO) as a polar aprotic solvent, and also depends on the nicotinamide adenine dinucleotide phosphate (NADPH) that is "a required cofactor, used to donate electrons and a hydrogens to reactions catalyzed by some enzymes". (Ali-Boucetta et al., 2021), (Hingorani et al., 2011), (Hashemzael et al., 2017). Cells must be alive to convert MTT, which is a yellow (3-[4,5-dimethylthiazol-2-yl]-2,5 diphenyl tetrazolium bromide) to insoluble purple formazan. DMSO solvent dissolves purple formazan (not dissolved in water) and convert them into a colored solution. Also, the MTT scale is used to check cell sensitivity by toxic drug effects on cell lines (Hingorani et al., 2011). Because of the light sensitivity, this test is performed in the dark. The absorbance of the colored solution is determined using a spectrophotometer (between 500 and 600 nm), (Hingorani et al., 2011). The degree of light absorption depends on the accumulation of formazan inside the cell and on the surface. When the concentration of Formazan increases, the violet color increases and the absorbance becomes less. This indicates the survival of the cell (Hingorani et al., 2011), (Jiao et al., 2015).

2.2 Measure cell viability Method (Ali-Boucetta et al., 2021), (Hashemzael et al., 2017), (Jiao et al., 2015):

1. Use a dilution chain (10, 20, 40, 80 and 120 μ M)) of quercetin to test (MTT) and prepare the MTT solution.

2. All 9 cancer cell lines (shown in table 1) are classified and treated with a set of concentrations in triplicate in 96 plates and incubated overnight.

3. Dilute the MTT and add the chain (10, 20, 40, 80 and 120 μ M) of quercetin

4. Cells were coated in 96 well plates at 37°C for 72 hours.

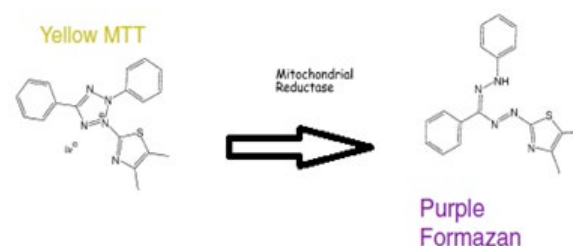
5. After incubation, the wells were suctioned and the dye dissolved in DMSO

6. Absorption was measured at 570 nm.

7. Compared to untreated control cells.

8. The percentage of cell survival is calculated using this formula:

$$\% \text{ Cell viability} = \frac{A_{570\text{nm}} \text{ of treated cells}}{A_{570\text{nm}} \text{ of untreated cells}} \times 100.$$



2.3 The BD Annexin V FITC Assay: (Hingorani et al., 2011),¹⁹

In the healthy cell, membrane phosphatidylserine (PS) is located on the inner plasma membrane, but when the phosphatidylserine (PS) is transported from the inner side of the plasma membrane to the surface, the plasma membrane is completely lost, and it becomes an invalid cell. Because of the electronic affliction, "Annexin V, a Ca²⁺-dependent phospholipid-binding protein" can bind to the cellular phosphatide membrane on the outer surface of the cell's plasma membrane. The BD Annexin V FITC Assay on the BD FACSVersTM System used to detect the location of membrane phosphatidylserine (PS), which caused apoptosis.

2.4 Measuring apoptosis by tracking cells (Abcam, 2016), (Hingorani et al., 2011), (Jin et al., 2019).

There are two processes that work to determine the difference between cells that have had early death and those that have a late death are shown in figure 5-a .

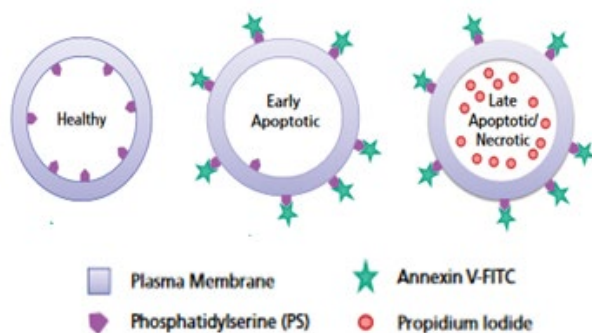


Figure (5-a): Diagram shows The healthy and apoptotic cells. (Abcam, 2016), (Hingorani et al., 2011).

The process of staining with Annexin V is called early apoptosis and the process of using propidium (PI) is termed late apoptosis. Consider the following:

1- Viable cells with healthy membranes cannot be stained with the use of Annexin V or penetrate the propidium dye (PI) so that the expression used for the description will be negative-negative (Foo et al., 2019), while in late apoptosis the membranes of dead cells penetrate the PI and the expression Annexin V and PI is positive – positive (Hingorani et al., 2011).

2- In early apoptosis with intact membranes will be Annexin V and PI positive - negative While the death stage apoptosis the expression used for description is Annexin V and PI positive as shown below in Figure 5-b (Hingorani et al., 2011).

2.5 Detection of Cell Apoptosis Method (Hingorani et al., 2011):

1- The affected cells were implanted into 12-well plates (2 x 10⁵ cells / well).

2- The cells were incubated (at 5% CO₂ and 95% air) at 37 ° C.

3- DMSO was used to dissolve quercetin in the following concentrations (10, 20, 40, 80 and 120 μM)

4- After the cells were incubated for 48 hours in the dark, the cells were analyzed.

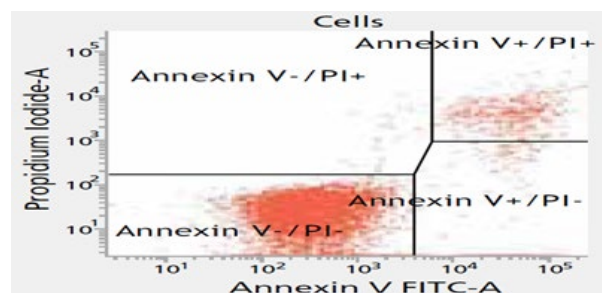


Fig (5-b). Using the BD Annexin V FITC assay on the BD FACVerse™ System to detect apoptosis (Hingorani et al., 2011), (Foo et al., 2019).

3. Results

The MTT assay was performed to assess the viability of all nine tumor cell lines illustrated in table 1 applied for 24, 48 and 72 h. Using three doses of quercetin (10, 40 and 120 μM) for the treatment purpose illustrated in Table 2 (Hashemzael et al., 2017). At the time of 24 h, there was no inhibition at a concentration of 120 μL for both PC3 and CHO cells, respectively, and at the same time, the inhibition of all other cells was apparent in Table 2. This means that the most significant shifts will be for (Raji, MOLT-4 and CT-26 equal to 0.18 ± 0.09 , 2.1 ± 0.9 , and 5.5 ± 0.38 , respectively, while the least significant shifts are observed for PC3 and LNCaP equal to 31.5 ± 3.7 and 30.7 ± 2 , respectively.

Table (1). Symbols used for cancer cell lines

Name of cancer cell lines	Symbols of lines
Colon carcinoma cells	CT-26
Prostate adenocarcinoma cells	LNCaP
Human prostate cells	PC3
Pheochromocytoma	PC12
Michigan Cancer Foundation-7, estrogen receptor positive breast cancer cells	MCF-7
Acute lymphoblastic leukemia cells	MOLT-4
Human myeloma cells	U266B1
Human lymphoid cells	Raji
Ovarian cancer cells	CHO

The use of 120 μM of quercetin had an effect on the rate of apoptosis of CT-26, LNCaP, MOLT-4 and Raji cell lines, and therefore the apoptosis of these lines was significant compared to the control group ($P < 0.001$).

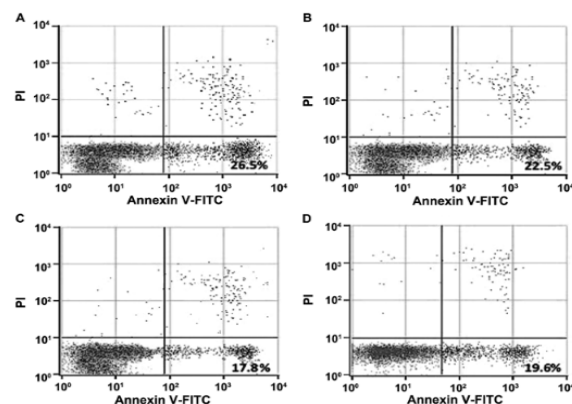


Figure (6). Apoptotic rate determined by Annexin V/PI staining in (A) CT-26, (B) LNCaP, (C) MOLT-4 and (D) Raji cell lines following 48 h of treatment with quercetin at 120 μM. Early apoptotic cells are Annexin V-positive and PI-negative (lower right quadrant). PI, propidium iodide (Hashemzael et al., 2017).

Figure 6 and 7 examine the rate of apoptosis in 4 cell lines “CT-26, LNCaP, MOLT-4 and Raji, respectively” that have high and low sensitivity to quercetin. In these cells, quercetin initiated the apoptosis process in a dose-dependent manner. The results of the MTT assay were in agreement with the Annexin V/PI assay, as the cell lines showed extreme sensitivity to quercetin at high concentrations that led to apoptosis at ($P < 0.001$) (Hashemzael et al., 2017).

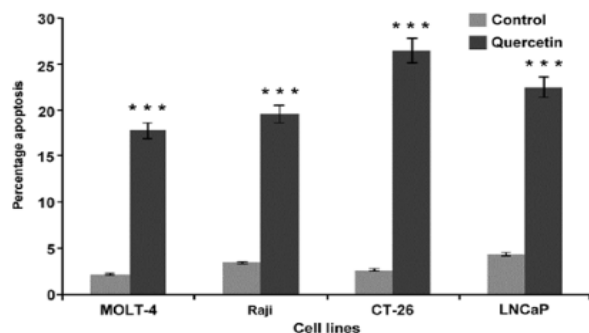


Figure (7). Induction of apoptosis in LNCaP, CT-26, MOLT-4 and Raji cell lines treated with quercetin, (Hashemzael et al., 2017).

While the effect of quercetin doses (10, 20, 40, 80 and 120 μ M) was great on cell lines in vitro, these doses of quercetin did not affect the in vivo. Therefore, different concentrations of quercetin (50, 100 and 200 mg/kg) were used on Mice bearing CT-26 and MCF-7 tumors. The treatment was completed and the tumor size decreased on days 18 and 20 as shown in Figure 8.

Table (2). Comparison of Hashemzael et al. data obtained from the MTT assay by using doses of quercetin applied to different cancer cell lines for 24, 48 and 72 hour.

Cell line	24h			48h			72h		
	10 μ M	40 μ M	120 μ M	10 μ M	40 μ M	120 μ M	10 μ M	40 μ M	120 μ M
CT-26	94.2 \pm 4.4	75.1 \pm 4.2	49.7 \pm 5.9	87.4 \pm 5.4	70.3 \pm 4.1	42.1 \pm 3	65.5 \pm 1.5	35.9 \pm 0.83	25 \pm 2.3
LNCaP	96.8 \pm 5.4	71.7 \pm 2.2	45.1 \pm 5.0	91.5 \pm 6.3	66.6 \pm 5.7	38.5 \pm 3.8	58.4 \pm 2.9	39 \pm 1.9	30.7 \pm 2
PC3	96.4 \pm 5.0	80.1 \pm 4.6	73.2 \pm 4.1	89.9 \pm 3.6	70.7 \pm 2.8	28.5 \pm 3.4	61.7 \pm 2.1	46.9 \pm 1.4	31.5 \pm 3.7
PC12	91.1 \pm 6.5	68.5 \pm 6.8	40.3 \pm 4.4	94.4 \pm 5	62.5 \pm 4.6	30.7 \pm 3.8	50.4 \pm 3.6	40.8 \pm 1.8	22.1 \pm 1.1
MCF-7	94.8 \pm 6.1	77.5 \pm 5.1	47.1 \pm 4.2	81.3 \pm 4.1	55.5 \pm 3.4	25.2 \pm 2.1	51.6 \pm 3.2	35.7 \pm 2.5	19.1 \pm 1.4
MOLT-4	88.6 \pm 3.6	57.5 \pm 4.0	42.8 \pm 3	70.6 \pm 2.8	43.1 \pm 1.9	21.6 \pm 1.4	11.5 \pm 0.5	10 \pm 0.37	2.1 \pm 0.9
U266B1	95.1 \pm 4.9	53.8 \pm 4.6	33.8 \pm 4.7	68.5 \pm 2.3	37.2 \pm 2	20.4 \pm 2.1	15.9 \pm 0.8	4.8 \pm 0.72	5.5 \pm 0.38
Raji	85.6 \pm 4.1	68.1 \pm 2.8	29.4 \pm 4.6	60.6 \pm 3.6	30.3 \pm 2.4	14.6 \pm 3.3	5.5 \pm 0.4	1.3 \pm 0.25	0.18 \pm 0.09
CHO	97.7 \pm 5.2	74.4 \pm 4.1	70.5 \pm 5.2	97.4 \pm 4.4	64.6 \pm 2.8	21.9 \pm 3.5	57.8 \pm 3.9	39.2 \pm 2.7	20.7 \pm 3.7

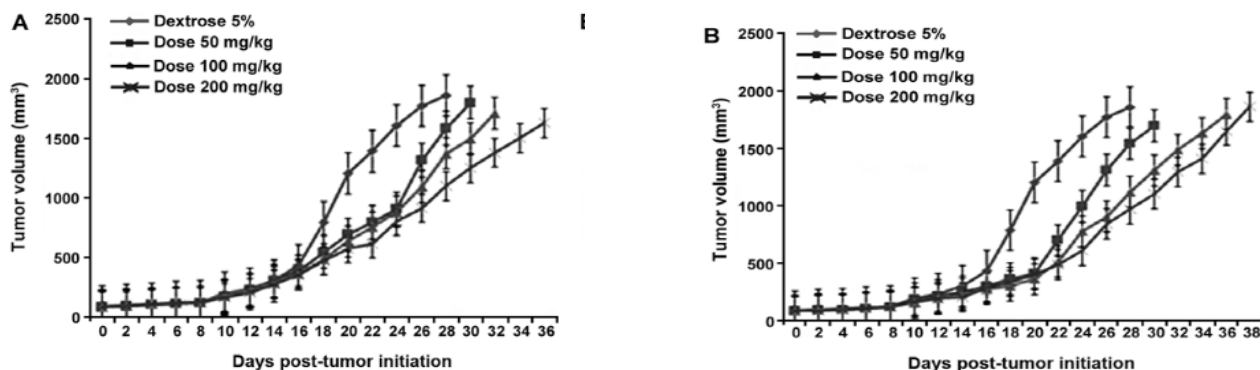


Figure (8). The relationship between tumor volume and days after tumor initiation. Whereas (A) CT26 and (B) MCF 7 cell lines were treated with (50, 100 and 200 mg/kg) doses of quercetin for several days (Hashemzael et al., 2017).

Discussions

The effect and activity of quercetin have been studied as an anti-cancer drug (Niu et al., 2011), (Mukherjee et al., 2019). In the vitro, different concentrations of quercetin were applied to different cancer cells. After hours of taking the quercetin doses, the inhibition effect of some cancer cell lines was very high, as shown by the IC50 values calculated in Table (2). The IC50 scale was used to describe the relationship between a series of drug dose concentrations and the response to the effectiveness of these concentrations in inhibiting 50% of the activity of cancer cell lines (it means inhibiting half of the total response to get 50% of the effect), and it was found that quercetin inhibited the activity of cancer cell lines. (Hashemzael et al., 2017)

In Figure 6, the study also showed apoptosis of the following: CT 26, LNCaP, MOLT 4 and Raji cell types by used flow cytometry Annexin V/PI and compared with control group (Hashemzael et al., 2017). Also, in the vivo, models of mice with positive breast cancer of estrogen receptor "MCF 7" and CT 26 were treated with different doses of the quercetin at concentrations of about (50, 100, and 200 mg / kg) for several days. The results from using quercetin showed in Figure (8) that the tumor size for each of these mice became small after receiving the required doses. (Hashemzael et al., 2017)

Both in vivo and in vitro, quercetin was also successful in suppressing the growth of human LM3 hepatocellular carcinoma by collecting the LM3 cell line treated with different doses of quercetin at different time intervals resulting in apoptosis at $P < 0.05$. (Wu et al. 2019). Treatment with 160 μM quercetin for 24 h suppressed the viability of oral squamous cell carcinoma "OSCC" cells by inducing cell cycle arrest on "OSCC" cell lines using MTT assay, flow cytometry and blot analysis ($p < 0.01$), "whereas treatment with low concentrations 10–40 μM) reduced cell viability slightly" ($p < 0.05$) compared to the control. (Kim et al, 2020)

Conclusions

Most of the chemical treatments for cancer have annoying side effects, so nature has been taken care of in terms of eating vegetables, fruits and seeds because of their benefits on the human body. The balance of food in your diet is important when you are trying to eat healthy food. Eating these healthy things would enhance the body's immunity and provide it with the necessary antioxidants, which target the elimination of increasing free radicals. In order to provide the best ways to treat cancer and help cancer patients, a review was discussed about the causes of cancer and quercetin extract and its applications in vitro and in vivo rather than many methods used in treatment such as chemotherapy. In

vitro, the inhibition effect of all cancer cell lines was very high, as the study showed apoptosis by using Annexin V/PI flow cytometer and comparing it with the control group. The results of using quercetin showed that the tumor size for each of these live models was small after receiving the required doses.

Acknowledgements

The author would like to acknowledge those who always encourage and give their guidance, mom and dad.

References

- Phaniendra, A., Jestadi, D. B., & Periyasamy, L. **2015**. Free radicals: properties, sources, targets, and their implication in various diseases. *Indian journal of clinical biochemistry*, 30(1), 11-26.
- Shi, G. J., Li, Y., Cao, Q. H., Wu, H. X., Tang, X. Y., Gao, X. H., ... & Yang, Y. **2019**. In vitro and in vivo evidence that quercetin protects against diabetes and its complications: A systematic review of the literature. *Biomedicine & Pharmacotherapy*, 109, 1085-1099. Available at: <https://pubmed.ncbi.nlm.nih.gov/30551359/> [Accessed 2 Oct. 2020].
- Widowati, W., Wijaya, L., Wargasetia, T. L., Bachtiar, I., Yellianty, Y., & Laksmiawati, D. R. **2013**. Antioxidant, anticancer, and apoptosis-inducing effects of Piper extracts in HeLa cells. *Journal of Experimental & Integrative Medicine*, 3(3).
- Tavsan, Z., & Kayali, H. A. **2019**. Flavonoids showed anticancer effects on the ovarian cancer cells: Involvement of reactive oxygen species, apoptosis, cell cycle and invasion. *Biomedicine & pharmacotherapy*, 116, 109004. Available at: <https://www.semanticscholar.org/paper/Flavonoids-showed-anticancer-effects-on-the-ovarian-TavsanKayali%20C4%B1%2013a2e823b9fbfc9446fcf0ac8621b083d8ae489b> [Accessed 6 Dec. 2020].
- Prieto-Bermejo, R., & Hernández-Hernández, A. **2017**. The importance of NADPH oxidases and redox signaling in angiogenesis. *Antioxidants*, 6(2), 32.
- Pham-Huy, L. A., He, H., & Pham-Huy, C. **2008**. Free radicals, antioxidants in disease and health. *International journal of biomedical science: IJBS*, 4(2), 89.
- Suarez, R. K. **2012**. Energy and metabolism. *Comprehensive physiology*, 2(4), 2527-2540. Available at: <https://onlinelibrary.wiley.com/doi/10.1002/cphy.c110009> [Accessed 11 Dec. 2020].
- Nicholson, L. B. (2016). The immune system. *Essays in biochemistry*, 60(3), 275-301.
- ab214484 Annexin V – DY-634/ PI Apoptosis Detection Kit. *Abcam*, **2016**. 1, 9, Available at: <https://www.abcam.com/ps/products/214/ab214484/documents/ab214484%20Annexin%20V%20DY634%20PI%20A>

- apoptosis%20Detection%20Kit%20v1a%20(website).pdf* [Accessed 20 Sep. 2020].
- Xiong, S., Mu, T., Wang, G., & Jiang, X. **2014**. Mitochondria-mediated apoptosis in mammals. *Protein & cell*, 5(10), 737-749.
- Apoptosis. **2020**, 1-3. Available at: <https://www.cancerquest.org/cancer-biology/apoptosis> [Accessed 15 Sep. 2021].
- Ramalalingam et al. **2015**, In Vitro Free Radical Scavenging and Anticancer Potential of Aristolochia Indical (MCF-7) Cell Line. *Int J Pharm Pharm Sci*, 7, (6), 392.
- Niu, G., Yin, S., Xie, S., Li, Y., Nie, D., Ma, L., ... & Wu, Y. **2011**. Quercetin induces apoptosis by activating caspase-3 and regulating Bcl-2 and cyclooxygenase-2 pathways in human HL-60 cells. *Acta Biochim Biophys Sin*, 43(1), 30-37.
- Mukherjee, A., Mishra, S., Kotla, N. K., Manna, K., Roy, S., Kundu, B., & Talukdar, A. **2019**. Semisynthetic quercetin derivatives with potent antitumor activity in colon carcinoma. *Acs Omega*, 4(4), 7285-7298. Available at: file:///C:/Users/ALAMAL/Downloads/Semisynthetic_Quercetin_Derivatives_with_Potent_An.pdf [Accessed 3 Nov.. 2021].
- Rather, R. A., & Bhagat, M. (2020). Quercetin as an innovative therapeutic tool for cancer chemoprevention: Molecular mechanisms and implications in human health. *Cancer medicine*, 9(24), 9181-9192.
- Ali-Boucetta, H., Al-Jamal, K. T., & Kostarelos, K. **2011**. Cytotoxic assessment of carbon nanotube interaction with cell cultures. In *Biomedical Nanotechnology* (pp. 299-312). Humana Press. Available at: https://www.researchgate.net/publication/50597901_Cytotoxic_Assessment_of_Carbon_Nanotube_Interaction_with_Cell_Cultures [Accessed 3 Jan. 2021].
- Biosciences, B. D. **2011**. Detection of Apoptosis Using the BD Annexin V FITC Assay on the BD FACSVerser™ System. Available at: https://www.bdbiosciences.com/content/dam/bdb/marketindocuments/BD_FACSVerse_Apoptosis_Detection_App_Note.pdf [Accessed 13 Jan. 2021].
- Hashemzaei, M., Delarami Far, A., Yari, A., Heravi, R. E., Tabrizian, K., Taghdisi, S. M., & Rezaee, R. **2017**. Anticancer and apoptosis-inducing effects of quercetin in vitro and in vivo. *Oncology reports*, 38(2), 819-828. Available at: <https://www.ncbi.nlm.nih.gov/pmc/articles/PMC5561933/pdf/or-38-02-0819.pdf> [Accessed 28 Jan. 2021].
- Jiao, G., He, X., Li, X., Qiu, J., Xu, H., Zhang, N., & Liu, S. **2015**. Limitations of MTT and CCK-8 assay for evaluation of graphene cytotoxicity. *Rsc Advances*, 5(66), 53240-53244. Available at : [https://www.researchgate.net/publication/278162083_Limitations_of_MTT_and_CCK-](https://www.researchgate.net/publication/278162083_Limitations_of_MTT_and_CCK-8_assay_for_evaluation_of_graphene_cytotoxicity)
- 8_assay_for_evaluation_of_graphene_cytotoxicity [Accessed 4 Dec. 2020].
- Foo, J. B., Ng, L. S., Lim, J. H., Tan, P. X., Lor, Y. Z., Loo, J. S. E., ... & How, C. W. **2019**. Induction of cell cycle arrest and apoptosis by copper complex Cu (SBCM) 2 towards oestrogen-receptor positive MCF-7 breast cancer cells. *RSC advances*, 9(32), 18359-18370. Available at: <https://pubs.rsc.org/en/content/articlelanding/2019/ra/c9ra03130h> [Accessed 24 Dec. 2020].
- Jin, H.; Ko, Y. S.; Park, S. W.; Chang, K. C.; Kim, H. J. **2019**, 13-Ethylberberine Induces Apoptosis through the Mitochondria-Related Apoptotic Pathway in Radiotherapy-Resistant Breast Cancer Cells. *Molecules*. 24(13), 2448. Available at: <https://www.ncbi.nlm.nih.gov/pmc/articles/PMC6651458/pdf/molecules-24-02448.pdf> [Accessed 1 Dec. 2020].
- Wu, L., Li, J., Liu, T., Li, S., Feng, J., Yu, Q., & Guo, C. **2019**. Quercetin shows anti-tumor effect in hepatocellular carcinoma LM3 cells by abrogating JAK2/STAT3 signaling pathway. *Cancer medicine*, 8(10), 4806-4820.
- Kim, S. R., Lee, E. Y., Kim, D. J., Kim, H. J., & Park, H. R. **2020**. Quercetin inhibits cell survival and metastatic ability via the EMT-mediated pathway in oral squamous cell carcinoma. *Molecules*, 25(3), 757.



Measuring the Content of 16 PAH in Plant (potato) from Bradford in the UK

Heiam Hamed

Occupational Health & Safety Department, Higher Institute of Engineering Technology, Benghazi, Libya.

DOI: <https://doi.org/10.37375/sjfsu.v2i2.461>

A B S T R A C T

ARTICLE INFO:

Received 19 July 2022.

Accepted 14 August 2022.

Published 27 October 2022.

Keywords: PAHs, Potato Vegetable, GC-MS

The objective of this study was to determine the spatial distribution of the PAH (polycyclic aromatic hydrocarbons) concentrations in a sample of potatoes from Bradford, this objective will be achieved by solvent extraction and analysis of potato samples using gas chromatography with mass spectrometry (GC-MS). The potato samples were collected from four sites in the city of the Bradford-middle north of the United Kingdom. The exact location of each sample was recorded using a Global Positioning System (GPS). In site 1 the average concentration of Benzo[b]fluoranthene was (9.82 ng/g). This compound had the highest concentrations level of the 16 PAHs in all sites, while the average (1.023 ng/g) in site 2 of the compound with the low-value Pyrene. The total concentration of 16 PAHs range was between 50.87 -78.31 ng/g.

1. Introduction

Polycyclic Aromatic Hydrocarbons (PAHs) have been of increasing concern due to their ubiquitous presence in urban air. Some of these compounds have toxic, carcinogenic, and mutagenic properties (Abdel-Shafy and Mansour, 2016)

As a category of widely known carcinogenic compounds derived from incomplete combustion (IARC, 1983; Harvey, 1991), because of the transportation, storage, and use of crude oil and its products, petrogenic PAH sources are ubiquitous in cities. Storage tank leaks and the accumulation of tiny discharges of motor oil, gasoline, and other transportation-related substances are major sources of petrogenic PAHs (Abdel-Shafy and Mansour, 2016). Among the most important environmental pollutants are polycyclic aromatic hydrocarbons compounds (Dong et al., 1999).

Because diet is thought to be the primary source of human exposure to PAHs (Phillips, 1999), and vegetables are a basic food, scientists are interested in how much PAHs accumulate in vegetable production. Many studies have been conducted to investigate the uptake of PAHs by plants. (Wild et al., 1992; Voutsas and Samara, 1998; Kipopoulou et al., 1999)

PAH contamination was discovered in a variety of dietary categories, including vegetables. (Howard and Fazio, 1980).

It seems that gas emissions from fossil fuel combustion are the main way that PAHs accumulate in vegetables nearby, and this affects the PAH levels and profiles in those vegetables. (Kipopoulou et al., 1999)

The absorption of PAHs by vegetables can occur through the absorption of the leaves or roots, and their absorption is directly related to the nature of the PAH compounds, their physico-chemical characteristics and the physiological conditions of the plant. (Wang et al., 2011)

The PAH content of foliage is mainly correlated to ambient air. The relationship with soil PAH concentrations is not strong due to the relatively weak influence of root uptake mechanisms related to the low degree of soil/plant separation resulting from the lipophilic properties of PAH molecules. (Tuteja et al., 2011)

Direct contact between some leaf crops and contaminated soil can lead to increased levels of PAHs (Delschen et al., 1999). Vegetables usually reflect short-term changes in air pollution, while the soil is subject to long-term changes resulting from cumulative deposition (Jones, 1991).

Contaminants found in plants grown in cities usually come from previously contaminated soil or air pollution (Säumel et al., 2012; de Temmerman et al., 2015). It has

been previously shown that the accumulation of elements and genotoxic effects due to air pollution are absorbed by the leafy vegetables in the UCG. (Amato-Lourenco et al., 2016a,b). To determine the spatial distribution of the PAH concentrations in sample of potatoes from Bradford, this objective will be achieved by solvent extraction and analysis of potato samples using gas chromatography with mass spectrometry (GC-MS).

2. Materials and Methods

a. Study Area

The potato samples were collected from an area in the city of Bradford, West Yorkshire. The exact location for each sample was recorded using a Global Positioning System (GPS), as shown in table (1).

Table 1: Coordinates of the potato sample locations from Bradford.

Coordinates for samples from Bradford	
East	North
413107	432166
414882	432141
416861	432127
417888	432137

b. Sampling and Sample Preparation

The sample preparation after being collected then transported to the laboratory, potatoes were washed with distilled water to remove surface dust and freeze-dried. Cut 5g skin of potato mixed with equal amount of anhydrous Na₂SO₄ after that Soxhlet extraction 6h with CHCl₃ then rotary evaporation to ~0.5 ml. The extraction evaporation to dryness under N₂ stream then redissolution in CH₃CN the samples are now ready to analysis GC-MS (Kipopoulou and Manoli 1999).

c. GC-MS Method

An Agilent technologies 7890A GC system with 5975c mass selective detector (MSD) was used to separate, identify and determine the concentrations of PAHs in soil extracts. 1µl of each sample extract was injected into a splitless injector at a temperature of 300°C. The samples were separated with a HP5 capillary column (30 mm × 0.25 mm × film 0.25 µm film). The initial oven temperature was at 40°C for 1 min, rising to 120°C at 25 °C/min, then to 160°C at 10°C/min, and finally to 300°C at 5°C/min, this final temperature was held for 15 min. The interface temperature was kept at 280°C. Helium was the carrier gas used at a constant flow rate of 1 mL/min. The 16 PAHs standards were analysed with a Selected Ion Monitoring (SIM) mode (Dong, 2012).

3. Results

By choosing the molecular masses of interest for each molecule, contamination analysis can be avoided. In fact, each PAH has a distinct mass that is well-known and documented in the literature (Dong, 2012), and if the retention duration is known, it is possible to choose which masses should be detected. In this investigation, the SCAN mode was used to analyze the 16 PAH standard in order to determine the retention times of each chemical of interest. The technique has been developed, as shown in table (2) below, with the specific masses and retention times of each PAH.

Table (3) shows the average concentration individual 16 PAH and total PAH level. The average concentration of Benzo[b]fluoranthene in site 1 was (9.82 ng/g). This compound had the highest overall concentrations level of the 16 PAHs in all sites. while the average 1.023ng/g in site 2 of the compound with the low overall value Pyrene. The 16 PAHs levels range between 50.87 -78.31ng/g in potato samples were found to be more or less similar to other regions. Bishnoi et al. (2006) found 16 EPA PAH values in range of 59.78-128.47 ng/g in underground vegetables collected from various places of Mumbai city, India. Also, the result of this study was less similar 48-94 ng/g in root vegetables in a Greek (Kipopoulou et al. 1999).

Table 2: SIM parameter of MS for PAH analysis

Abbreviation	m/z	Rt [min]
NA	127, 128, 129	4-7
ACY	151, 152, 153, 154, 165, 166, 167	7-12
ACE		
FL		
PH	176, 178, 179	12-15
AN		
FLU		15-22
PY	101, 200, 202, 203	15-22
BaA	226, 228, 229	22-25
CH		
BbF	125, 252, 253	25-33
BkF		

BaP		
IP	138, 134, 276, 277, 278, 279	33-46
DA		
BP		

Table 3: Average Concentration individual 16 PAH and total PAH level.

	Site1	Site2	Site 3	Site 4
Abbreviation Compound	Average [ng/g]	Average [ng/g]	Average [ng/g]	Average [ng/g]
NA	9.581	4.956	1.762	2.874
ACY	6.428	2.835	1.910	2.293
ACE	1.05	1.290	2.110	2.495
FL	4.349	3.469	2.798	5.557
PH	7.599	7.680	2.738	6.147
AN	5.614	2.937	1.814	2.098
FLU	1.600	1.170	3.832	5.954
PY	1.490	1.023	3.632	5.185
BaA	3.505	6.618	7.400	1.411
CH	2.997	4.099	5.866	1.0578
BbF	9.820	1.187	6.629	1.528
BkF	6.391	8.313	2.702	1.294
BaP	5.117	7.549	3.852	1.738
IP	8.316	4.029	2.155	2.141
DA	8.806	3.237	2.991	2.136
BP	2.080	1.168	3.572	6.965
Total PAH [ng/g]	78.315	61.56	55.763	50.873

4. Discussion

Table (4) presents a statistical comparison was made using Analysis of variance of the differences between the four study areas in order to assess whether these areas are significantly different in their PAH concentrations. The total concentration data for all PAHs combined, as well as the data for each individual compound separately, were analysed using one-way ANOVA with the individual sampled sites being the replicates within each study area, to determine whether data from the four areas

There are significantly different. Results are presented in Table (5). There are significantly different in individual PAH concentrations. The result of this test ($F = 4.65$, $df = 99$, $p = 0.01$) that indicated a strongly significant difference between the four areas

Table 4: Results from one-way Analysis of Variance calculations, testing for differences between the four study areas in Bradford, for individual PAH compounds and for the combined total PAH concentrations. Number of degrees of freedom are (2, 97) in all cases. Key to symbols: ns indicates

$p > 0.05$, * indicates $P < 0.05$, ** indicates $P < 0.01$, *** indicates $p < 0.001$

PAH	All sites		
F-value	Probability	Significance	
NA	17.8	0.0001	***
ACY	15.9	0.0001	***
ACE	29.8	0.0001	***
FL	30.7	0.0001	***
PH	16.4	0.0001	***
AN	29.1	0.0001	***
FLU	20.8	0.0001	***
PY	43.8	0.0001	***
BaA	50.4	0.0001	***
CH	70.4	0.0001	***
BbF	7.5	0.001	**
BkF	10.6	0.001	**
BaP	3.2	0.01	*
IP	15.4	0.0001	***
DA	9.8	0.001	**
BP	10.2	0.001	**

The total PAH concentration in table (4) showed values ranged between 50.87 and 78.32 ng/g, all of which would be diagnosed as low by Dong (2012).

The total PAH compounds which showed a relative standard deviation (%RSD) greater than 10% were presented in table (4), 10% being an arbitrary threshold chosen to highlight that the compound has a comparatively high amount of variability.

The Shapiro-Wilk test indicated that these samples were not normally distributed in Bradford. For total PAH compounds a Grubbs' test was carried out to check for outliers. The Grubbs' test (G values which are less than the critical value 1.481 and therefore there is no outlier

for any compound. This means there were no other outliers within these compounds.

Table 5: Statistical analysis table for total concentration of the 16 PAHs from all sites

All sites	
Mean ng/g	62
Range ng/g	50.87-78.32
Standard deviation SD	12
Relative standard deviation RSD (%)	19
Shapiro-Wilk test probability	0.364 ns
Grubbs' test statistic (G)	0.898ns

5. Conclusions

To sum up above it is probably the large variability between individual results within a study area, as noted above, that lead to differences between means being able to be shown to be statistically significant. While the data had a one-way ANOVA result ($F = 4.65$, $df = 99$, $p = 0.01$) that indicated a strongly significant difference between the four areas.

Acknowledgements

I thank Ms Belinda Hill who provided insight and expertise that greatly assisted in conducting this research.

Conflict of Interest: The author declares that there are no conflicts of interests.

References

- Abdel-Shafy, H. I., and Mansour, M. S. M. 2016. A review on polycyclic aromatic hydrocarbons: source, environmental impact, effect on human health and remediation. *Egypt. J. Petrol.* 25, 107–123. doi: 10.1016/j.ejpe.2015.03.011.
- IARC. Monographs on the evaluation of the carcinogenic risk of chemical to humans, Polynuclear aromatic compounds, Part 1, Chemical, environmental and experimental data, 1983, p. 32.
- Dong RB, Xu DF, Liu LD. Behavior of PAHs in the environment. *Environ Dev (in Chinese)* 1999; 14:10–11.
- Phillips DH. Polycyclic aromatic hydrocarbons in the diet. *Mutat Res* 1999; 443:139–147.
- Wild SR, Berrow ML, McGrath SP, Jones KC. Polynuclear aromatic hydrocarbons in crops from long term sewage sludge amended field experiments. *Environ Pollut* 1992; 76:23–31.

Voutsas D, Samara C. Dietary intake of trace elements and polycyclic aromatic hydrocarbons via vegetables grown in an industrial Greek area. *Sci Total Environ* 1998; 218:203–216.

Kipopoulou AM, Manoli E, Samara C (1999). Bioconcentration of polycyclic aromatic hydrocarbons in vegetables grown in an industrial area. *Environ Pollut.* 106:369–380.

Howard JW, Fazio T (1980). Review of polycyclic aromatic hydrocarbons in foods. *J Assoc Of Anal Chem.* 63:1077–1104.

Harvey RG (1991). Polycyclic aromatic hydrocarbons: Chemistry and carcinogenicity. New York: Cambridge University Press.

Wang, W., Simonich, S. L. M., Xue, M., Zhao, J., Zhang, N., Wang, R., and Tao, S (2011). Concentrations, sources and spatial distribution of polycyclic aromatic hydrocarbons in soils from Beijing, Tianjin and surrounding areas, North China. *Environmental Pollution*, 158(5), 1245-1251.

Tuteja, G., Rout, C., and Bishnoi, N. R (2011). Quantification of polycyclic aromatic hydrocarbons in leafy and underground vegetables: a case study around panipat city, haryana, india. *J. Environ. Sci. Technol.* 4, 611–620. doi:10.3923/jest.2011.611.62.

Jones, K. C (1991). Contaminant trends in soils and crops. *Environ. Pollut.* 69, 311–325. doi: 10.1016/0269-7491(91)90119.

Delschen, T., Hembrock-Heger, A., Leisner-Saab, J., and Sopczak, D (1999). UWSF-Z. *Umweltchem. Ökotoxicol.* 11, 79–87.

de Temmerman, L., Waegeneers, N., Ruttens, A., and Vandermeiren, K (2015). Accumulation of atmospheric deposition of As, Cd and Pb by bush bean plants. *Environ. Pollut.* 199, 83–88. doi: 10.1016/j.envpol.2015.01.014.

Säumel, I., Kotsyuk, I., Hölscher, M., Lenkerei, C., Weber, F., and Kowarik, I (2012). How healthy is urban horticulture in high traffic areas? Trace metal concentrations in vegetable crops from plantings within inner city neighbourhoods in Berlin, Germany. *Environ. Pollut.* 165, 124–132. doi: 10.1016/j.envpol.2012.02.019.

Amato-Lourenco, L. F., Lobo, D. J. A., Guimarães, E. T., Moreira, T. C. L., Carvalho-Oliveira, R., Saiki, M., et

al. (2016a). Biomonitoring of genotoxic effects and elemental accumulation derived from air pollution in community urban gardens. *Sci. Tot. Environ.* 575, 1438–1444. doi: 10.1016/j.scitotenv.2016.09.221.

Dong, C.D., Chen, C.F. and Chen, C.W (2012). Determination of polycyclic aromatic hydrocarbons in industrial harbour sediments by GC-MS. *International Journal of Environmental Research and Public Health*, 9(6), pp.2175-2188.

Bishnoi, N.R., U. Mehta, U. Sain and G.G. Pandit (2006). Quantification of polycyclic aromatic hydrocarbons in fruits and vegetables using high performance liquid chromatography. *Indian J. Chem. Technol.*, 13: 30-35.



Mode of Formation of the Coastal Sabkha Sediments in the Coastal Plain of Al-Dafna Plateau

Ahmed A. Mohammed¹, Tarek I. Anan² and Amin M. Gheith²

¹Geology Department, Science Faculty, Tobruk University, Tobruk, Libya.

²Geology Department, Science Faculty, Mansoura University, Mansoura, Egypt.

DOI: <https://doi.org/10.37375/sjfssu.v2i2.516>

A B S T R A C T

ARTICLE INFO:

Received 19 August 2022.

Accepted 21 September 2022.

Published 27 October 2022.

Keywords:

Intertidal and supratidal sabkhas
coastal sand dune
mouth of wadis
Al-Dafna plateau

Two types of sabkhas are distinguished in the study of coastal area; the first type was developed at the mouths of wadis where sea water enters the wadis through high tides; these include; Omm El-Shawesh, Wadi Al-Ain sabkha and Wadi Rizk sabkha. A generalized hydrodynamic model for the formation of this type of sabkha was constructed. The second type of sabkha is stretching behind the dunes, and is divided into a longitudinal strip from east to west where saline crusts appear in some parts and approach the groundwater level. These sabkhas are subjected to flooding during the winter and plant grows within this sabkha. Behind the shore sand hummocks, sea water enters the sabkhas area by seepage and mix with groundwater, and then rises upward to the surface through capillary action and evaporates. This type of sabkha include; Alaqila, Omm Rukbah and Wadi Al-Sawani. The generalized hydrodynamic model suggested for the formation of this kind of sabkha was constructed too.

1 Introduction

Sabkhas are widespread geomorphological features in the coastal landforms of the Mediterranean Sea of Libya. Wadis sabkhas always subjected to flash floods during the rainy season in the main Wadis and/or recharge from tidal flow. A tidal pool partially filled with seawater during high tide flood seasonally and daily thus intertidal and supratidal sabkhas are developed. A marine sabkha is a near coastal salt dominated by marine-derived brines and processes; a continental sabkha is an inland salt flat dominated by continental brines and processes (Prudencio et al., 2007). According to Kleo and Al-Otaibi (2011) there are three types of geomorphic sabkhas which are as follows: 1) sabkhas that are connected to the coastal inlets; 2) sabkhas that are connected to the tidal flats and 3) sabkhas that lie behind the shore sand hummocks.

The study area is characterized by the presence of many geomorphological coastal landforms and bays. The coastline extends from the Wadi El-Shawash estuary in the west to the Ramla well in the east at the

western border of the Arab Republic of Egypt. Sand dunes, sabkhas and pockets are abundant in this area (Al-Haram, 1997). Sabkha is an Arabic word for a salt-flat area found mainly along hot and arid climate typically formed on shoreline (coastal sabkhas) and inland present within the sand dunes areas. Marine sabkhas represent transitional environments between the land and the sea. Marginal marine sabkhas that bordered by tidal flats display a range of sedimentary features according to the frequency of flood by sea water and the providing of terrigenous material from nearby high mountains. A marine sabkha is a near coastal salt dominated by marine-derived brines and processes; whereas, a continental sabkha is an inland salt flat dominated by continental brines and processes (Prudencio et al., 2007).

The area is subdivided into two geomorphic units; the northern scarped terrain is marked by the presence of many prominent scarps running in an ESE-WNW direction while the southern part of Al Bardia area is

flat, monotonous plain (El Deftar and Issawi, 1977; Mazhar and Issawi, 1977; Sweedan and Issawi, 1977).

Coastal sabkha spreads within a boundary between the coastline and the interior at different distances depending on the topography of the surface. Sediments of sabkha were observed close to the mouths of some wadis at the northeast part of the studied area. It was subjected to all changes affecting the coastal plain because its development is closely related to coastal conditions (Ashour, M., 1993).

2 Techniques of Study

Two field trips were carried out on the coastal stretch of the Al-Dafna plateau in the summer and winter times (2017-2018) where six sites in the coastal area were chosen for collecting samples from intertidal and supratidal flat sediments developed at the mouths of different wadis; wadi Omm El-Shawesh, Alaqila, wadi Al-Ain, Omm Rukbah, wadi Ritzk and wadi Al Sawani. Sabkha features were described photographed, logged and samples.

3 Study Area

The study area occupies the northeastern part of Libya; where sabkhas are common in the coastal area of Al-Dafna plateau which extends from the mouth of Wadi Omm El-Shawash, in the west (east of Tobruk City), to Bir Al Ramla Well in the eastern border of Libya with Egypt for about 130 km long. The area lies between Latitude $31^{\circ} 45''$ to $32^{\circ} 21''$ N and Longitude between $24^{\circ} 00''$ to $25^{\circ} 08''$ E (Fig. 1). The study area has a Mediterranean climate where arid to semiarid conditions are dominant. The average temperature is ranging from 25 to 40° C in summer months and from 10 to 20° C

during winter. The rainy season is limited and often concentrated in few showers from October to March. While December and January months are the wet.

The geomorphology of the Al-Dafna Plateau area occupy the eastern-north part of Libya. It extends from the Wadi Omm El-Shawesh, east of Tobruk City, to Bir Al Ramla Well in the eastern border of Libya to Egypt for about 130 km long. The total area included in this study is estimated to 5638.3 km² with maximum height of 223 m above the mean sea level. He further mentioned that the sabkhas are significantly spread along the coastal area, behind the sand dunes in Ras Azaz, Omm Rukbah, Mursi and Jazour. Sabkha is a shallow coastal area of marginal seas, particularly those in catchment areas of populated and industrialized regions, are endangered by the increasing of substances or heavy metals at a rate faster than the environment can accommodate (Saleh, 2013).

The supratidal and intertidal sabkha areas are flooded with sea water seasonally and daily. The main recharge to the sabkha area is from tidal flow and flash flood from different wadis. A tidal pool partially filled with seawater during high tide flood always occurs.

4 Study Objective

The objective of this paper is to construct the hydrodynamic model of sabkha formation.

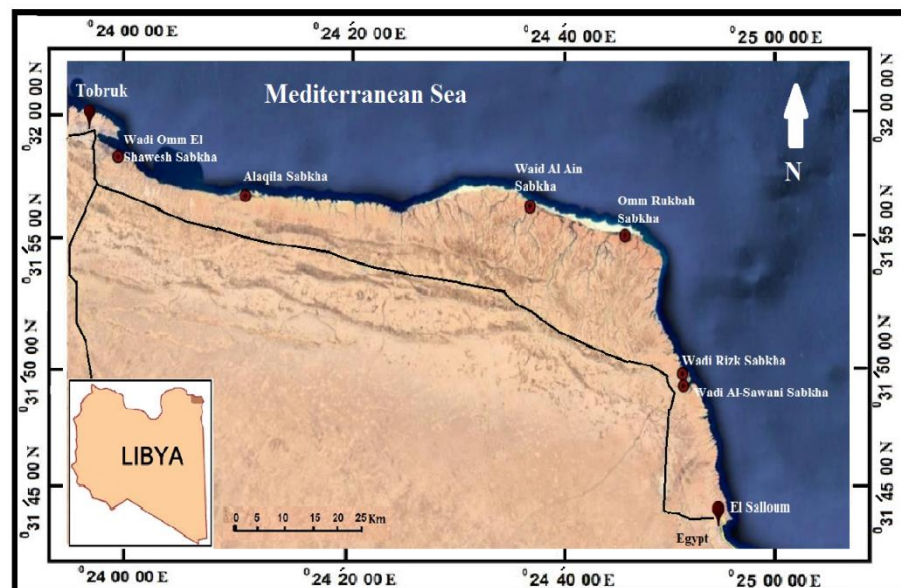


Figure (1). Satellite image showing the location of the studied coastal sabkhas in Al-Dafna plateau.

The sabkhas are significantly spread along the coastal area behind the sand dunes. Supratidal and intertidal sabkhas are developed in the wadis mouths in the coastal area of Al-Dafna plateau where desiccation in the tidal flat areas causes precipitation of gypsum and halite.

Sabkhas are subjected to all changes affecting the coastal plain because its development is closely related to coastal conditions. Sediments are composed of fine to medium sand and muds with gypsum. They are deposited by wind and water carried by the valleys to the sea sabkha areas. Fine sediments can be brought to sabkhas through the tidal currents and storm waves too. Marshes and plants (halophytes) are well developed in the study area where groundwater covers some sabkhas. The water table rises in winter due to the tyranny of the sea with the rising waves, in addition to the water of the floods brought by wadis. While in summer, the high temperatures and the high evaporation rate cause lowering of water table. Depending on the topography of the surface, coastal sabkha spread between the coastline and the interior of the land. Sabkha sediments were observed close to the mouths of some wadis at the northeast part of the studied area.

The wadis draining the inland part of the surrounding limestone terrain wash in this flat surface fine-grained terrigenous materials admixed with the almost stagnant sea water. Evaporation helps the formation of sediments which consist of very fine calcite sand and salt grains with various components of clay. Gypsum and salt form a thin cover on the sabkha surface in dry season; and saline crusts in some parts appear frequently.

5 Results and Discussion

The recognized sabkhas are subdivided into intertidal and supratidal sabkhas. These sabkhas are occurred either in mouth of wadis or behind the coastal sand dune. Each type has its characteristic textural and mineralogical composition. The dunes cover very small patches at the central part of the area with 2 m rise from the surrounding surface. It is composed of quartz sands mixed with carbonate particles.

Sabkhas developed in these areas are formed under complex hydrochemical system includes sea water seepage, groundwater percolation, and surface drainage water. Wadis sabkhas always subjected to flash floods during the rainy season in the main wadis and/or recharge from tidal flow, thus intertidal and supratidal sabkhas are developed. Tidal flats are desiccated and are marked by mud cracks with the growth of gypsum and halite crystals in muds according to Boggs (1987),

especially in arid and semiarid regions. In correlation with the Trucial sabkha, gypsum and anhydrite are the dominant evaporite minerals (Kinsman, 1969). Although there is a common tendency to regard tidal flats as primarily sites of siliciclastic deposition, carbonate sediments, and evaporites accumulate on many modern tidal flats. On the other hand, Kleo and Al-Otaibi (2011) distinguished three types of geomorphic sabkhas; these include, sabkhas that connected to the coastal inlets, sabkhas connected to the tidal flats and sabkhas lie behind the shore sand hummocks.

The studied area of the sabkha is a flat and shallow embayment filled with sea water during high tides. Lands filled with water are formed throughout the year as a result of the decline and exposure to rain water during the winter and spread the edges of some veneers salt. Evaporation helps the formation of sediments which consist of very fine calcite sand and salt grains with various components of clay. Gypsum and salt form a thin cover on the sabkha surface in dry seasons.

Two types of sabkhas are distinguished in the study coastal area; the first type was developed at the mouths of wadis where sea water enters the wadis through high tides; these include Omm El-Shawesh, Wadi Al Sawani sabkha and Wadi Rizk sabkha (Fig. 2). A generalized hydrodynamic model for the formation of this type of sabkha is shown in (Fig. 3). The second type of sabkha is stretching behind the dunes, and is divided into a longitudinal strip from east to west. Saline crusts appear in some parts and approach the groundwater level. In meantime, these sabkhas may be subject to flooding during the winter and plant grow within this sabkha. Behind the shore sand hummocks, sea water enters the sabkhas area by seepage and mix with groundwater, and then rises upward to the surface through capillary action and evaporates. Sometimes this sabkha is subject to flooding of wadis through rainy season. This type of sabkha includes Alaqila, Omm Rukbah and Wadi Al-Ain (Fig. 4). The generalized hydrodynamic model suggested for the formation of this kind of sabkha is demonstrated in (Fig. 5). During the winter season rainfall results in the increase of the flow of groundwater through wadis and thus the level of water table is increased. This mechanism is reversed through summer season, where the increase of evaporation rate causes lowering of the water table, this leads to evaporative concentration of near surface water and displacive growth of the gypsum and halite crystals. The occurrence and abundance of evaporite minerals are controlled by local environmental factors such as topography of the sabkha, emergence or submergence of tidal areas and contribution of meteoric water as a result of floods from the adjoining mountains.

Furthermore, during the rise of groundwater part of the old gypsum is dissolved and redeposited again at the ground surface under arid climate. This is probably modified by dissolving some of the lagoon gypsum under the sabkha (Ali; 1981, Ali and West, 1983). In addition, there is a role of active wind deflation which eroded the surrounded high carbonate outcrops then transported and deposited into the sabkha basin. The carbonate minerals present in the sabkha deposits are formed of calcite and dolomite that occur as sand and mud material resulted from weathering products.

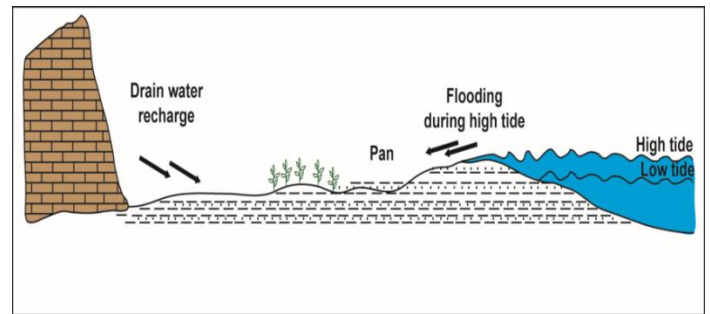


Figure (3). Hydrodynamic model of the first type of sabkha formation

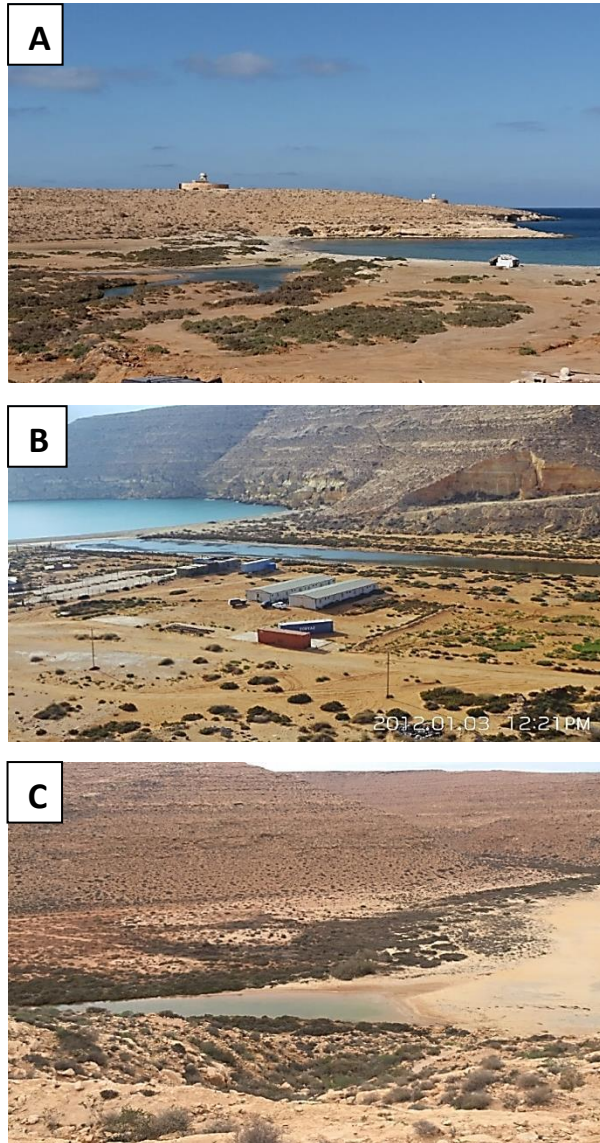


Figure (2). First type of sabkha formed at the Wadi mouths, where sea water enter sabkha basin during the high tide. (A) Omm El-Shawesh sabkha, (B) Al Sawani sabkha, (C) Wadi Rizk sabkha.

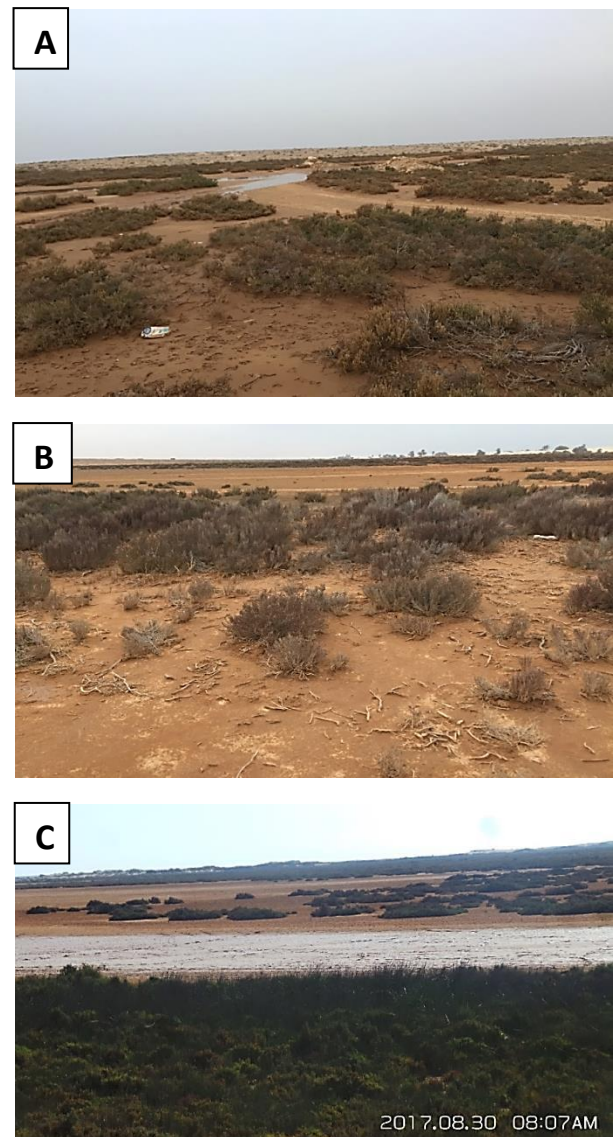


Figure (4). Second type of sabkha formed behind sand dunes, where sea water seepage and mix with groundwater. (A) Alaqila sabkha, (B) Omm Rukbah sabkha, (C) Wadi Al-Ain sabkha.

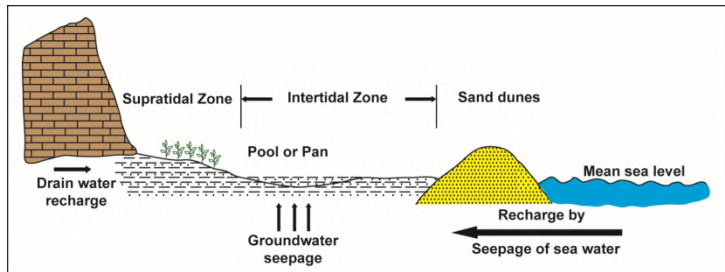


Figure (5). Hydrodynamic model of the second type of sabkha formation

6 Conclusion

Three mechanisms were suggested for the formation of sabkha deposits in the coastal area of Al-Dafna Plateau:

- 1) Direct influx of the sea water during the high tides into the low land with probability of mixing with drainage surface water, later then evaporated.
- 2) Seepage of seawater through the very permeable sediments under the coastal dune sediments which formed the groundwater brines that upward raised by capillary movement, then subjected to evaporation.
- 3) Downward flow of concentration brines moving through the sediments enriched with residual Mg^{++} and formation of dolomite crystals.

References

- Al-Harram, F. (1997). *The Libyan Coast*. Publications of the Center for Research and Consultations, University of Garyounis, Benghazi, First Edition. (Translated From Arabic).
- Ashour, M. (1991). *The sabkhas in the Peninsula of Qatar: Biogeological and Geomorphology Study*, Center for Documentation and Humanities, Qatar University, First Edition. (Translated From Arabic).
- Ali, Y. A. (1981). *Mineralogical, geochemical and Sedimentological studies on recent sabkha sediments west of Alexandria, Egypt, and some Upper Jurassic evaporites from Dorset, England* (Unpublished Ph.D. Thesis, Faculty of Science, Ain Shams University, Cairo, 332 pp).
- Ali, Y. A., and West, I. (1983). Relationships of modern gypsum nodules in sabkhas of loess to compositions of brines and sediments in northern Egypt. *Journal of Sedimentary Research*, 53 (4), 1151-1168.
- Boggs, S. (1987). *Principal of Sedimentology and Stratigraphy*. Macmillan Publishing Company, New York, 519 pp.
- El Deftar, T., and Issawi, B. (1977). *Geological Map of Libya*, 1: 250 000, Sheet Al Bardia NH 35-1. In

Explanatory Booklet (p. 93). Ind. Res. Centre Tripoli, Libya.

- Kleo, A. A., and Al- Otaibi, O. (2011). The sustainable development of Kuwaiti Sabkhas. *Digest of Middle East Studies*, 20 (1), 27-49.
- Kinsman, D. J. (1969). Modes of formation, sedimentary associations, and diagnostic features of shallow-water and supratidal evaporites. *Bull. Am. Ass. Petrel. Geol. Vole 53 (4)*, p. 830-840.
- Mazhar, A., and Issawi, B. (1977). *Geological map of Libya: 1: 250,000 sheet, Zt. Msus NH34-3*, Explanatory Booklet, Indust. Res. Cent., Tripoli, 80p.
- Mohamed, A. (1993). *Depositional environments of some Miocene rocks in northern Western Desert, Egypt*. Unpublished M.Sc. Thesis, Alexandria Univ., Egypt, 144 pp.
- Prudêncio, M. I., Gonzalez, M. I., Dias, M. I., Galan, E., and Ruiz, F. (2007). Geochemistry of sediments from El Melah lagoon (NE Tunisia): a contribution for the evaluation of anthropogenic inputs. *Journal of Arid Environments*, 69 (2), 285-298.
- Sweedan, A. and Issawi, B. (1977). *Geological map of Libya, 1: 250,000 Sheet NH 34-4 Bir Hacheim*. Explanatory Booklet, Industrial Research Center, Tripoli, 80p.
- Saleh, M. (2013). *Al-Dafna Plateau, Northeast of Tobruk, Libya: Geomorphological Study*. Unpublished Ph.D. Thesis in Natural Geography, Faculty of Arts, Ain Shams University, Egypt. 338 pp. (Translated From Arabic).



Muco-adhesion Evaluation of Polysaccharides in Simulated Physiological Fluids

Hana A. S. Binhamad¹ and Ramadan Diryak²

¹Chemistry Department, Science Faculty, Omar al-Mukhtar University, al-Bayda, Libya.

²Medicine Faculty, Sirte University, Sirte, Libya.

DOI: <https://doi.org/10.37375/sjfsu.v2i2.510>

A B S T R A C T

ARTICLE INFO:

Received 19 August 2022.

Accepted 04 September 2022.

Published 27 October 2022.

Keywords: Gellan gum, Methylene blue, Retention time, Gellan gel, Drug delivery.

Gellan gum is a microbial exopolysaccharide, water-soluble polymers secreted by microorganisms during fermentation. The biopolymer gellan gum is a relatively recent addition to the family of microbial polysaccharides that is gaining much importance in food, pharmaceutical and chemical industries due to its novel properties. The purpose of this work is to investigate the impact of physiological fluids on both the physical and chemical properties of gellan gum, and to understand the role of polymers gel in muco-adhesion and drug delivery to prolong the residence time of the drug inside the body. Muco-adhesion measurements of retention time were performed using bespoke retention apparatus to determine the retention of labelled gellan gum dose. The physiological fluids used in this work are artificial gastric juice, artificial saliva fluid, and artificial tears fluid. Results of this work show that in general the viscosity of gellan increased with high concentration and the gel formation is strong with artificial gastric juice (HCL) and weak gel formation with artificial saliva and tears but the retention time is longer with saliva and tears than with artificial gastric juice.

1 Introduction

Hydrocolloids or gums is a type of polysaccharide which is commercially available and it is used in food industries as stabilizers, crystallization inhibitors, thickening and gelling agents and in some non-food industries it is used as encapsulating agent. Due to the strong interlinked connections in the molecules, polysaccharides have a characteristic strength. In nature it is present in plant cell wall as a component or exist as extracellular substance e.g., Gellan gum. Gellan gum is a high molecular weight compound with a negative charge on its molecule. It is produced by microorganism named *Sphingomonas elodea* as a fermentation product. It can also be produced commercially on demand with a consistent quality (Jansson et al., 1983).

Physical characteristics of gellan Gum

The gelatinization of gellan gum is dependent on

ambient temperature and cationic strength. The process of gelatinization involves the formation of double helical junctions which further form complexes with cations and hydrated with water molecules by hydrogen bonds.

The gelatinization of gellan gum in aqueous environment is a two-step process. In step one double helices of random coil chains are formed leading to aggregation of pairs of double helices, this is also called Coil-helix transition. In step two it makes electrostatic interaction with co-existing cations in the solutions and this is affected by varying the pH of the solution.

Chemical Characteristics of gellan Gum

The molecular structure of it consists of a tetra saccharide repeating unit made of glucose, glucouronic acid and rhamnose residue in a ratio of 2:1:1. In the negative charged molecule two acyl substituent; glyceryl at O (2)

and an acetyl at O (6) are present on the 3 linked glucose molecule (Fig. 1). The gellan gum can deacetylate by alkali treatment.

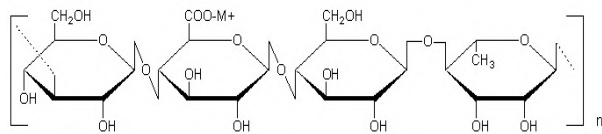


Figure (1). The structure of Gellan Gum ([Matricardi et al., 2009](#))

Gellan gum has been characterized into the three groups on the following basis: Polysaccharide content, the percentage of O-acetyl substitution on the molecule, and the protein content (including the nucleic residues and other organic nitrogen sources).

Acyl content has a profound impact in the physical characteristics of gel. Gels with high acyl content are very soft, elastic and not brittle whereas gels with low acyl content are firm, brittle and are inelastic. Both forms of acyl gels (high content which is the native form and the synthetics low content form) have similar linear structure having a tetra saccharide unit repeat. The tetra saccharide contains three different molecules which are glucose, rhamnose and glucouronic acid with a molar ratio of 2:1:1. Glucose residues in the molecule have an acetyl group and L-glyceryl groups on it ([Jansson et al., 1983](#)). The molecular formula of gellan gum can vary as it depends on the glucouronic acid neutralization with various salts. The anionic nature of the gum is due to the presence of the carboxylate groups in molecular structure which gives it the ability to undergo gelatinization in the presence of monovalent or divalent cations. The gum form complexes with them by electrostatic interactions. It has been reported by [Sanderson and Clark \(1983\)](#) that the gum has greater affinity for the divalent cations.

Physiological Fluids

The weight of water in the human body is in the range of 45-75%. The percentage of it varies with age and gender. The adipose tissue of the human body holds up to 10% water whereas the lean tissues contain approximately 70 to 75 percent of water. The total body water is with varying percentage in intracellular fluid and extracellular fluid. Transcellular fluid like cerebrospinal fluid, humours of eye, digestive secretions and the renal tubular fluid secretions contain 1-2% of body water.

Gastric Juice

Several factor like hormonal (by gastric hormones), neural and intestinal factors affect the secretion of gastric acid from the stomach. Food intake and the deficient level of glucose in the brain result in the reflex secretion of gastric juice. The reflex system has optic, gustatory and olfactory afferent nerves which are responsible for partial conditions reflex and the impulse then flows through an efferent vagus nerve. When the HCl secretion is on the peak the pH of the stomach drops to ca. 0.8. The

food being swallowed buffers the pH and increases it up to 1.8 to 4. This is the optimum pH for the enzymatic action of pepsin and gastric lipase. The low pH provides a bactericidal effect and it also denatures dietary protein making it easier to be degraded of protein enzymes.

Saliva

The human saliva is a complex mixture of different fluids; it is secreted by a set of major and minor salivary glands. There are three major salivary glands which are parotid, sublingual and submandibular glands. All these glands are under the control of autonomic nervous system. A human has salivary secretion of 1.5 litres in a day. It has slightly alkaline pH which is 7.4. Some organic and inorganic substances which are suspended in water make the saliva. It has glycoprotein Mucin along with some enzymatic proteins like lipase and salivary amylase. Some other compounds like lactoferrins, cystatin histatins, immunoglobulins and some thiocyanate ions are also present ([Humphrey and Williamson, 2011](#)).

Tear Fluid

A smooth ocular surface is responsible for the good visual activity. This property is provided to eye by Tear fluid or TF which covers the whole ocular surface and protects it. It serves as a barrier, lubricant, nutrient and an anti-microbial protectant. It improves the optical properties of eye and the maintenance of a normal Tear fluid is thus important for a smooth ocular surface.

Tear fluid lipids and proteins give high surface pressure and thus help in the stability of it. The average value of TF surface tension was found to be 70 mN/m ([Glasgow et al., 2010](#)). Tan and his fellows reported in 1993 that during sleep all major protein and water secretion is inhibited but Immunoglobulin A is the exception and it's secreted during the sleep. Na^+ , K^+ , Cl^- , HCO_3^- and low levels of Mg^{+2} and Ca^{+2} are the principal electrolytes in the basal tear fluid. The TF is usually isotonic in nature with serum but it has got a higher concentration of K^+ ions comparing to it ([Gilbard, 1994](#)).

In this paper the effect of the physiological fluids discussed above on the gellan gum will be discussed. Muco-adhesion of gel on the living tissue will be discussed in the context of bio-responsiveness in drug delivery systems.

Muco-adhesion

Muco-adhesion phenomenon is defined as a process in which two molecules, one of which is biological in nature interact with another with an interfacial force for an extended period of time. It's also defined as the ability of biological material or a synthetic material to stick on a tissue for a longer period of time. The tissue on which mucoadhesive adhere are actually mucous membrane. There are two steps which are involved in the muco-adhesion phenomenon. In the first step a contact between

the mucous membrane and the mucoadhesive polymer is established. This can be achieved by either good wetting of mucoadhesive surface or by promoting swelling of mucoadhesive substance. Once a good contact is established between them, the second step starts in which mucoadhesive penetrates the tissue surface or an interpenetration of mucoadhesive chains with the mucosal ones occurs the two surfaces are then stabilized by low energy chemical bonds (Duchene et al., 1988).

Muco-adhesion was used as a novel strategy for the improvement of therapeutic effect of various drugs in the early 1980s. Some water-soluble polymers have bio-adhesive properties i.e., they adhere to the mucous membrane on hydration. This property of bio-adhesive polymers was employed for designing mucoadhesive drug delivery systems. These polymers on the basis of this property can target the desired drug to the target tissue and keep it there for a longer period of time. The idea of using Mucoadhesive in drug delivery system was the result of need to localize drugs at target site for an extended period of time to optimize the action of delivered drug (Nagai and Machida, 1985).

The absorption of drug is constrained by the residence time of it at the target site e.g., in ocular drug delivery system a residence time of two minutes is available for the absorption of drug right after the instillation of it in the eye. But most of the drug washes away due to the solution drainage and rendering it unavailable for the absorption. This created the need development of drug delivery system which will keep the target at the target site for an extended period of time. Innovative formulations were developed with the use of gellan gum for the drug delivery to the target sites. The presence of gellan gum ensures the bioavailability of the drug for effective absorption by the tissue by adhering it to mucosal linings. From the research it has been observed that this gum is a very effective carrier and some attractive formulations were formulated that make the delivery of drug to the target tissues very specific (Kamath and Park, 1994). Following are the features that made the basis for the gellan gum drug delivery system:

- The delivery of the drug to the pharmacological specified sites can be controlled by using this gum.
- Another remarkable feature of it is that it increases the permeability of the cell membrane and thus helps in the effective drug uptake by the cell membranes.
- It stabilizes the drug product which is supposed to be delivered in the body.
- The solubility of the dug product is also increased in the body fluids (e.g., intestinal fluid) due to the presence of gellan gum.
- The drug metabolism is also reduced by its use thus it prevents the elimination of drug from the body.

Mao et al. (2000) explained the most remarkable feature of gellan which is its swelling ability which can be triggered by altering the environment surrounding to the delivery system (Fig. 2). The environmental factors that have an effect on the efficiency of the gel are pH, temperature or ionic strength. These factors can either swell or shrink the delivery system if changed from their normal values. The gellan gum is a pH sensitive compound and the functioning of the drug delivery having gellan gum can be monitored or optimized by changing the ambient pH. The most effective pH for it is alkaline. At alkaline pH the gel swells and releases the drug content inside it whereas at low pH the delivery system is collapsed. This property of gellan gum makes it an ideal candidate to be used in oral drugs in which it is rendered ineffective on its passage to the stomach where the pH is too low. When it reaches the upper intestine with high pH, the drug is released here to perform its function (Huang, 2004)

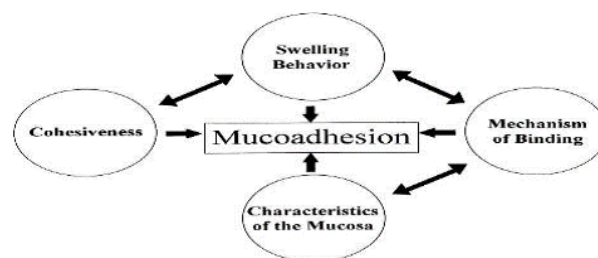


Figure (2). Schematic presentation of effects influencing Muco-adhesion. (Bernkop-Schnürch & Steininger 2000)

2 Materials and Methods

Gellan gum polysaccharide (Kelcogel) was from CP Kelco (Leatherhead, UK). Six well plates and dialysis tube supplied from Sigma-Aldrich (Poole UK). All other chemicals which were used in this study were supplied by the chemicals store, University of Huddersfield.

Gellan Gum Solutions

Three different concentrations of gellan gum solutions were prepared (0.5, 1.0 and 1.5 % (w/v) by slowly adding a weighed amount of gellan gum to hot deionised water (80°C) with continuous stirring until fully dissolved and then left at room temperature to cool before it was transferred into a 100 ml volumetric flask.

Gastric Juice (artificial)

Artificial gastric fluid was prepared from concentrated hydrochloric acid (HCl) mixed with deionised water in 1000 ml volumetric flask to produce a 0.1M solution and was adjusted to pH 1.2 using concentrated NaOH or HCl.

Artificial Saliva Fluid

The preparation of artificial saliva was developed by (Parker et al., 1999) and prepared in g/l by using 0.34 g

KH_2PO_4 , 0.43 g Na_2HPO_4 , 1.5 g KHCO_3 , 0.58 g NaCl, 0.14 g MgCl_2 , 0.22 g CaCl and 0.03 g Citric Acid dissolved together in a 1-liter deionised water and then the pH of solution was adjusted to 6.7 using concentrated of NaOH or HCl.

Artificial Tears Fluid

The preparation of artificial tear fluid was adopted from a tear fluid analysis (Stjernschantz and Astin, 1993) and made using 6.8 g NaCl, 2.2 g NaHCO, 0.084 g CaCl, 1.4 g KCl in 1 l of deionised water.

Methylene Blue Stock Solution

The stock solution was prepared by dissolving 0.1 mg/ml of Methylene blue crystals (methylthioninium chloride) in 100 ml volumetric flask with deionised water and then seven different amounts from the stock were taken (0.5, 1, 2, 4, 6, 8 and 10 ml) respectively to prepare different concentration from the stock as standards for plotting standardization curve. AUV-V is spectrophotometer in scanning mode was used to identify the peak maxima (λ_{max}) for Methylene blue which was measured at 658nm. This wavelength was used to measuring the absorbance of the standards.

Preparation of Methylene Blue Labelled Gel for Retention Time Measurement

Labelled gel was prepared by dissolving the gellan powder and Methylene blue crystal in deionised water (hot water 80°C) while stirring until completely dissolved. Four different concentrations from Methylene blue were prepared (0.01, 0.025, 0.05 and 0.1 mg/ml) to find out the suitable concentration for the experiment which was 0.1 mg/ml. The three different concentrations from gellan gel were prepared by the same way that mention above (0.5, 1.0 and 1.5 g %) after finish preparation the gel leaved at room temperature for 24 hours before measure the retention time.

Retention Time Measurement

Measurements of retention time were performed using bespoke retention apparatus shown in Fig. 3 (Batchelor et al., 2002). The apparatus used to determine the retention of labelled gellan gum dose on dialysis tube as a tissue. A Perspex® mounting block was manufactured with dimensions 100 mm length by 60 mm width and 15 mm deep. A groove was cut into this block in a central position; the dimensions of the groove were 100 mm long by 12 mm wide and 5 mm deep. The mounting block was permanently attached to a clamp that was able to rotate through approximately 120°. The clamp was attached to a stand and placed within a temperature and humidity-controlled environment, an adapted Gallenkamp industrial humidity cabinet (model BR185H). This apparatus allowed the temperature and

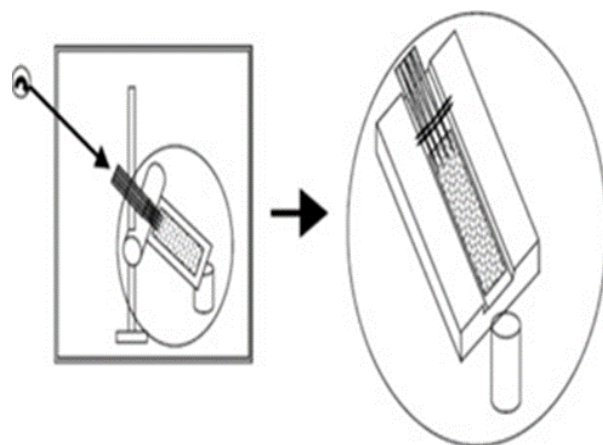


Figure (3). Apparatus used to determine the retention of a *vivo* tissue in presence three different type of artificial physiological fluids (Gastric juice HCl, saliva and tears).

humidity to be controlled and maintained via the water bath. The cabinet had sealed glove access to enable procedures to be performed during the experiment. The washing medium delivered to the tissue was supplied via a peristaltic pump (Watson Marlow model 202). The flow was split into three channels to provide an even distribution of the media over the entire tissue section. labelled gellan gum on dialysis tube as a tissue instead The Methylene blue labelled gellan gel (0.5, 1.0 and 1.5 %) were prepared and kept in room temperature for 24 hours before measuring retention. The retention time was examined for each concentration of the gel with the three fluids.

A 60 mm by 12 mm longitudinal section of dialysis tube (used as a model for epithelial tissue) was cut and placed into the groove cut on the stand and fixed with super glue. Then 1 ml of the gel sample was taken by syringe and put on the dialysis tube and the artificial fluid was allowed to flow over the gel controlled by an automatic pump at a rate of 4 ml per minute. The eluted physiological fluid was collected at time intervals up to 60 minutes and the absorbance was then measured at 658nm.

Calculation of Retention Time

The retention time can be calculated by using the equation from the calibration curve of Methylene blue standards.

$$Y = 197.42x - 0.0146, \text{ where } Y \text{ is the absorbance value}$$

Concentrations of the Methylene blue were calculated in different period of time, concentration versus absorbance was plotted on the curve.

3 Results

By using UV spectrophotometer, it can be able to identify the suitable wavelength for Methylene blue solution. The UV spectrophotometer allows a user to identify electronic transitions within the various regions of the

electromagnetic spectrum. UV can be measured by a spectrophotometer most readily when it is in the 400 to 700 nanometre (nm) region to quantify and determine the features of colour perception. The wavelength which will be used to measuring the absorbance for standards is (658 nm). Table 1 shows the absorbance for all concentration of standards which were taken at 658 nm for plotting a calibration curve.

The calibration curve of Methylene blue for seven different standards which give good linearity and the coefficient of determination (R^2) = 0.98 which is close to one (Fig. 4). The equation obtained from the curve is used to calculate the retention time.

Table (1). shows the absorbance for all concentration of standards

Concentration mg/ml	Absorbance (658nm)
0.0005	0.102
0.001	0.205
0.002	0.407
0.004	0.764
0.006	1.090
0.008	1.393
0.01	2.141

Calculation of Retention Time

1- Labelled Gel with Artificial Gastric Juice (HCL)

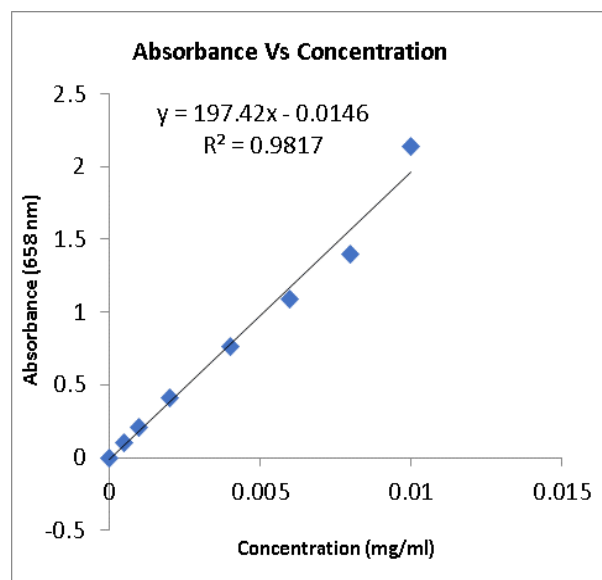


Figure (4). Calibration curve of Methylene blue standards

Calculation and comparing between the retention time of Methylene blue in three different concentrations of gel:

1- 0.5 % w/v labelled gel:

Absorbance (658nm) = 0.329, Amount of all volume collected = 204 ml

$$Y = 197.42X - 0.0146$$

$$X = 0.329 + 0.0146/197.42 = 0.0017 \text{ mg/ml}$$

$$\text{Dilution factor} = 0.0017 \times 204 = 0.35 \text{ mg/ml}$$

$$\text{Retention concentration} = 1 - 0.35 = 0.65 \text{ mg/ml (65\%)}$$

2- 1.0 % w/v labelled gel:

Absorbance (658nm) = 0.374 Amount of all volume collected = 244 ml

$$Y = 0.374, X = 0.374 + 0.0146/197.42 = 0.002 \text{ mg/ml}$$

$$\text{Dilution factor} = 0.002 \times 244 = 0.49 \text{ mg/ml}$$

$$\text{Retention concentration} = 1 - 0.49 = 0.51 \text{ mg/ml (51\%)}$$

3- 1.5 % w/v labelled gel:

Absorbance (658nm) = 0.421 Amount of all volume collected = 244ml

$$Y = 0.421,$$

$$X = 0.421 + 0.0146/197.42 = 0.0022$$

$$\text{Dilution factor} = 0.0022 \times 244 = 0.54 \text{ mg/ml}$$

$$\text{Retention concentration} = 1 - 0.54 = 0.46 \text{ mg/ml (46\%)}$$

2- Labelled Gel with Artificial Saliva

Calculation and comparing between Retention and Removed amount of Methylene blue in different concentration of gel with saliva

1- 1.0 % w/v labelled gel:

For all volume (124ml) = $0.141 + 0.0146/197.42 = 0.0008$ Amount

Dilution factor = $0.0008 \times 124 = 0.1 \text{ mg/ml}$
Remaining concentration = $1 - 0.1 = 0.9 \text{ mg/ml (90\%)}$

2- 1.5 % w/v labelled gel:

Amount for all volume (184ml) = $0.192 + 0.0146/197.42 = 0.001$

Dilution factor = $0.001 \times 184 = 0.18 \text{ mg/ml}$
Remaining concentration = $1 - 0.18 = 0.82 \text{ mg/ml (82\%)}$

3- Labelled gel with artificial tear

Calculation and comparing between Retention of Methylene blue in different concentration of gel

1- 0.5 % w/v labelled gel:

Amount for all volume (124ml) = $0.186 + 0.0146/197.42 = 0.001$

Dilution factor = $0.001 \times 124 = 0.124$ mg/ ml
 Remaining concentration = $1 - 0.124 = 0.88$ mg/ ml (88%)

2- 1.0 % w/v labelled gel:

Amount for all volume (124ml) = $0.171 + 0.0146/197.42 = 0.0009$.

Dilution factor = $0.0009 \times 124 = 0.112$ mg/ ml
 Remaining concentration = $1 - 0.112 = 0.89$

mg/ ml (89%)

3- 1.5 % w/v labelled gel:

Amount for all volume (184ml) = $0.232 + 0.0146/197.42 = 0.0012$

Dilution factor = $0.0012 \times 184 = 0.221$ mg/ ml
 Remaining concentration = $1 - 0.221 = 0.78$ mg/ ml (78%)

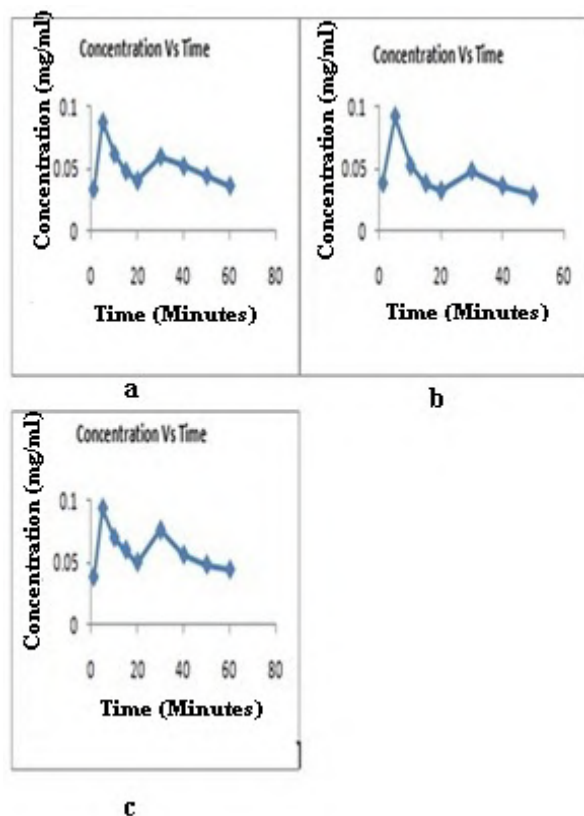


Figure (5). Concentrations of gellan gel forming with artificial gastric juice (HCL) in three different concentrations (a: 0.5, b: 1.0 and c: 1.5 %)

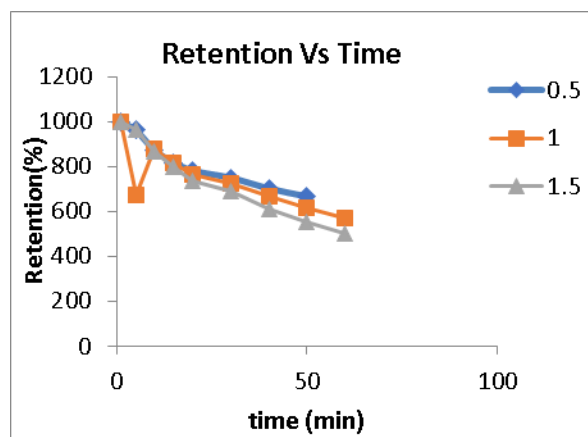
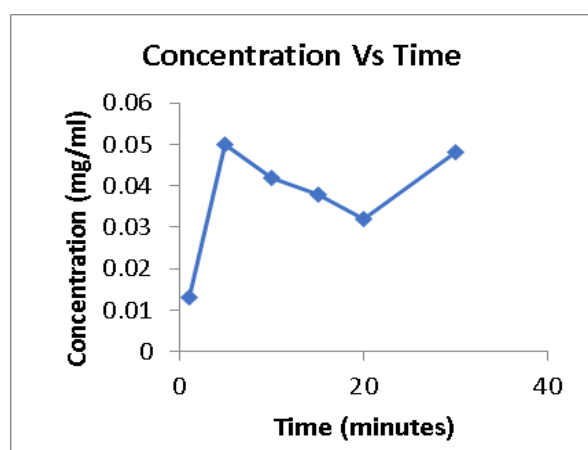
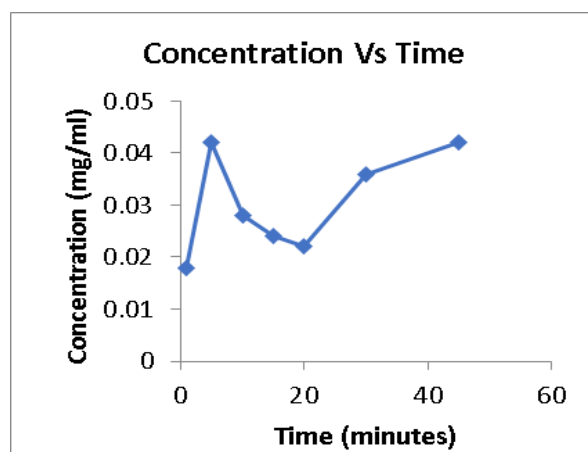


Figure (6). Comparing between retention amount of Methylene blue in different concentrations of labelled gel



(a)



(b)

Figure (7). Concentration of Methylene blue in various concentrations of labelled gel (a: 1.0 and b: 1.5 %)

4 Discussion

Figs. 5, 7, and 9 show the concentrations of Methylene blue which removed from the gel throughout 60 minutes intervals time by flowing physiological fluids over the gel. The results which can be obtained from the graphs show that the adhesion of Methylene blue stain with artificial saliva and tear better than with artificial gastric juice (HCL).

Figs 6, 8, and 10, illustrates the retention time of Methylene blue with three types of physiological fluids that mentions above in three different concentrations (0.5 %, 1%, 1.5 %) w/v. The graphs show that the retention time increases with low concentrations of labelled gel and decreases with high concentrations in three types of fluids.

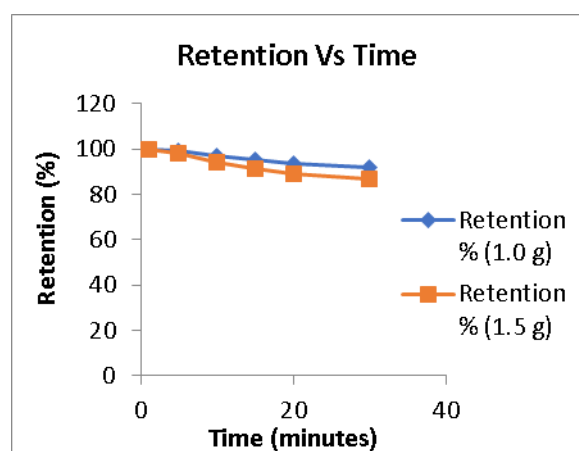


Figure (8). comparing between retention amounts of Methylene blue in different concentrations of labelled gel

5 Conclusion

Gellan gum is a bacterial polysaccharide, discovered through the screening of thousands of bacteria and prepared commercially by aerobic submerged fermentation from *Sphingomonas elodea*. The rheological behaviours like viscosity and oscillation effected by temperature, concentration, shear rate and stress.

The polymer as secreted by the microorganism contains approximately 1.5 acyl substituent per tetra saccharide repeating unit. The strength of gellan gum gels increases with the cations mono and divalent (Ca^+ , k^+ , H^+ and Mg^+) which present in physiological fluids such as gastric juice, saliva and tear fluid. Muco-adhesive polymers can be used as means of improving drug delivery through different routes like gastrointestinal and ocular.

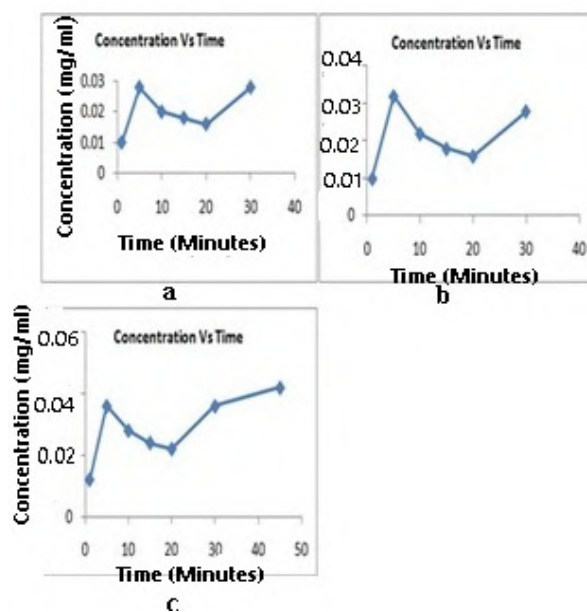


Figure (9). shows concentrations of gellan gel forming with artificial tear in three different concentrations (a:0.5, b:1.0, and c:1.5 %)

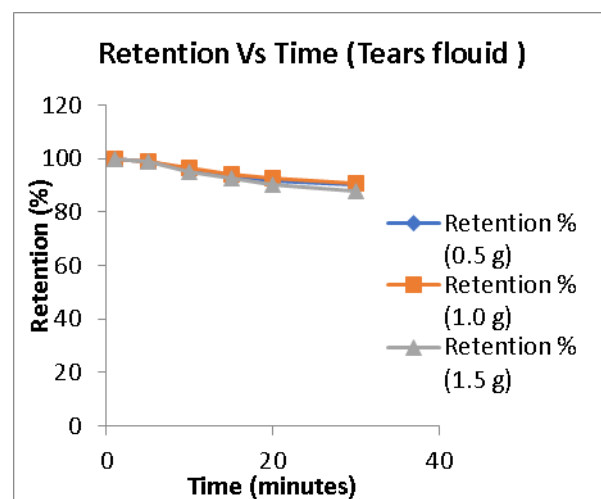


Figure (10). shows comparing between retention amounts of Methylene blue in different concentrations of labelled gel

References

- Batchelor, H. K., Banning, D., Dettmar, P.W., Hampson, F.C., Jolliffe, I. G., Craig, D. Q. M., (2002) An in vitro mucosal model for prediction of the bio-adhesion of alginate solutions to the oesophagus, *International Journal of Pharmaceutics*, 238: 1–2, 123-132.
- Bernkop-Schnürch, A., & Steininger, S. (2000). Synthesis and characterisation of mucoadhesive thiolated polymers. *International journal of pharmaceutics*, **194**(2), 239–247.
- Duchene, D., Touchard F., Peppos, N.A., (1988). *Drug Dev, Ind Pharm*, 14:283.

- Gilbard, J. P., Human tear film electrolyte concentrations in health and dry-eye disease, *Int Ophthalmol Clin.* 1994, 34:27-36.
- Glasgow, B. J, Gasymov, O. K., Abduragimov, A. R., Engle, J. J., Casey, R. C., (2010) Tear lipocalin captures exogenous lipid from abnormal corneal surfaces. *Invest Ophthalmol Vis Sci.* 51:1981-7.
- Huang, Y., (2004). Gelling temperatures of high acyl gellan as affected by monovalent and divalent cations with dynamic rheological analysis, *Carbohydr. Polym.* 56, 27-33.
- Humphrey, S. P., Williamson, R. T., (2001). A review of saliva: normal composition, flow, and function. *The Journal of Prosthetic Dentistry*, Vol. 85, 162.
- Jansson, P. E., Lindberg, B., and Sandford, P. A. (1983) Structural studies of gellan gum, an extracellular polysaccharide elaborated by *Pseudomonas elodea*, *Carbohydr. Res.*, 124, 135-139.
- Kamath, K. R, Park, K., (1994). Mucosal adhesive preparations, in *Encyclopaedia of Pharmaceutical Technology*; J. Swarbrick and J. C. Boylan, eds., Vol. 10 Marcel Dekker, New York, 133.
- Mao M., Tang J., Swanson B.G. (2000). Texture properties of high and low acyl mixed Gellan gels, *Carbohydr. Polym.*, 41, 331-338.
- Matricardi, P., Cencetti, C., Ria, R., Alhaique, F., and Coviello, T. (2009). Preparation and Characterization of Novel Gellan Gum Hydrogels Suitable for Modified Drug Release, *Molecules*, 14, 3376-3391.
- Nagai T, Machida Y. (1985). Mucosal adhesive dosage forms, *Pharm Int*, 6: 196-200.
- Sanderson, G. R., Clark, R. C., (1983). Gellan gum, *Food Technology*, 37, 62-70.
- Stjernschantz, J., Astin, M., (1993). Anatomy and physiology of the eye physiological aspects of ocular drug therapy, In: *Biopharmaceutics of Ocular Drug Delivery*, Edman, P. ed., CRC Press, Boca Raton, pp. 1-25.



Petrophysical Characterizations of Some Reservoir Formations in Ghani Oilfield, Libya

Ibrahim M. Abou El Leil¹, Farag Adam² and Ahmed Mohammed^{2*}

¹Petroleum Engineering Department, Engineering Faculty, Tobruk University, Libya.

²Geology Department, Science Faculty, Tobruk University, Libya.

DOI: <https://doi.org/10.37375/sjfsu.v2i2.515>

A B S T R A C T

ARTICLE INFO:

Received 19 August 2022.

Accepted 03 September 2022.

Published 27 October 2022.

Keywords:

Petrophysical properties, core samples relative permeability, resistivity index formation factor, correlation

This study has been conducted on three types of reservoir rocks for core analysis of samples denoted by R-1, R-2 and R-3 of Ghani oil field from three reservoir include Farrud, Facha and Mabruk formations respectively. This analysis includes determination of physical characteristics e. g. porosity (ϕ), permeability (k), formation factor (FF) and resistivity index (RI). The purpose of this study is to how core petrophysical data might be most investigating effectively applied to the petrophysical prediction of petrophysical properties from core samples analysis. For Farrud reservoir of R-1 shows that the relation between degree of saturation (S_w) and relative oil permeability (K_{ro}) equal the relative permeability of water (K_{rw}) at which the intersection point between the two curves; whereas, the flow with the same rate. FF and RI are vary with ϕ and the RI is a function of S_w . The gas-oil relative permeability have been expressed graphically. Whereas, the intersection point between the two curves (K_{ro}) equal the (K_{rg}), at which both oil and gas are flow with the same rate. A similar results were obtained from Facha reservoir, R-2. The petrophysical properties of core samples for R-3 of Mabruk Formation have been performed including ϕ , k, and S_w . The comparison between the three reservoirs by correlation between the average values such as ϕ , k, grain density and RI; shows that the average of Mabruk reservoir k greater than the other two reservoirs, while the other properties seem to be close together.

1 Introduction

The analysis of petrophysical data seeks to describe the formation under study by quantifying certain of its properties such as porosity, permeability, fluid saturation and mineralogy. The natural ordering of geological systems arising from the controlling influences of sedimentary environment, other rock-forming processes and rock mechanics imparts an ordering to the petrophysical properties of interest. Recognition of the inherent ordering, usually manifest as structure in the petrophysical data available for analysis, assists both in the identification of the petrophysical interpretation model to be applied, and in the characterization of the

variation present in the formation to facilitate the quantification of geologically distinctive genetic units in terms of their petrophysical properties.

A definition of petrophysical rock types might be 'classes of rock characterized by differences in physical properties. The properties of interest could be the basic formation properties that we seek to measure in petrophysical analyses, viz. density, resistivity, hydrogen, index, acoustic travel time or they might be the formation parameters of porosity, permeability, capillarity, saturation etc. that we infer from out

measurements of the basic properties. The fundamental controlling phenomena for nearly all of these properties are the quantity, shape, size and connectivity of the pore system (i.e. the pore geometry of the rock). Together with the mineralogy and texture of the rock fabric, both of which, jointly and severally, control the pore geometry, these are the fundamental subjects of importance in petrophysical investigations (Steve Cannon., 2016).

Figure 1 illustrated the integrated petrophysical evaluation data. On the other hand, logs do not measure porosity, permeability or water saturation; they make measurements of various parameters and relationships between the rock and the fluids to allow computer programs to process and interpret the results. The petrophysicist role is to validate and organize the input data and to understand and calibrate the results.

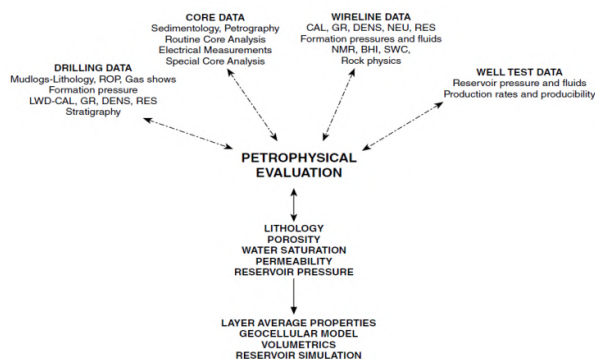


Figure (1). The integrated petrophysical evaluation data (Steve Cannon., 2016)

2 Cores and Logs

The two primary sources of reservoir information acquired during drilling of a well are cores and logs. Coring can be an expensive and time-consuming process that is usually reserved for potential reservoir sections. When the top reservoir is reached, signaled by a rapid increase in drilling rate and the presence of hydrocarbon shows, drilling is halted and the drill string recovered and the bit replaced with a core barrel. Core barrels are usually made up of 30 ft lengths of pipe with a special coring head and retrieval mechanism, the catcher.

There are in fact an inner and an outer barrel that can rotate independently; the inner barrel is the repository for the core as it is being cut. Upon retrieval at the surface, the core is stabilized and sent to shore for analysis; on occasion, some samples are evaluated at the well site, but this is becoming less and less common (Steve Cannon., 2016).

3 Study Objectives

This study is mainly aimed to take some initial steps towards this goal by how core petrophysical data might be most investigating effectively applied to the petrophysical prediction of petrophysical properties from core samples analysis. Also, to integrate petrophysical data of core samples to qualify and quantify reservoirs in order to assess the production potential of Farrud, Facha and Mabruk reservoirs in Ghani oilfield. The objectives include:

1. Interpretation of porosity, permeability and saturation data.
2. Comparison of the petrophysical core data of investigated formations with each other's.
3. Integration of all the available data to evaluate the wells performance.

4 Materials and Methods

4.1. Sample Preparation

Full diameter cores from different sections of Farrud, Facha and Mabruk reservoirs in the Ghani field (Figure 2), were supplied for use in this special core analysis study. From each formation, a full diameter core piece was taken for conventional core analysis determinations, and three one and half inch diameter plug samples were drilled for core analysis tests using tap water as the bit lubricant. These samples are briefly described with respect to depth and lithology. The rock types of these formations can be characterized as carbonate rocks represented by limestone and dolomitic.

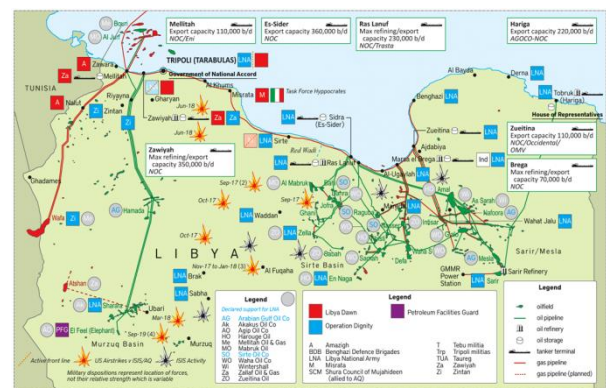


Figure (2). Location map of Ghani and other oilfields (Arabian Gulf Petroleum Company., 2018)

The size and form of samples used in laboratory vary from drilling cuttings, loose sands and coarse pieces of consolidated rocks up to samples of regular geometrical shape. The most commonly core samples used form is the cylinder. The cylindrical samples or as known as core plugs are cut from the full diameter cores, about 10 cm in diameter sampled (Figure 3).



Figure (3). Full diameter core (left) and core plugs (right) cut for laboratory measurements

The plug and full diameter samples were trimmed to right cylinder cleaned in hot refluxing xylene and methanol to remove residual hydrocarbons and salts and dried in an oven at 60°C.

4.2. Water-Oil Relative Permeability

Following gas-oil relative permeability tests four samples were scheduled to undergo water-oil relative permeability testing. Water-oil relative permeability were performed using simulated formation brine as a displacing phase. Incremental volumes of water and oil produced were recorded as a function of time.

4.3. Factor of Formation Resistivity and Resistivity Index

Eight core plug samples, labeled 1A through 8A were scheduled to undergo electrical resistivity tests. The clean dry samples were evacuated and pressure saturated with simulated formation brine.

4.4. Gas-Oil Relative Permeability

Eight core plug samples were scheduled for gas-oil relative permeability tests. The clean dry samples were evacuated and pressure saturated with simulated formation brine.

5 Literature Review

Several authors have been studied the petrophysical using cores, logs, well test, publications, and production data.

5.1. Overview

(Paul & Gaffney., 2003) the role of core samples for the investigation of reservoir petrophysical characterizations and correlation between the static and dynamic reservoir models.

The integrated analysis petrophysical well core data is required for the study essentially focused on reservoir

properties e. g. lithology, depositional environments, shale volume porosity (Φ), permeability (K), fluid saturation, net pay thickness, among others from well logs and cores, which are variables that determine reservoir quality. The relationships between these parameters showed linear trends (Ulasi et al., 2012).

An engineer or geologist or geophysicist can interpret the log readings to reach certain conclusions about the formation. Fresh water, oil and gas are poor conductors of electricity, so they are high resistivity. By contrast, the formation waters are salty enough that they conduct electricity with ease. The formation waters generally have low resistivity because of high salinity. Hydrocarbon saturation and formation porosity are the two key parameters determined from core that are used in the evaluation of a subsurface reservoir as a potential hydrocarbon producer (Ahammad et al., 2014).

Presented study which performed on the core samples to determine and evaluate the petrophysical properties of oil field. The evaluated properties include porosity, permeability, fluid saturation, net/gross thickness and mobility which are all inferred from geophysical wire-line logs. He concluded that these reservoir parameters are significant to evaluate reservoir performance and satisfactory for hydrocarbon production (Amigun & Odole., 2003).

was studied the Gir Formation at Ghani and Ed Dib Fields, Eastern Libya of Eocene (Ypresian) age comprises which a 500-1000m sequence of carbonates and evaporites deposited. He demonstrated that 70% of dolomites previously considered to be reservoir have little or no mobility and thus no reservoir potential, and permitted refined and more reliable calculations of oil in-place and producible reserves (Henry Williams., 2014).

Found that the analyses of well log data evaluate the hydrocarbon potential of reservoirs and quantitative interpretation determined parameters useful to compute the volume of identified oil and gas within the reservoir as well as estimate reservoir properties required for ease of developing and producing the field (Osinowo et al., 2018).

6 Results and Discussion

6.1. Core Analysis Techniques

The present study shows the experimental results of core analysis carried out on samples from three wells are R-1, R-2 and R-3 of Ghani oil field from three reservoir formations include Farrud, Facha and Mabruk formation respectively. This analysis includes:

1. Determination of physical characteristics e. g. porosity, permeability.
2. Formation factor and resistivity index measurements.

6.2. Core Analysis of Well No. R-1

6.2.1. Farrud Reservoir

6.2.1.1. Measurements of Water-Oil Relative Permeability

These measurements of water-oil relative permeability with connate water were carried out on four samples from Farrud Formation with numbers 3V, 5V, 9V and 13V.

6.2.1.2. Relative Permeability Investigations

All the tests previously mentioned were conducted in two-fluid systems, one of which was always gas. From these data we can concluded which are shown in Figure 4 through Figure 11 that relative permeability was substantially independent of fluid viscosity but was some function of pore-size distribution, pressure and fluid saturations.

The fluids used in obtaining these data were water and air in the core sample tests, where water is the wetting fluid. The curve labeled K_{rw} denotes the relative permeability to water, while that labeled K_{ro} denotes the relative permeability to oil.

The trends which are presented in these figures The K_{rw} curve is typical of the trend of relative permeability curves for the wetting phase in a porous system regardless of whether that phase is water. The relative permeability to the wetting phase shows a rapid decline in value for a small decreases in an original high saturation of that particular phase. The relative permeability for the wetting phase normally approaches zero or vanishes at saturations of the wetting phase greater than zero. Likewise, the K_{ro} curve is typical of the relative permeability to a non-wetting phase, whether that phase is gas, oil, or water.

From relation between degree of saturation and relative permeability, we can noted that the intersection point between the two curves, the relative permeability of oil (K_{ro}) equal the relative permeability of water (K_{rw}), at which both oil and water are flow with the same rate. This does not mean that the amount of flow of both two fluids are equal, because of their different viscosities, hence the water will flow in great amount comparing with oil. This point is varies from sample to another due to the different porosities and permeability.

On the other hand, water-oil relative permeability have been presented in Tables 1 through 4 (Appendix A); and expressed graphically for the different samples as shown in Figure 4 through Figure 7.

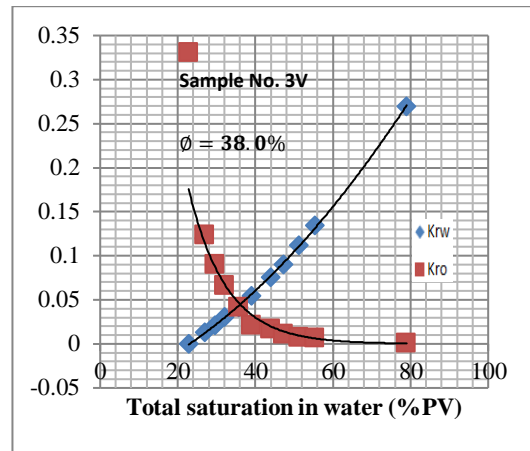


Figure (4). k_{ro}/k_{rw} versus total saturation in water (%PV)

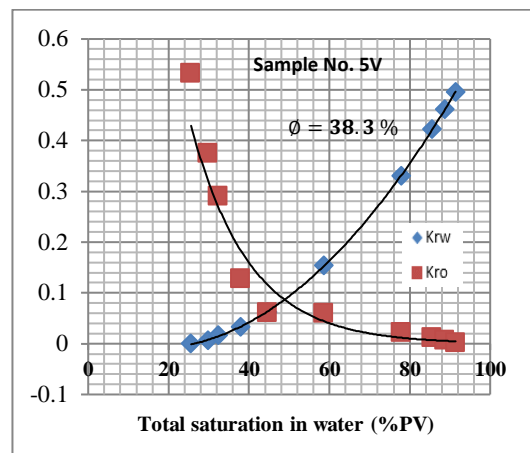


Figure (5). k_{ro}/k_{rw} versus total saturation in water (%PV)

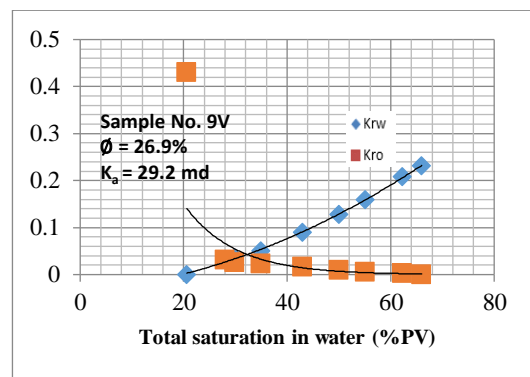


Figure (6). k_{ro}/k_{rw} versus total saturation in water (%PV)

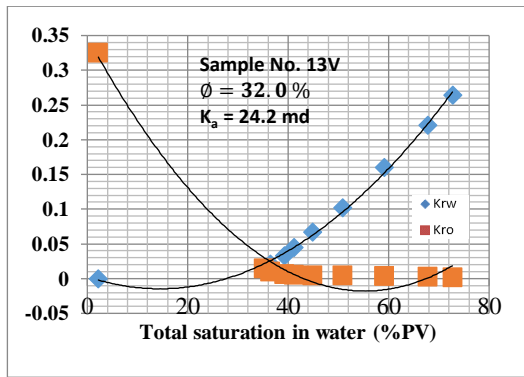


Figure (7). k_{ro}/k_{rw} versus total saturation in water (%PV)

Bilogarithmical crossplots of k_w/k_o , k_{ro}/k_{rw} ratios and total saturation in water (%PV), are illustrated in Figure 8 through Figure 11.

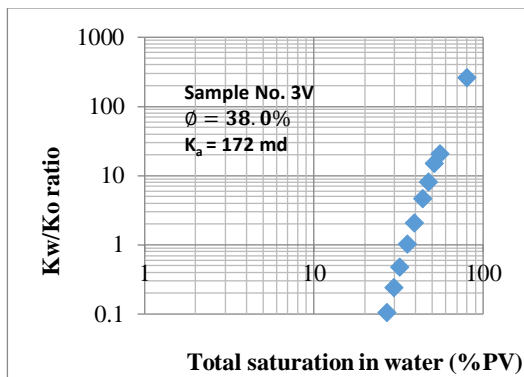


Figure (8). $\frac{k_w}{k_o}$ ratio versus total saturation in water (%PV)

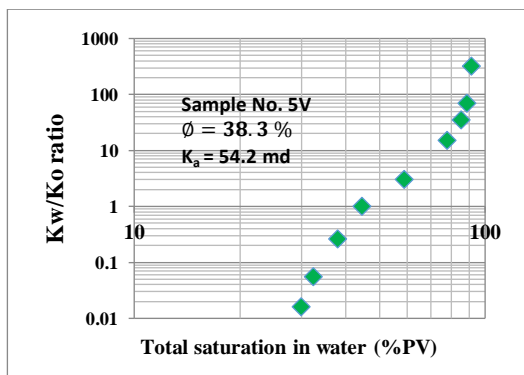


Figure (9). The $\frac{k_w}{k_o}$ ratio versus total saturation in water (%PV)

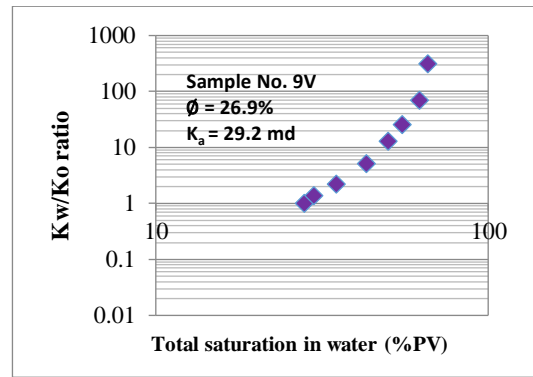


Figure (10). $\frac{k_w}{k_o}$ ratio versus total saturation in water (%PV)

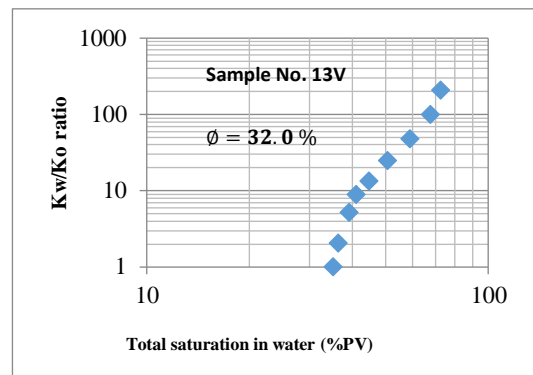


Figure (11). $\frac{k_w}{k_o}$ ratio versus total saturation in water (%PV)

6.2.1.3. Formation Resistivity Factor and Resistivity Index

There are some petrophysical characterization parameter such as formation resistivity factor, permeability, porosity, grain density, water saturation and resistivity index have been estimated for core samples are presented in Table 5 (Appendix A).

Resistivity and formation factor vary with porosity in somewhat the manner described by the previously. Rarely do natural formations have such uniform pore geometry. It is more common to express formation factor as:

$$FF = a\phi^{-m} \quad [1]$$

Where a and m are unique rock properties.

By plotting F factor against porosity on a log-log plot for a number of similar rock types, it is possible to obtain the slope of the line, m , or the cementation factor (Figure 12). The value of m varies for different rock types as a function of degree of cementation, ranging from < 1.6 for poorly cemented rocks to > 3.5 for very well cemented rocks; the default_value of m is usually 1.8-2.2 (Figure 13). The tortuosity factor, a reflects the complexity of the

connected pores and is usually set to 1.0. The principle of estimation and experimental determination. Plotting the results of each measurement determines a slope *m* that relates FF to porosity, known as the exponent of cementation.

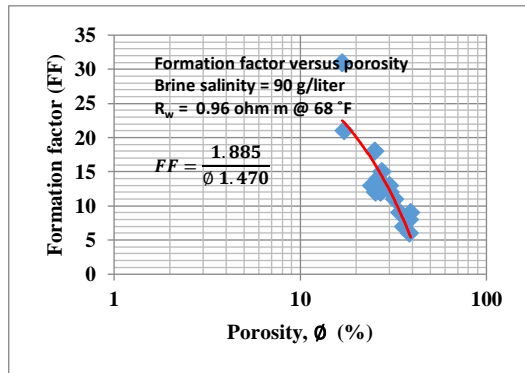


Figure (12). Correlation diagram between FF and porosity ϕ

Oil and gas are not electrical conductors. Their presence in an element of reservoir or in a core sample will reduce the mean cross sectional area of the flow path for an electric current and increase the length of the flow path, thus increasing the resistivity.

Resistivity index is defined as the ratio of rock at any condition of gas, oil and water saturation to its resistivity when completely saturated with water:

$$RI = \frac{R_t}{R_o} = S_w^{-n}, \quad \text{or} \quad \frac{1}{S_w^n} \quad [2]$$

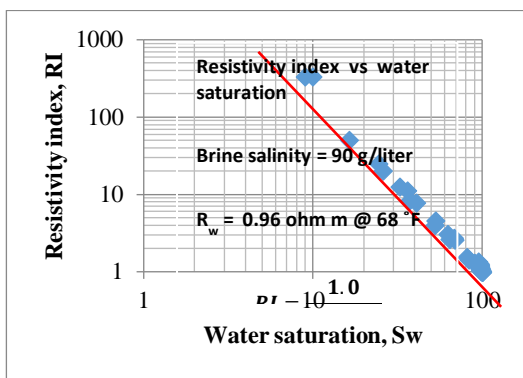


Figure (13). Correlation diagram between S_w and RI

Thus, the resistivity index is a function of water saturation. It is also a function of the pore geometry. The presence of cation exchangeable clays (smectites, or mixed layer clays), cause apparently low resistivity index values to be observed.

6.3. Core Analysis of Well No. R-2

6.3.1. Facha Reservoir

The core samples analysis of well R-2 of Facha reservoir include water saturation and permeability.

6.3.1.1. Water Saturation and Porosity

Also, from the results of experimental work on a core samples of Facha Formation of water saturation, height above free water level and porosity, exhibit that the water saturation as a function of height above free water level and porosity are presented in Table 1 (Appendix B) and Figure 14.

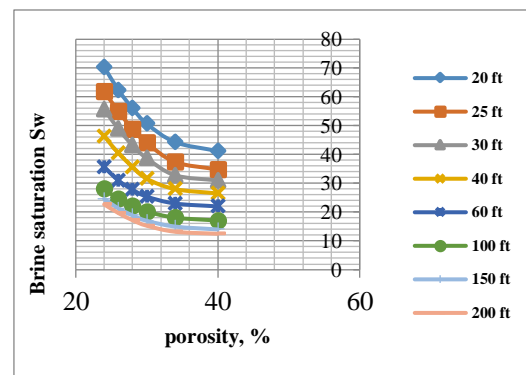


Figure (14). Water saturation as a function of height above free water level and porosity

6.3.1.2. Porosity–Permeability Correlations

Both porosity and permeability play an important role in reservoir description because the former describes reservoir storage capability, while the later describes the ability of the rock formation to transmit fluids. However, cross plots of these reservoir variables show that porosity seldom has a statistical correlation to permeability significant enough to develop predictive models.

Since permeability depends on the interconnection between pore space there is not theory, or in fact, a unique relationship between the porosity of a rock and its permeability. For unconsolidated rock, it's possible to establish relationships between porosity and either some measure of apparent pore diameter and permeability. However, these have very limited application.

In some cases, there is sometimes a reasonable relationship between the porosity of a rock and its permeability, although for a given porosity, permeability can vary widely. Figure 15 shows porosity–permeability correlation obtained from core analysis.

The correlation of Figure 15 consists of different reservoir samples from core analysis. It is obviously that increase of permeability with an increase in porosity, the

correlation shows the wide spread, lack of close relation between porosity and permeability.

The core porosity values were plotted against to permeability values as shown in Figure 15, and both regression equation and correlation coefficient (r) were computed for set points. The computed regression equation of $y = 0.0567x + 24.421$ was used to fit a regression line to the points for Facha reservoir. The correlation coefficient r of 0.7356 shows strong linear relationship between the two variables in this reservoir by linear fitting.

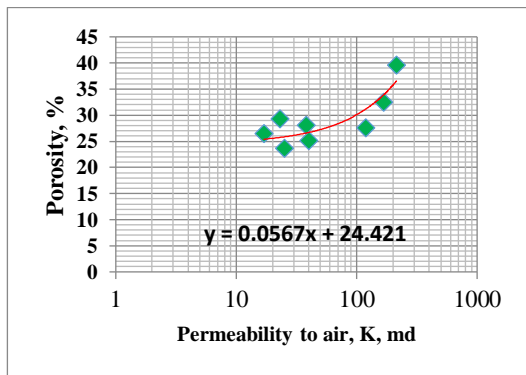


Figure (15). Relationship between porosity and permeability

On the other hand, Figure 16 shows the relationship between porosity and formation resistivity factor (FF) on a bilogarithmical plot. While Figure 17 gives the relation between brine saturation and resistivity index (RI), both of them illustrate a linear regression coefficient.

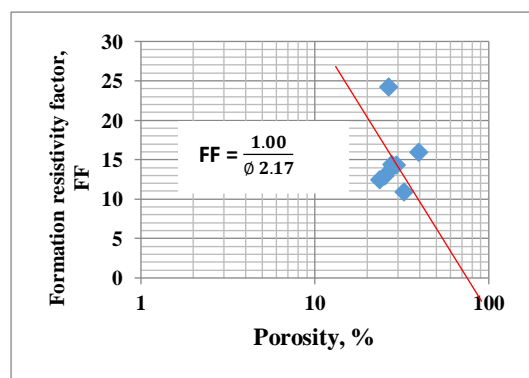


Figure (16). Relationship between porosity and formation resistivity factor (FF)

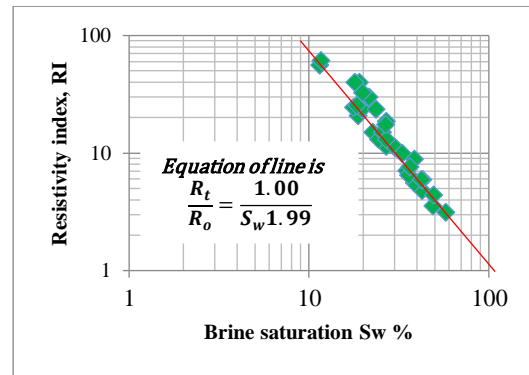


Figure (17). Relationship between brine saturation and resistivity index (RI)

6.3.1.3. Gas-Oil Relative Permeability

On the hand, the same eight core samples have been investigated for gas-oil relative permeability. The gas-oil relative permeability have been expressed graphically for the different samples as shown in Figure 18 through Figure 25, also, given in Tables 2 to 9 (Appendix B).

From relation between degree of saturation and relative permeability, we can noted that the intersection point between the two curves the relative permeability of oil (K_{ro}) equal the relative permeability of gas(K_{rg}), at which both oil and gas are flow with the same rate. This does not mean that the amount of flow of both two fluids are equal, because of their different viscosities, hence the gas will flow in great amount comparing with oil. This point is varies from sample to another due to the different porosities and permeability.

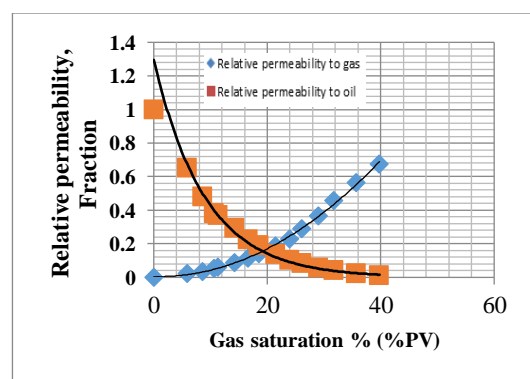


Figure (18) Relative permeability to oil and gas for sample 1C

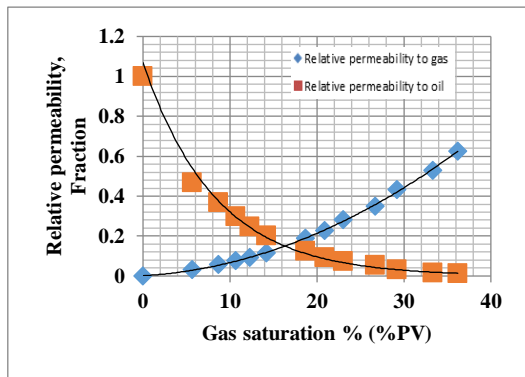


Figure (19) Relative permeability to oil and gas for sample 2C

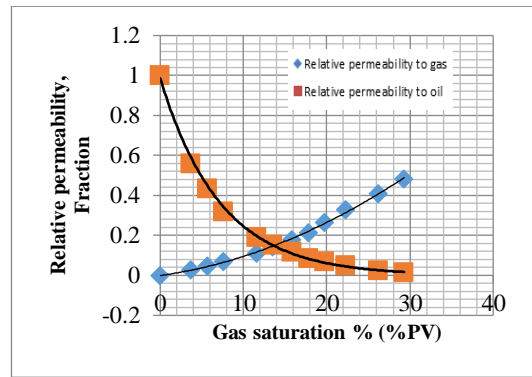


Figure (23) Relative permeability to oil and gas for sample 6C

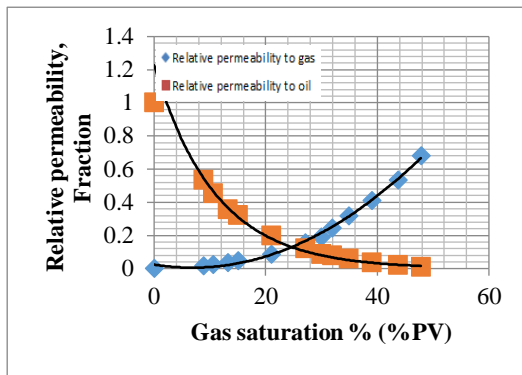


Figure (20) Relative permeability to oil and gas for sample 3C

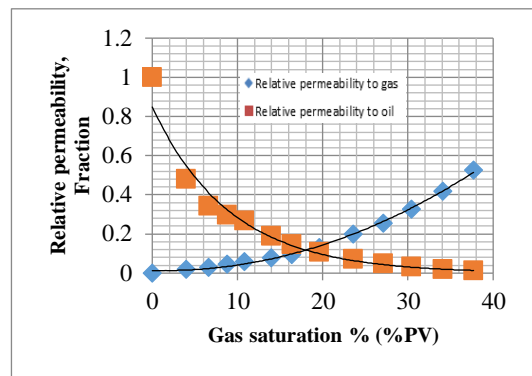


Figure (24) Relative permeability to oil and gas for sample 7C

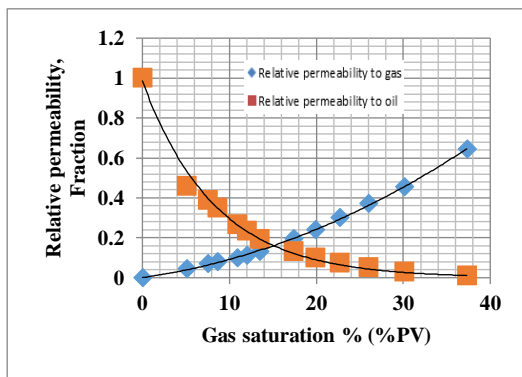


Figure (21) Relative permeability to oil and gas for sample 4C

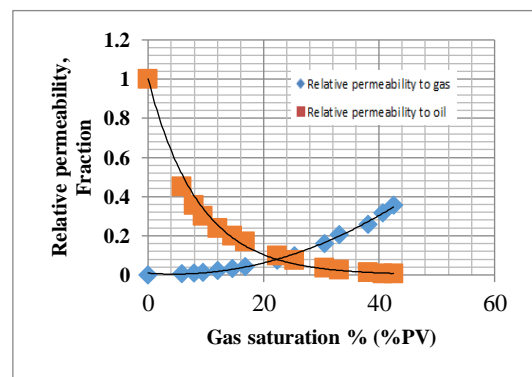


Figure (25) Relative permeability to oil and gas for sample 8C

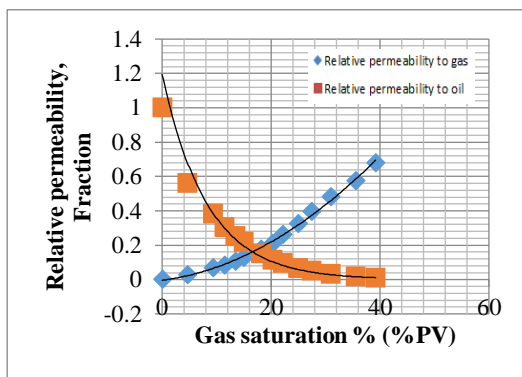


Figure (22) Relative permeability to oil and gas for sample 5C

6.4. CORE ANALYSIS OF WELL NO. R-3

6.4.1. MABRUK RESERVOIR

The petrophysical properties of twelve core samples from well No. R-3 of Mabruk Formation have been performed on include porosity, permeability and brine saturation as depicted in Table 1 (Appendix C).

The correlation of Figure 26 consists of different reservoir samples from core analysis. It is obviously that the increase of permeability is slightly with an increase in porosity, the correlation shows the wide spread, lack of close relation between porosity and permeability. However, Figure 26 depicts the relationship between porosity and permeability with a simple linear regression of weak correlation coefficient 0.1971.

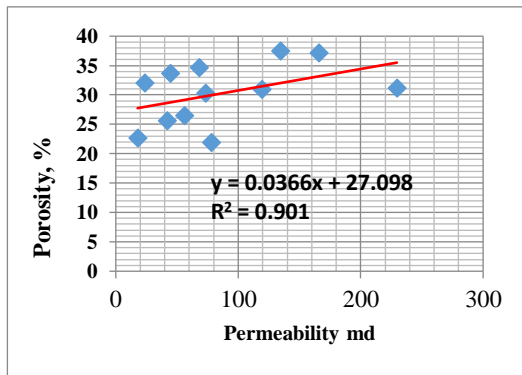


Figure (26). Correlation between porosity and permeability of investigated samples

Figure 27 gives a correlation between the average values of some petrophysical properties such as porosity, permeability, grain density and formation resistivity factor of investigated reservoirs of Farrud, Facha and Mabruk. It is obviously that the average of Mabruk reservoir permeability greater than the other two reservoirs, while the other properties seem to be close to each other's.

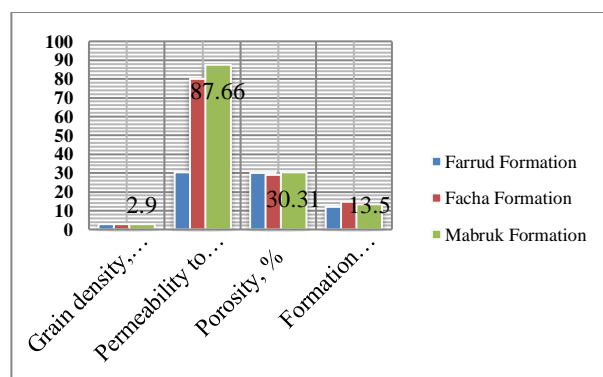


Figure (27). Correlation between the petrophysical properties of investigated reservoirs

7 Conclusions

From the previous study that have been carried out on three different reservoir rocks for Farrud, Facha and Mabruk to estimate the petrophysical properties of formation bearing hydrocarbons through different analyses include porosity (ϕ), permeability (k), formation

factor (FF) and resistivity index (RI) we can concluded the following:

The laboratory investigations of relative permeability of *Farrud reservoir* for well R-1 show that the relation between degree of saturation (S_w) and relative permeability gives an intersection point between the two curves, the relative permeability of oil (K_{ro}) equal the relative permeability of gas (K_{rg}), at which both oil and gas are flow with the same rate.

Bilogarithmical crossplots of k_w/k_o , k_{ro}/k_{rw} ratios and total saturation in water, illustrated variable trends, this is attributed to the different properties of studied samples.

The core samples analysis of well R-2 of *Facha reservoir* include S_w , and k . The relation between S_w is a function permeability. Also, the results of water saturation, ϕ and k are obviously show that S_w is a function of permeability.

The relationship between porosity and formation resistivity factor (FF) on a bilogarithmical plot and the relation between brine saturation and resistivity index (RI), both of them gives a linear regression coefficient.

From relation between degree of saturation and relative permeability, we can noted that the intersection point between the two curves the relative permeability of oil (K_{ro}) equal the relative permeability of gas (K_{rg}), at which both oil and gas are flow with the same rate. This point is varies from sample to another due to the different porosities and permeability.

For well No. R-3 of *Mabruk Formation* study performed on ϕ , k , and S_w , the results revealed that the correlation of different reservoir samples from core analysis show that the increase of k is slightly with an increase in ϕ .

The comparative study between the three reservoir rocks has been carried out by correlation between the average values of some petrophysical properties such as ϕ , k , grain density and formation resistivity factor of investigated formations of *Farrud*, *Facha* and *Mabruk*. Whereas, the average of Mabruk reservoir k greater than the other two reservoirs, while the other properties seem to be close together.

8 Recommendations

In the light of the previous study we can recommend the following:

1. It is important to study the petrophysical properties of formation bearing hydrocarbons to evaluate this formation and enable us to estimate the hydrocarbon reserves.
2. Petrophysical parameters must be study to determine reservoirs performance.

3. To perform a correlation between the different formation to evaluate these parameters.
4. Comparing between laboratory investigations of petrophysical properties and results that have been obtained by different well logs.

References

- Arabian Gulf Petroleum Company, AGOCO, (2018).
- Paul, F., & Gaffney, W. (2003). The application of cutoffs in integrated reservoir studies. *Society of Petroleum Engineers*, 84387, 1-16.
- Ahammod, S., Hai, M. A., Islam, M. R., & Abu, S. M. (2014). Petro-Physical Analysis Of Reservoir Rock Of Fenchuganj Gas Field (Well# 03) Using Wireline Log. *American Journal of Engineering Research (AJER)*, 3(8), 37-48.
- Amigun, J. O., & Odole, O. A. (2013). Petrophysical properties evaluation for reservoir characterisation of Seyi oilfield (Niger-Delta). *International Journal of innovation and applied studies*, 3(3), 756-773.
- Henry Williams (2014) The Eocene Gir Formation of the Ghani and Ed Dib Fields, Eastern Libya -An example of "Virtual Core Study" Search and Discovery Article #20288 (2014).
- Osinowo, O. O., Ajayi, F. S., & Akeye, N. A. (2018). Petrophysical Properties' Evaluation for Reservoir Characterization of AK Field, Onshore Eastern Niger Delta, Southern Nigeria. *Advances in Petroleum Exploration and Development*, 15(1), 30-40.
- Steve Cannon (2016) *Petrophysics: A Practical Guide*, First Edition, John Wiley & Sons. Ltd. Published 2016 by John Wiley & Sons. Ltd.
- Ulasi, A. I., Onyekuru, S. O., & Iwuagwu, C. J. (2012). Petrophysical evaluation of Uzek Well using well log and core data, Offshore Depobelt, Niger Delta, Nigeria. *Advances in applied science research*, 3(5), 2966-2991.

Appendices

Appendix A

Table (1) Relative permeability water/oil measurements

<u>Sample No.: 3V</u>			
Permeability to air $K_a = 172$ md		Porosity $\phi = 38\%$	
Permeability to liquid $K_L = 155$ md		Connate water $S_{cw} = 22.8\%$	
Permeability to oil $K_o = 51.3$ md		Oil in place (%PV) $S_o = 77.2\%$	
Permeability to water $K_w = 31.4$ md and with residual oil		Residual saturation (% PV) $S_{ro} = 34.3$	
		Oil recovery (% PV) $R_o = 42.9\%$	
Total saturation in water (%PV)	$\frac{k_w}{k_o}$ ratio	Rel. perm. to water (Fraction) k_{rw}	Rel. perm. to oil (Fraction) k_{ro}
22.8	0	0	0.331
27.0	0.105	0.013	0.124
29.6	0.240	0.021	0.090
32.1	0.470	0.031	0.066
35.7	1.01	0.042	0.042
39.1	2.05	0.055	0.021
44.0	4.60	0.076	0.017
47.3	8.10	0.090	0.011
51.2	15.0	0.112	0.0075
55.3	20.6	0.135	0.0066
79.0	260	0.270	0.0008

Table (2) Relative permeability water/oil measurements

<u>Sample No.: 5V</u>			
Permeability to air $K_a = 54.2$ md		Porosity $\phi = 38.3\%$	
Permeability to liquid $K_L = 46.2$ md		Connate water $S_{cw} = 25.6\%$	
Permeability to oil $K_o = 24.6$ md		Oil in place (%PV) $S_o = 74.4\%$	
Permeability to water $K_w = 22.9$ md and with residual oil		Residual saturation (% PV) $S_{ro} = 8.6$	
		Oil recovery (% PV) $R_o = 65.8\%$	
Total saturation in water (%PV)	$\frac{k_w}{k_o}$ ratio	Rel. perm. to water (Fraction) k_{rw}	Rel. perm. to oil (Fraction) k_{ro}
25.6	0	0	0.532
29.9	0.016	0.006	0.375
32.4	0.055	0.016	0.290
37.9	0.26	0.033	0.127
44.6	1.01	0.062	0.061
58.6	3.05	0.154	0.059
77.9	15.0	0.330	0.022
85.5	35.0	0.423	0.012
88.8	70.5	0.462	0.0066
91.4	317	0.495	0.0016

Table (3) Relative permeability water/oil measurements

<u>Sample No.: 9V</u>			
Permeability to air $K_a = 29.2$ md		Porosity $\phi = 26.9\%$	
Permeability to liquid $K_L = 24.2$ md		Connate water $S_{cw} = 20.6\%$	
Permeability to oil $K_o = 10.4$ md		Oil in place (%PV) $S_o = 79.4\%$	
Permeability to water $K_w = 5.6$ md and with residual oil		Residual saturation (% PV) $S_{ro} = 34.0$	
		Oil recovery (% PV) $R_o = 45.4\%$	
Total saturation in water (%PV)	$\frac{k_w}{k_o}$ ratio	Rel. perm. to water (Fraction) k_{rw}	Rel. perm. to oil (Fraction) k_{ro}
20.6	0	0	0.430
28.0	1.0	0.032	0.032
29.9	1.4	0.036	0.026
34.9	2.2	0.050	0.023
43.0	5.2	0.090	0.017
50.0	13.1	0.128	0.0097
55.1	26.1	0.159	0.0061
62.2	70.0	0.208	0.0030
66.0	315	0.231	0.0008

Table (4) Relative permeability water/oil measurements

Sample No.: 13V			
Permeability to air $K_a = 24.2$ md		Porosity $\phi = 32.0\%$	
Permeability to liquid $K_L = 21.2$ md		Connate water $S_{cw} = 32.2\%$	
Permeability to oil $K_o = 6.9$ md		Oil in place (%PV) $S_o = 67.8\%$	
Permeability to water $K_w = 5.6$ md and with residual oil		Residual saturation (% PV) $S_{ro} = 27.3$	
		Oil recovery (% PV) $R_o = 40.5\%$	
Total saturation in water (%PV)	$\frac{k_w}{k_o}$ ratio	Rel. perm. to water (Fraction) k_{rw}	Rel. perm. to oil (Fraction) k_{ro}
2.2	0	0	0.325
35.1	1.0	0.015	0.015
36.4	2.05	0.021	0.010
39.2	5.20	0.033	0.0063
41.1	8.90	0.045	0.0051
44.8	13.50	0.067	0.0049
50.8	25.0	0.102	0.0041
59.1	48.0	0.160	0.0033
67.8	100.0	0.221	0.0022
72.7	210.0	0.264	0.0013

Table (5) Petrophysical characterization parameter of core samples

Sample No.	Depth, ft.	Grain density, gr/cm ³	Permeability to air, K, md	Porosity, %	Formation resistivity factor, FF	Water saturation S_w	Resistivity index, RI
3V	5947	2.83	119	38.5	8.0	100	1
						98.1	1.05
						83.6	1.41
						64.4	2.63
						37.4	8.33
						16.4	50.00
						10.0	333.23
5V	5954	2.84	32.9	38.5	6	100	1
						99.5	1.01
						99.2	1.05
						98.0	1.12
						96.5	1.23
						36.1	11.11
						9.0	333.23
7V	5955	2.75	2.1	26.1	14	100	1
						98.9	1.02
						98.0	1.05
						96.8	1.09
						81.7	1.54
						52.7	4.00
						26.0	20.00
9V	9560	2.74	15.3	27.0	12	100	1
						99.2	1.03
						97.7	1.08
						90.1	1.30
						68.6	2.70
						53.0	4.55
						32.5	12.50
13V	5982	2.70	11.6	32.0	11	100	1
						99.0	1.04
						98.1	1.09
						96.8	1.27
						62.6	3.03
						40.8	7.69
						24.5	25.00
17V	5993	2.74	0.4	17.2	21	100	1
						98.8	1.01

						98.2	1.12
						97.7	1.18
						97.4	1.23
						95.0	1.35
						69.0	2.56
\bar{x}		2.77	30.22	29.88	12.0		

\bar{x} = Values average

FACHA FORMATION

Appendix B

Table (1) Water saturation, height above free water level and permeability of Facha reservoir

Selected Permeability to air, md	Water saturation S_w (% VP) Height above free water, feet							
	Height above free water, feet							
	20	25	30	40	60	100	150	200
	Water saturation S_w (% VP)							
15	90.6	78.3	70.8	59.7	46.8	40.0	36.2	34.0
20	81.4	71.4	64.4	53.7	41.3	35.2	31.5	29.4
30	69.3	60.6	54.3	45.2	36.0	30.3	26.7	24.8
40	64.5	56.2	50.2	41.1	33.7	27.8	24.2	22.3
50	60.4	52.3	46.4	38.0	31.7	26.2	22.6	20.7
70	55.9	48.0	42.3	35.3	29.8	24.6	21.1	19.2
100	51.3	43.6	38.3	32.8	27.9	23.2	19.6	17.8
200	45.8	38.7	34.3	29.9	25.6	21.2	18.2	16.4

Table (2) Gas-oil relative permeability

Sample identification: 1C Sample depth: 5,772 feet Permeability to air: 47 md		Porosity: 26.3 % Initial water saturation: 12.8 % Effective permeability to air: 39 md	
Gas saturation % (%PV)	Gas-oil relative permeability ratio	Relative permeability to gas*, fraction	Relative permeability to oil*, fraction
0.0	0.000	0.000	1.000
5.9	0.032	0.021	0.652
8.6	0.073	0.035	0.481
10.6	0.136	0.052	0.381
11.3	0.162	0.060	0.370
14.3	0.303	0.089	0.293
16.6	0.500	0.112	0.223
18.5	0.739	0.141	0.190
21.5	1.360	0.188	0.138
23.9	2.220	0.228	0.103
26.1	3.520	0.291	0.083
29.0	6.440	0.365	0.057
31.7	11.20	0.458	0.041
35.7	24.40	0.564	0.023
39.8	62.40	0.674	0.011

* Relative to the effective permeability to oil at initial water saturation

Table (3) Gas-oil relative permeability

Sample identification: 2C Sample depth: 5,775 feet Permeability to air: 27 md		Porosity: 25.6 % Initial water saturation: 8.0 % Effective permeability to air: 20 md	
Gas saturation % (%PV)	Gas-oil relative permeability ratio	Relative permeability to gas*, fraction	Relative permeability to oil*, fraction
0.0	0.000	0.000	1.000
8.8	0.034	0.018	0.533
10.5	0.051	0.023	0.452
13.2	0.097	0.035	0.358

15.0	0.146	0.047	0.322
21.0	0.435	0.087	0.199
27.1	1.270	0.156	0.123
29.9	2.160	0.190	0.088
31.9	3.130	0.243	0.078
34.9	5.240	0.318	0.061
39.0	10.90	0.411	0.038
43.7	26.40	0.536	0.020
47.8	61.20	0.683	0.011

* Relative to the effective permeability to oil at initial water saturation

Table (4) Gas-oil relative permeability

Sample identification: 3C Sample depth: 5,789 feet Permeability to air: 68 md		Porosity: 28.4 % Initial water saturation: 18.10 % Effective permeability to air: 52 md	
Gas saturation % (%PV)	Gas-oil relative permeability ratio	Relative permeability to gas*, fraction	Relative permeability to oil*, fraction
0.0	0.000	0.000	1.000
5.7	0.066	0.031	0.468
8.7	0.156	0.057	0.368
10.7	0.251	0.075	0.297
12.3	0.374	0.092	0.245
14.2	0.576	0.116	0.201
18.7	1.540	0.189	0.123
20.9	2.450	0.228	0.093
23.0	3.770	0.280	0.074
26.7	6.530	0.349	0.054
29.2	13.00	0.432	0.033
33.3	30.50	0.529	0.017
36.2	57.80	0.626	0.011

* Relative to the effective permeability to oil at initial water saturation

Table (5) Gas-oil relative permeability

Sample identification: 4C Sample depth: 5,792 feet Permeability to air: 38 md		Porosity: 26.7 % Initial water saturation: 12.8 % Effective permeability to air: 33 md	
Gas saturation % (%PV)	Gas-oil relative permeability ratio	Relative permeability to gas*, fraction	Relative permeability to oil*, fraction
0.0	0.000	0.000	1.000
5.1	0.095	0.044	0.456
7.5	0.176	0.068	0.388
8.6	0.227	0.079	0.350
10.9	0.377	0.100	0.265
12.0	0.474	0.110	0.232
13.5	0.687	0.129	0.191
17.4	1.510	0.194	0.129
19.9	2.460	0.239	0.097
22.7	4.190	0.299	0.072
26.0	7.660	0.372	0.049
30.1	15.80	0.454	0.029
37.3	74.80	0.642	0.0086

* Relative to the effective permeability to oil at initial water saturation

Table (6) Gas-oil relative permeability

Sample identification: 5C Sample depth: 5,805 feet Permeability to air: 26 md		Porosity: 29.5 % Initial water saturation: 13.0 % Effective permeability to air: 18 md	
Gas saturation % (%PV)	Gas-oil relative permeability ratio	Relative permeability to gas*, fraction	Relative permeability to oil*, fraction
0.0	0.000	0.000	1.000
4.6	0.052	0.029	0.560

9.3	0.176	0.067	0.380
11.5	0.283	0.085	0.302
13.5	0.430	0.107	0.250
15.0	0.586	0.127	0.217
18.2	1.160	0.175	0.152
20.3	1.850	0.211	0.114
22.2	2.760	0.261	0.094
25.0	5.100	0.324	0.063
27.4	8.170	0.397	0.049
30.9	18.70	0.481	0.031
35.5	38.30	0.576	0.015
39.2	91.00	0.681	0.0075

* Relative to the effective permeability to oil at initial water saturation

Table (7) Gas-oil relative permeability

Sample identification: 6C Sample depth: 5,831 feet Permeability to air: 115 md		Porosity: 35.2 % Initial water saturation: 11.6 % Effective permeability to air: 85 md	
Gas saturation % (%PV)	Gas-oil relative permeability ratio	Relative permeability to gas*, fraction	Relative permeability to oil*, fraction
0.0	0.000	0.000	1.000
3.7	0.048	0.027	0.560
5.7	0.105	0.046	0.436
7.6	0.216	0.069	0.320
11.6	0.580	0.111	0.192
13.5	0.919	0.142	0.154
15.8	1.530	0.180	0.117
17.8	2.460	0.215	0.087
19.7	3.750	0.266	0.071
22.3	6.610	0.329	0.050
26.2	15.70	0.408	0.026
29.3	34.30	0.482	0.014

* Relative to the effective permeability to oil at initial water saturation

Table (8) Gas-oil relative permeability

Sample identification: 7C Sample depth: 5,849 feet Permeability to air: 56 md		Porosity: 29.5 % Initial water saturation: 17.0 % Effective permeability to air: 44 md	
Gas saturation % (%PV)	Gas-oil relative permeability ratio	Relative permeability to gas*, fraction	Relative permeability to oil*, fraction
0.0	0.000	0.000	1.000
4.0	0.038	0.018	0.479
6.6	0.084	0.029	0.342
8.8	0.150	0.044	0.296
10.8	0.217	0.058	0.266
14.0	0.406	0.077	0.189
16.4	0.649	0.095	0.147
19.6	1.220	0.130	0.107
23.6	2.740	0.199	0.073
27.1	5.240	0.256	0.049
30.4	10.40	0.328	0.031
34.1	21.50	0.417	0.019
37.7	45.60	0.525	0.012

* Relative to the effective permeability to oil at initial water saturation

Table (9) Gas-oil relative permeability

Sample identification: 8C Sample depth: 5,857 feet Permeability to air: 249 md		Porosity: 37.3 % Initial water saturation:19.2% Effective permeability to air: 211 md	
Gas saturation % (%PV)	Gas-oil relative permeability ratio	Relative permeability to gas*, fraction	Relative permeability to oil*, fraction
0.0	0.000	0.000	1.000
5.8	0.018	0.008	0.451
7.9	0.031	0.011	0.357
9.5	0.047	0.014	0.301
12.0	0.091	0.022	0.238
14.6	0.166	0.033	0.200
16.8	0.254	0.043	0.171
22.3	0.752	0.075	0.099
25.3	1.23	0.098	0.074
30.5	4.470	0.162	0.036
33.1	7.650	0.206	0.027
38.1	21.10	0.258	0.012
40.6	36.90	0.318	0.0086
42.5	55.80	0.355	0.0064

* Relative to the effective permeability to oil at initial water saturation

Appendix C**Table (1)** Petrophysical properties of Mabruk Formation

Sample No.	Depth, ft.	Perm. To air, md	Porosity, %	Water saturation S_w (% V_P) versus Pressure (psig)						
				Pressure (psig)						
				1	2	4	8	15	35	40
Brine saturation S_w (% V_P)										
3S	6118	67.95	34.65	100	100	47.50	33.12	17.50	14.30	14.12
6S	6121	134.30	37.45	100	100	66.25	35.63	20.00	17.14	16.75
7S	6124	44.64	33.62	100	100	100	51.25	34.06	25.00	24.00
8S	6125	73.17	30.27	100	100	75.00	43.75	26.25	18.57	17.00
14S	6131	23.61	32.06	100	100	100	71.38	41.58	15.46	12.24
18S	6135	165.67	37.10	100	100	65.91	36.33	17.75	7.61	6.64
32S	6151	42.23	25.57	100	100	93.75	50.63	31.25	25.00	23.75
33S	6153	119.18	30.92	100	90.45	59.96	38.31	26.58	21.45	21.48
36S	6155	55.84	26.43	100	100	100	54.38	40.31	28.86	27.50
38S	6157	229.53	31.09	100	100	36.17	18.71	14.69	12.24	11.79
39S	6160	77.96	21.85	100	90.00	55.00	31.25	15.00	7.90	7.60
40S	6162	17.80	22.65	100	100	100	75.63	44.10	33.30	33.30
\bar{x}		87.66	30.31							

 \bar{x} = Values average



Effect of Active Compounds for *Quercus* Fruit on Some Biochemical Parameters and Tissue Aorta in Induced Atherosclerosis Rats

Intisar G. Taha¹ and Nashwan I. AL-Lehebe²

¹science Department, Basic education Faculty, Mosul University, Mosul, Iraq.

²chemistry Department, education for pure sciences Faculty, Mosul University, Mosul, Iraq.

DOI: <https://doi.org/10.37375/sjfsu.v2i2.511>

A B S T R A C T

ARTICLE INFO:

Received 15 August 2022.

Accepted 17 September 2022.

Published 27 October 2022.

Keywords:

atherosclerosis,
Quercus,
polyphenol,
oil.

This research included extractions of the active compounds from *Quercus* fruit, the identification of active compounds extract by using the capillary gas chromatography technique CGC and with high-performance liquid chromatography technology HPLC. The active dose of the aqueous extract (250 mg/kg) was studied in animals after induced arteriosclerosis with cholesterol (500mg/kg) dissolved in coconut oil for two weeks. The effect of the extracts oil, poly phenols, and at 7, 37.5, and 10 mg/kg respectively were studied also. The results showed a significant ($P \leq 0.05$) increase in catalase activity and the level of high density lipoprotein-cholesterol (HDL-C), However, there was a significant ($P \leq 0.05$) decrease in the high plasma kallikrein, caspase-3, cholesterol, triglycerides, and low-density lipoprotein cholesterol LDL-C in induced atherosclerosis rats treated with all extracts compared with affected control with the active extracts (oil, poly phenols) during the first and second week. The tissue aorta examination in the group of animals treated with the active extracts (aqueous, oily, flavonoid) after two weeks of the treatment showed that large parts of the tissues of the aorta were healed close to the normal state compared to the group of animals induced with atherosclerosis untreated whose tissues contained on thickenings and foam cells.

1 Introduction

The idea of a great healing power exists in medicinal plants for serious diseases that affect living organisms (humans and animals) (Tungmunnithum *et al.*, 2018).

The *Quercus is acorn oak* Dicotyle donae from type *Quercus aegilops* tree was used to treat cough and hoarseness, *Quercus* leaves were also used to treat stomach pain and heart disease (Bahmani *et al.*, 2015).

Use to dilate blood vessels, and dermatitis and as an anti-fungal and anti-inflammatory). *Quercus* leaves and fruits were used to treat stomach diseases and hemorrhoids (Taib., 2020). They are used to treat ulcers that affect diabetes, treat high blood fats, and as an anti-cancer by inhibiting cancer-causing chromosomes, especially in the treatment of colon cancer (Chokpaisarn., 2020; Amedi., *et al* 2020).

Atherosclerosis, which is one of the cardiovascular diseases (CVD), Atherosclerosis leads to the formation of active macrophages capable of producing enzymes that break down protein and break down collagen, which add strength. It has an adequate fibrous cover, making the cover brittle, weak, and more prone to rupture (Soehnlein *et al.*, 2021). Recent studies indicate a relationship between arteriosclerosis and lipids on the one hand, and inflammation on the other, according to the hypothesis of lipid oxidation, LDL-C cholesterol found in the lining of blood vessels increases absorption by macrophages (Libby, 2021 & Que *et al.*, 2018). The research aims to study the positive effects of *Quercus* in preventing atherosclerosis by reducing some enzymes and lipids and improving damage to the aortic tissue.

2 Materials and Methods

Quercus was the local oak found in the city of Dohuk / Iraq was used taken and dry and grain in a Blender machine, distilled water was added, mixed for the electric motor in an ice bath, then filtered. The fatty acids and volatile oils were isolated from the *Quercus* plant by using (100) g of the plant's powder in petroleum ether (60-80 °C) for one day, then placed in the Soxhlet extractor until the color of the solvent became clear (Sayyar *et al.*, 2013) The fatty acids of the oil isolated from the plant were diagnosed using capillary gas chromatography. Flavonoids were obtained from the remaining tissues (bagasse) were taken and dried to get rid of petroleum ether and then placed in the Soxhlet with absolute ethanol 90% until it became clear. The solvent became transparent (Kato *et al.*, 2010). Flavonoids were identified using HPLC.

3 Animal experiments

3.1. Experimental design:

Forty-five (45) adult male Albino rats (4) months old, with weights ranging about (250)g were used. Atherosclerosis was induced using cholesterol dissolved in coconut oil at a concentration of (500 mg/kg) (Ram *et al.* 2014) were dosed orally for 15 days, then animals were divided into (9) groups each group including (5) rats.

Three groups were used to determine the active dose of aqueous extract. Then six groups were used to study the extracts 1st was healthy +ve control 2nd unhealthy -ve 3-6 groups were orally treated with active extracts table 1.

Table (1): effect of doses from *Quercus* on rate induced atherosclerosis.

Dose (mg/ kg)	<i>Quercus</i> extracts
250	aqueous extract
7	Oil
37.5	Flavonoids

Then the tissue samples (aorta) were taken in the experimental end and placed in a neutral physiological saline solution at a concentration of (0.9%) (Kassim., 2012).

3.2. Biochemical analysis in plasma

▪ Determination activity of Plasma Kallikrein PK in blood plasma.

The activity of the enzyme in blood plasma was estimated using chromogen by monitoring the change in absorbance at wavelength in (405) nm (Ito & Statland., 1981).

- **Estimation of the activity of enzyme caspase-3 in blood plasma (CasP-3)**

The activity of enzyme caspase-3 in was estimated (ELISA) kit from Nanjing Duly Biotech of China (Rica & Molly., 2012).

- **Determination of Plasma Catalase Activity (CAT)**

The activity of the catalase enzyme in plasma was estimated by the followed method (Hadwan & Abed., 2016) using hydrogen peroxide as a substrate.

- **Determination of lipid profile in plasma**

Lipid profile in blood was estimated using a ready-made analysis kit.

T-Cho., T.G French company (Biolabo), by the enzymatic method (Burtis *et al.*,2012). HDL-C was measured by the enzymatic method using a ready-made assay kit (Kostner, 1976). LDL-C in the blood plasma was calculated according to the equation (Friedewald *et al.*, 2000):

$$\text{LDL-C} = \text{Total Cholesterol} - (\text{HDL-C} + \text{T.G}/5)$$

- **Statistical analysis**

The values of biochemical variables were analyzed using the statistical program SPSS 25, to find the standard statistical methods for determining the mean and standard deviation of the mean (SD). Duncun test was used to compare the results between more than two groups.

3.3 Results and Discussion

Active compounds were diagnosed using different techniques. The fatty acids were diagnosed using CGC technology, depending on the time of their purity in the separation rod, which in turn depends on the length of the

hydrocarbon chain of fatty acid and the degree of saturation of fatty acid as shown in the figure1 and the table 2 The oil extract of the Quercus plant contains saturated and unsaturated fatty acids, which are essential acids for building eicosanoids and have important effects on anti-inflammatory and maintaining blood pressure. The composition of fatty acids and their physical and chemical properties of Quercus oil are very similar to the fatty acids found in Olive oil in terms of flavor, as Quercus oil is enhanced with unsaturated fatty acids by (70 _90%), so the unsaturated fatty acids play an important role to protect against heart disease and reduce blood fat as well as modify the metabolism and reduce sugar and urea in blood (AL-Rousan *et al.*, 2013; Schulze., 2021).

Table (2): Fatty acids and their percentage in *Quercus* oil.

Fatty acid	Ratio
Palmatic	7.8
Oleic	41.8
Linoleic	42.4
Linolenic	7.6
Stearic	2.7
Elaidic	1.4
Heptadeanaoic	0.9
Eicosenoic	2.4
Behenic	3.2

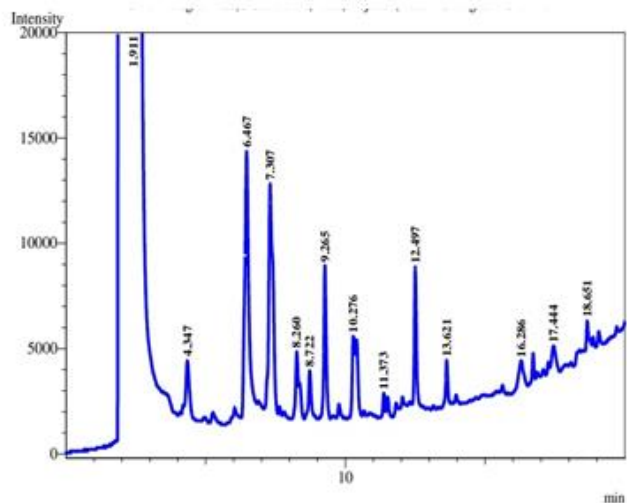


Figure (1). GC chromatogram of fatty acids extracted from Quercus fruit oil

The phenols and flavonoids were also identified by the standard compounds as shown in Table 3 and HPLC technique by comparing the retention time of Figure 3 .

Table (3): Retention time for standard substances and extract polyphenol

Peaks	Diagnosis of peaks	The retention time for standard substances	The retention time for polyphenol extract
1	Gallic	13.7	13.7
2	Rutin	15.1	15
3	Kaemferol	18.6	20.2
4	Quercetin	20.20	22
5	Epigenen	23.4	23.4
6	Catechin	24.3	24.13

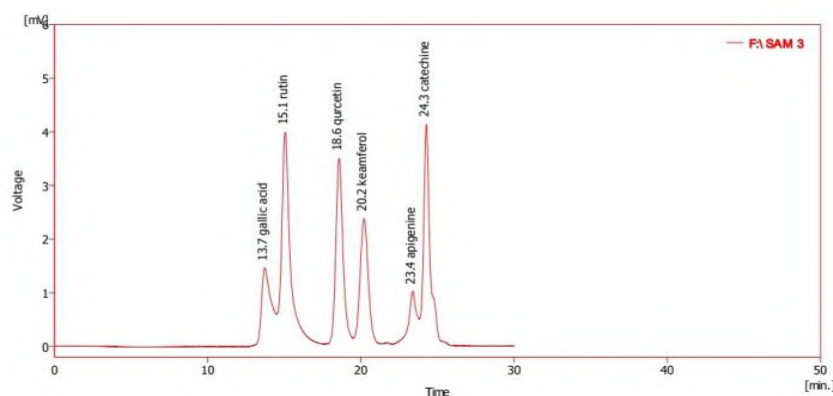


Figure. (2). HPLC chromatogram of flavonoids separated from Quercus

To study the effect of extracts of Quercus on the activity of the PK enzyme, The aqueous extract at a concentration of 250 mg/kg of body weight, which reduced the activity of the PK and casp-3 enzyme in induced atherosclerosis rats, the active doses of the extracts (oil, flavonoid) were calculated based on the active dose of the aqueous extract and the relationship between the effective dose of the extract and weight of extracts practically obtained. The doses for three extracts were (7, 37.5) mg/kg body weight for 2 weeks. Negative for infection through biochemical examinations and histological sections. The results are shown in Table (4) indicate an increase ($P \leq 0.05$) in the activity of PK enzyme in animals with induced atherosclerosis compared with the control group during treatment periods and for two weeks. High

blood fats are also associated with thrombosis and inflammation and apoptosis (Larsen *et al.*, 2000). Dosing animals with extracts (aqueous, oily, poly phenols) led to a significant increase ($P \leq 0.05$) for all extracts after 15 days of treatment. The decrease occurred from the first week with flavonoid and aqueous extract. The reason is attributed to the effective role of flavonoid compounds, as antioxidants in the night from oxidative stress to the active oxygen classes ROS that attack biomolecules, so the decrease of free radicals is related to a decrease in PK enzyme, as its chemical structure helps to endow hydrogen atom in hydroxyl group OH (Zhang *et al.*, 2020) Also, unsaturated oils reduce the activity of the PK and caspa-3 enzyme by decreasing apoptosis (Elrasoul *et al.*, 2021)

Table (4): Effect of Quercus extracts on parameters plasma of male rats

Parameters								
Groups		PK(U/L)	Casp-(U/ml)3	CAT(KU/L)	Chol. mmol/L	T.g mmol/L	HDL-c mmol/L	LDL-c mmol/L
Control		30.84± 0.597	42.7 ±1.494	9.915± 0.89	2.438 ±0.246	1.288± 0.203	2.131± 0.06	2.04 ±0.26
induced atherosclerosis	Time 0	35.38±1.305 a	47.6±1.1 a	7.256±0.75 a	4.22 ±0.66 a	1.96±0.25 a	1.91±0.3077 a	4.7 ±0.0.7 a
	1 week	35.3±1.83 a	48.99±2.0 b	7.64±1.187 b	7.256±0.819 b	2.4166±0.66 b	0.9±0.11 b	6.03±0.809 b
	2 week	37.83±1.753 b	49.311±2.19 b	6.4±0.345 c	9.232±1.127 c	3.833±1.169 c	0.69±0.164 c	7.93±1.1 c
induced atherosclerosis+Aqueous crude extract (250 mg/kg body weight)	Time 0	38.59±1.35 a	48.68 ±2.5 a	6.56±0.352 a	9.015 ±0.737 a	4.04±0.811 a	0.953±0.065 c,a	7.49 ±0.72 a
	1 week	36.3±0.87 b	47.66 ±0.64 a	7.17±0.602 a	6.895 ±1.162 b	2.65±0.207 b	1.22±0.032 b	5.13 ±1.19 b
	2 week	36.65±1.42 b	42.34 ±1.56 b	8.27±0.65 b	4.95 ±0.781 c	1.966±0.25 c	1.24±0.05 c	3.61 ±0.86 c
induced atherosclerosis+ oil extract (7mg/kg body weigh)	Time 0	38.53±1.35 a	48.86 ±1.9 a	6.49±0.427 a	8.65 ±0.62 a	3.27±1.01 a	0.72±0.164 a	7.27 ±0.62 a
	1 week	36.3±0.876 b	47.08 ±0.832 ab	6.83±0.526 a	5.958 ±0.76 b	1.74±0.438 b	1.24±0.05 b	4.71 ±0.76 b

	2 week	30.63±1.42 b	43.8±1.6 b	8.61±0.65 b	6.31 ±0.748 c	1.401±0.13 b	1.28±0.2 c	4.39 ±0.78 c
induced atherosclerosis+ poly phenol extract (37.5mg/kg body weight)	Time 0	37.68±1.54 a	48.73 ±2.07 a	6.66±0.387 a	8.546 ±0.733 a	3.76±1.16 a	0.69±0.213 a	7.08 ±0.68 a
	1 week	37.26±1.89 b	47.6±1.1 a	7.25±0.75 ab	6.31 ±0.76 b	2.221±1.22 b	1.105±0.273 b	4.76±0.8 b
	2 week	34.166±0.983 c	45.86±1.21 b	7.95±1.29 b	4.788 ±0.66 c	1.266±0.0708 b	1.818±0.602 c	3.36 ±0.61 c

* The values in the above table refer to the average Mean Standard ± Deviation

Different horizontal lowercase letters indicate a significant difference at the level of probability

The results in Table (4) show a significant decrease $P \leq 0.05$ in the activity of catalase enzyme in the blood plasma of animals used in atherosclerosis, especially during the last week, compared with the healthy control group. The reason for this is due to the antioxidant properties of the enzyme catalase. The formation of peroxy nitrite radical as a result of increased oxidative stress leads to inhibition of the activity of the CAT enzyme in atherosclerosis activity (Nandi *et al.*, 2019). Whereas, the treatment of animals with plant extracts led to a significant increase in the activity of catalase enzyme in blood plasma, especially in the last week of treatment for animals used with arteriosclerosis, due to the properties of these extracts' anti-oxidation and resistance to free radicals by inhibiting the enzymes producing them such as

Xanthine oxide enzyme, Reductase and NADPH - oxidase (Pedro *et al.*, 2019).

The treatment of animals with cholesterol at a concentration of 500 mg/kg of body weight led to their infection with atherosclerosis with a significant $P \leq 0.05$ increase in chol, T.G LDL-C in the blood plasma during the treatment period (15) days (Ram *et al.*, 2014; Kang *et al.*, 2019) as shown in Table (4). In the treatment of animals with extracts of Quercus (water, flavonoids, oil) there was a significant decrease ($P \leq 0.05$) for cholesterol in animals treated with extracts for 15 days compared with animals used with arteriosclerosis and the decrease occurred from the first week the reason for this decrease is that the extracts act as inhibitors of LDL receptors as they work On the inhibition of the enzyme HMG-COA responsible for the

formation of cholesterol and thus reduce the level of excess cholesterol to bile acids and then to the intestinal tract and thus excreted by the seed and activation lipoprotein lipase enzyme (Yokoyama., *et al.*, 2022 ;Wen *et al.*,2022), Also, results shown in table (4) indicate a significant decrease in the concentration of HDL-C $P \leq 0.05$ in animals used with arteriosclerosis compared with healthy animals from the beginning of the treatment until after two weeks of treatment. The transfer of cholesterol ester and cholesterol ester transfer protein from HDL particles to VLDL particles and thus HDL bodies become rich in small triglycerides and thus lead to their destruction inside the body and the loss of Apo A protein with urine, which is an important component for building HDL particles with a low number of HDL particles (Pikto – Pictkiewicz *et al.*, 2005; Casula *et al.*, 2021), when animals were treated with Quercus extracts, a significant $P \leq 0.05$ rise occurred in the level of HDL in animals induced with arteriosclerosis during two weeks of treatment if the increase was observed from the first week as shown in the table (4) as fatty acids work in extract Oily, oils have a high level of HDL-C (Mazidi., 2022). Also, flavonoids work in the extract. Vegetarians raise the level of HDL-C by increasing the activity of the lecithin cholesterol acyl transferase enzyme LCAT (Rograni & Baluchnejadomajard., 2010; Ahn *et al.*, 2020)

Histological examination in animals used for arteriosclerosis with cholesterol at a concentration of (500 mg/kg) dissolved in oil for 15 days, compared with normal tissues, shows in figure (3) the presence of histological

changes in the aorta compared with the control group through the presence of thickenings in three layers of the aorta with the existence of many Foam cells in cholesterol-containing macrophages with coagulation of smooth muscle fibers and cholesterol deposition in the artery. -1 (IL-1) in foam cells with artery stenosis due to inflammation and cholesterol accumulation. The reason for these histological changes is due to a metabolic disorder in lipids, oxidative stress, secretion of LDL-C cholesterol, and accumulation in the form of fat droplets with cell stimulation. foamy in the cytoplasm as shown in the figure (Poznyak *et al.*, 2021).

The treatment of animals suffering from cholesterol-induced atherosclerosis with extracts of natural products of Quercus (aqueous, polyphenol, oily) during two weeks of treatment daily led to the healing of large parts of the aortic tissues, which are close to the normal state compared to animals affected by atherosclerosis, and the reason for these changes Histological in the ability of extracts to repair and restore damaged tissues by improving the mechanical properties of tissues of aorta while strengthening the cross-links of collagen by increasing activity of the endogenous lysyl oxidase-1 enzyme and lysyl oxidase-2, which work to enhance the tensile balance and elasticity of internal tissues (through catabolic processes). And building by enhancing bonds between the collagen (responsible for tissue tension) and elastin (responsible for elasticity) with the formation of covalent cross-links and their natural remodeling in fibroblasts, endothelial cells, and vascular smooth muscle cells (Sawada *et al.*, 2022). Free radical formation on tissues (Martínez-González *et al.*, 2019) as shown in the figure (3).

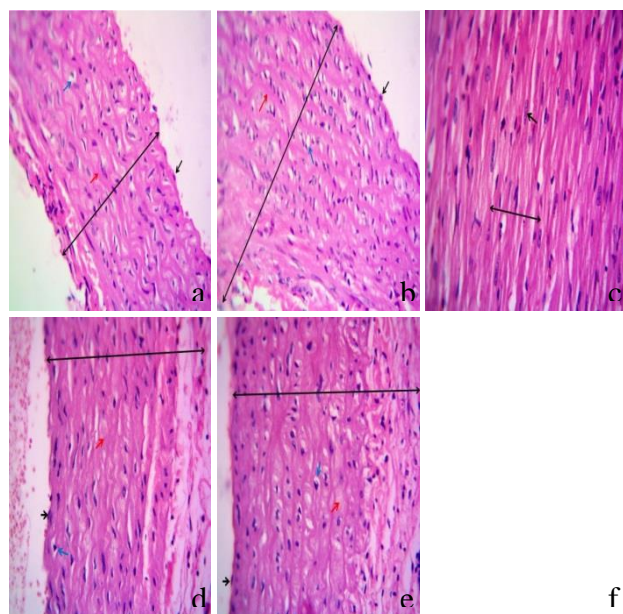


Figure (3). photomicrographs of aorta sections (a) Histological section of the aorta of a control rat showing the normal histological features of aortic layers (\leftrightarrow), endothelial cells (\leftarrow), cells, and smooth muscle fibers (\leftarrow), with the presence of some foamy cells (\leftarrow). Hematoxylin (b) - Histological section of the aorta of a cholesterol-treated rat shows thickening of the aortic layers (\leftrightarrow), spherification of endothelial cells (\leftarrow), thickening of smooth muscle fibers (\leftarrow), and the presence of many foamy cells (cholesterol-containing macrophages) (\leftarrow). Hematoxylin (c) Histological section of the aorta of a rat treated with Q aqueous extract showing the normal histological features of aortic layers (\leftrightarrow), endothelial cells (\leftarrow), smooth muscle cells and fibers (\leftarrow), with a slight presence of foamy cells (\leftarrow). (d) - Histological section of the aorta of a rat treated with alcoholic extract A showing the normal histological features of aortic layers (\leftrightarrow), endothelial cells (\leftarrow), cells and smooth muscle fibers (\leftarrow), with a very slight presence of foamy cells (\leftarrow). (e) - Histological section of the aorta of a rat treated with fatty extract F showing the normal histological features of aortic layers (\leftrightarrow), endothelial cells (\leftarrow), cells and smooth muscle fibers (\leftarrow), with a slight presence of foamy cells (\leftarrow). all tissue Hematoxylin and Eosin Tincture, 400X

Conclusions

The extractions of the active compounds from *Quercus* fruit decrease in the high plasma kallikrein, caspase-3, cholesterol, triglycerides, and low-density lipoprotein cholesterol LDL-C in induced atherosclerosis rats treated with all extracts compared with affected control with the active extracts (oil, poly phenols) during the first and second week. The tissue aorta examination in the group of animals treated with the active extracts (aqueous, oily, flavonoid) after two weeks of the treatment showed that large in rats induced atherosclerosis

Acknowledgements

The authors would like to Acknowledge those who always encourage and give their guidance, mom and dad.

References

- Ahn, S., Jun, S., & Joung, H. (2020). Association of total flavonoid intake with hypo-HDL-cholesterolemia among Korean adults: effect modification by polyunsaturated fatty acid intake. *Nature*, **12**(1), 195.
- Amedi, S.I., & Mohammed, B.M. (2020). Anticlastogenic properties of *Quercus* infectoria galls extract against DMBA induced genotoxicity in bone marrow cells of mice in vivo. *34*, 279-285. *I.J.V.S*
- Al-Rousana, W. M., Ajoa, R. Y., Al-Ismailb, K. M., Attleec, A., Shakerd, R. R., & Osailid, T. M. (2013). Characterization of acorn fruit oils extracted from selected mediterranean *Quercus* species. *Grasas y Aceites*, **64**, 5.
- Bahmani, M., Forouzan, S. H., Fazeli-Moghadam, E., Rafieian-Kopaei, M., Adineh, A., & Saberianpour, S. H. (2015). *Quercus* (*Quercus branti*): an overview. *J chem pharm res*, **7**(1), 634-9.
- Burtis C.A, Ashwood E.R. and Bruns D.E. (2012). *Tietz textbook of clinical chemistry and molecular diagnostics*. By Saunders, an imprint of Elsevier Inc. USA
- Casula., M, Colpani O., Xie S, Catapano A.L, Baragetti A. (2021). HDL in Atherosclerotic Cardiovascular Disease: In Search of a Role. *Cells*. **23**; **10**(8):1869.

- Mazidi M., Shekoohi N., Katsiki, N., Banach M., Meta-analysis Collaboration (LBPMC) Group, T. L. A. B. P. (2022). Omega-6 fatty acids and the risk of cardiovascular disease: insights from a systematic review and meta-analysis of randomized controlled trials and a Mendelian randomization study. *Arch. Med. Sic* **18(2)**, 466-479.
- Chokpaisarn, J., Chusri, S., & Voravuthikunchai, S. P. (2020). Clinical randomized trial of topical *Quercus infectoria* ethanolic extract for the treatment of chronic diabetic ulcers. *J. Herb. Med.*, **21**, 100301.
- Elrasoul, A. S. A., Mousa, A. A., Orabi, S. H., Mohamed, M. A. E. G., Gad-Allah, S. M., Almeer, R.,... & Eldaim, M. A. A. (2021). Antioxidant, anti-inflammatory, and anti-apoptotic effects of *Azolla pinnata* ethanolic extract against lead-induced hepatotoxicity in rats. *Antioxidants*, **9(10)**, 1014.
- Friedewald, W. T., Levy, R. I., & Fredrickson, D. S. (2000). Estimation of the concentration of low-density lipoprotein cholesterol in plasma, without use of the preparative ultracentrifuge. *Clin. Chem*, **18(6)**, 499-502.
- Hadwan, M. H., & Abed, H. N. (2016). Data supporting the spectrophotometric method for the estimation of catalase activity. *Data in brief*, **6**, 194-199.
- Ito, R., & Statland, B. E. (1981). Centrifugal analysis for plasma kallikrein activity, with use of the chromogenic substrate S-2302. *Clin. Chem*, **27(4)**, 586-593.
- Kang, I., Park, M., Yang, S. J., & Lee, M. (2019). Lipoprotein Lipase Inhibitor, Nordihydroguaiaretic Acid, Aggravates Metabolic Phenotypes and Alters HDL Particle Size in the Western Diet-Fed db/db Mice. *Int. J. Mol. Sci.*, **20(12)**, 3057.
- Kassim, H.M. (2012). Effect of Fenugreek seeds extraction liver cells and enzymes of albino male. *Int. J. Soc* , **53(1)**, 62-67.
- Kato, H., Li W., Koike, M. and Koike, K. (2010). Phenolic glycosides from *agrifonia pilosa*. *Phytochem. J Phtochem.*, **71(16)**: 1925-1929.
- Kostner G.M. (1976). Enzymatic determination of cholesterol in high density lipoprotein fraction prepared by polyanion precipitation. *Clin Chem.*, **22(5)**: 698.
- Larsen, L. F., Marckmann, P., Bladbjerg, E. M., Østergaard, P. B., Sidelmann, J., & Jespersen, J. (2000). The link between high-fat meals and postprandial activation of blood coagulation factor VII possibly involves kallikrein. *Scandinavian J. Clin. Lab*, **60(1)**, 45-54.
- Libby, P. (2021). The changing landscape of atherosclerosis. *Nature* **592**, 524–533
- Martínez-González, J., Varona, S., Cañes, L., Galán, M., Briones, A. M., Cachafeiro, V., & Rodríguez, C. (2019). Emerging roles of lysyl oxidases in the cardiovascular system: new concepts and therapeutic challenges. *Biomolecules*, **9(10)**, 610.
- Nandi, A., Jun-Yan, L., Jana, C. K. (2019). Oxidative stress and age-associated degenerative diseases. *Oxid. Med. Cell. Long.*, **2019**: 1-19.
- Pedro, A. C., Maciel, G. M., Riberio, V. R. and Isidoro, C. W. (2019). Fundamental and applied aspects of catechins, from different sources: A review. *Inter. J. Food Sic. Tech.*, **55(2)**: 1-14.
- Pikto - Pictkiewicz W., Wolkowska K., and Pasiński T. (2005). Treatment of Dyslipidemia in Patients Diabetes Mellitus. *Pharmacol Rep*, **57**: 10-19.
- Poznyak, A. V., Nikiforov, N. G., Starodubova, A. V., Popkova, T. V., & Orekhov, A. N. (2021). Macrophages and Foam Cells: Brief Overview of Their Role, Linkage, and Targeting Potential in Atherosclerosis. *Biomedicines*, **9(9)**, 1221.
- Que X., Hung MY., Yeang C., Gonen A., Prohaska TA., Sun X., Diehl C., Määttä A., Gaddis DE., Bowden K., Pattison J., MacDonald JG., Ylä-Herttuala S., Mellon PL., Hedrick CC., Ley K., Miller YI., Glass CK., Peterson KL, Binder CJ., Tsimikas S., Witztum JL (2018) Oxidized phospholipids are proinflammatory and proatherogenic in hypercholesterolaemic mice. *Nature*, **558(7709)**:301-306
- Ram, H, Jatwa, R., Purohit A. (2014) Antiatherosclerotic and Cardioprotective Potential of *Acacia senegal* Seeds in Diet-Induced Atherosclerosis in Rabbits. *Biochem Res. Int.*; 2014:436848.
- Rica, R., Molly, M. (2012). Plasmonic II ELISA for the ultrasensitive detection of disease biomarker with the naked eye: *Nat. Nanotechnol.*, **7(12)**:821-4.
- Rograni M., and Baluchnejadmojarad T. (2010). Hypoglycemic and Hypolipidemic effect and antioxidant activity of chronic

- epigallocatechin- gallate in streptozotocin - diabetic rats. *Pathophysiology*. **17**: 55-59.
- Sawada H., Beckner, Z. A., Ito S., Daugherty, A., & Lu H. S. (2022). β -Aminopropionitrile-induced aortic aneurysm and dissection in mice. *JVS-vascular science*, **3**, 64–72.
- Sayyar, S., Abidin, Z.Z. and Yunus, R. (2013). Optimisation of solid liquid extraction of jatropa oil using petrolum ether. *Asia-Pacific. J of Chem Eng.*, **8**:331-338.
- Schulze, M. B.(2021). Dietary Linoleic Acid: Will Modifying Dietary Fat Quality Reduce the Risk of Type 2 Diabetes?. *Diabetes Care*, **44(9)**, 1913-1915.
- Soehnlein O., Libby, P. (2021) Targeting inflammation in atherosclerosis — from experimental insights to the clinic. *Nat Rev Drug Discov* **20**, 589–610.
- Taib, M., Rezzak, Y., Bouyazza, L., & Lyoussi, B.(2020). Medicinal Uses, Phytochemistry, and Pharmacological Activities of Quercus Species. *Evid. Based.Complementary Altern. Med: eCAM*, 2020.
- Tungmunnithum, D., Thongboonyou, A., Pholboon, A., & Yangsabai, A. (2018). Flavonoids and Other Phenolic Compounds from Medicinal Plants for Pharmaceutical and Medical Aspects: An Overview. *Medicines (Basel, Switzerland)*, **5(3)**, 93.
- Wen, G., Yao, L., Hao, Y., Wang, J., & Liu, J. (2022). Bilirubin ameliorates murine atherosclerosis through inhibiting cholesterol synthesis and reshaping the immune system, *J. Transl. Med* , **20(1)**, 1-18.
- Yokoyama, H., Masuyama, T., Tanaka, Y., Tsubakihara, I., Kondo, K., & Yoshinari, K. (2022). Acyl-CoA: diacylglycerol acyltransferase 1 inhibition in the small intestine increases plasma transaminase activity via the activation of protein kinase C pathway. *J. Toxicol. Sci.*, **47(1)**, 19-30.
- Zhang W., An R., Li Q., Sun L., Lai X., Chen R., Li D., Sun S.(2020) Theaflavin TF3 Relieves Hepatocyte Lipid Deposition through Activating an AMPK Signaling Pathway by targeting Plasma Kallikrein. *J Agric Food Chem*. **68(9)**:2673-2683.



Micropropagation of *Paulownia elongata* tree through Plant Tissue Culture Technology

Ahmed Shaaban, Salem Hammud, Mohammed Abo Sneena, Elmundr Abughnia

Libyan Center for Biotechnology Research Department of Plant Tissue Culture.

DOI: <https://doi.org/10.37375/sjfsu.v2i2.512>

A B S T R A C T

ARTICLE INFO:

Received 21 August 2022

Accepted 02 October 2022

Published 27 October 2022

Keywords:

Paulownia elongata, plant Tissue culture, Micropropagation, Plant growth regulators

The study was carried out at biotechnology research center laboratories for the purpose of Micropropagation of *Paulownia elongata* tree by using plant tissue culture technique for the purpose of identifying the best plant Micropropagation conditions. The plants were sterilized superficially by immersing them in the Clorox solution, then the sterilized plants were cultured in MS media supplemented with several concentrations of (BA and Kinetin) for the purpose of obtaining the best vegetative growths. Obtained plants were also cultured in MS media supplemented with different concentrations of (IBA and NAA) for the purpose of obtaining the best root growth. Finally plants were moved for the adaptation stage. The results indicated that single-nods cultured in (MS) media supplemented with a concentration of 2 and 2.5 mg / L of (BA) growth regulator resulted in good vegetative growth represented in the number of leaves, while the best treatment of branches growth was using 2 mg / L concentration of the Kinetin (K) growth regulator but For the length of the plant, the treatment of the control achieved the best results. For the root site, the results showed that the culture media (MS) plus 0.2 mg / L of the growth regulator (NAA) resulted in the best root growth. As for the adaptation, the results showed that 85% of the plants could be adapted to the sterile environment of soil with 1: 1 size / volume before transferring them to the greenhouse.

1 Introduction

Paulownia, a hardwood tree, which belongs to the family Paulowniaceae (Scrophulariaceae), is characterized by a fast-growing and short-rotation plant with large leaves arranged in opposite pairs on the stem. The tree is able to grow under several weather conditions and in different types of soil even poor ones. *Paulownia* tree is a large, fast- vertical growing tree that is considered to be not evergreen tree. Nowadays, Paulownia species are considered the most important forestry crops in the world. There are nine species of Paulownia but the most

important of them include *P. kawakamii*, *P. australis*, *P. catalpifolia*, *P. elongata*, *P. fargesii*, *P. fortunei*, *P. albiphloea*, and *P. tomentosa* (A fahmy and H gendy , 2018). In fact *paulownia elongate* is considered one of the most important trees producing wood, especially in the last ten years, whereas the global demand on this tree is clearly increased in the global market due to the high quality of wood obtained from *paulownia elongate* tree . Furthermore, the most famous one is *Paulownia tomentosa* originated from China which is a very fast

growing specie (Oprea, 2007). The length of this tree is 12-15m with large leaves shaped as a heart with the length of 15-40cm. The flower appears at the beginning of the spring with length of 10-30 cm (Atanas Chunchukov and SvetlaYa, 2015). Paulownia wood is good for making paper pulp (Latibari et al., 2012). The paper produced from Paulownia trees is of high quality, comparable to Eucalyptus (Feria et al., 2013). Due to these qualities, *Paulownia* species are among the most important forestry crops in the world. The *Paulownia* tree is widely used for reclamation of wooded areas, furniture industry, wooden parts of the aircraft (Zhu, 1986) and musical instruments industry (Ayan et al., 2003). The tree cultivated in Europe for the purpose of decoration and woodwork (Kaymakci et al., 2013). Moreover the tree has been used to improve the properties of soils contaminated with condensate (Miladinova et al., 2014). On the other hand the tree has the potential to grow in several different types of soil and adapt to different types of climate also it has the ability to grow in the tropical climate and regions which have low rainfall rates of 20 inches per year and high temperatures of up to 40°C (Md. Atiqur et al., 2013). However *Paulownia* tree adapted easily to environmental different condition. In the first season after culture of the seedling it reaches of 5-6 meters long when suitable conditions are available (Md. Atiqur et al., 2013; El-Showk, 2003). The trees grow to marketable size in 5-8 years, much faster than other tree species. The plantation does not need re-planting after harvest as new trees grow from the stumps. Paulownia wood is very light, with densities around 0.300 g/cm³ (Akyildiz and Kol, 2010; Kiaei, 2012). In the age of 3-5 years, the length of the tree may be 15-20 meters, and the urine can be used as feed for the farm animals because it has a good nutritional value that corresponds to wheat straw and alfalfa, and can be used in the production of compost (Lyons, 1993) or as source of the organic matter in soil (Wang and Shogren, 1992), as well as polyuria and phosphorus, are rich in nitrogen and can be used as fertilizer for soil (Md. Atiqur et al., 2013). Polonia wood of finest wood, which is characterized by a bright color and has the ability to dry quickly, it has cracks, cracks and does not distort quickly (Atanas Chunchukov and SvetlaYa, 2015).

Using of traditional methods for propagation of Paulownia tree requires large areas and large numbers of workers (Crisanand Petrus, 2016). However, it is very difficult to reproduce Paulownia by traditional methods. However, increasing demand on *Paulownia* in the market has pushed researchers to found appropriate method of

propagation, whereas using plant tissue culture technique is one of the most important methods used in the propagation of Paulownia tree, which will be studied in this research. Obtaining to large quantities of plants in a short period is one of the most important challenges facing the scientific researchers. Use of plant biotechnology such as tissue culture technique as tool for propagation of plants normally provides some advantages such as obtaining plants that are genetically identical with the mother plant, large numbers in a short period of time and cultivation of plants in sterile condition.

In general the most commonly used culture media in plant Micropropagation side is Murashige and Skoog media (MS), which usually depend on addition of micro and macro elements to culture media supplemented with growth regulators. However (MS, DKW, N6 and QL) culture medias are used for Micropropagation of Paulownia tree, with different concentrations of growth regulators (BA and IBA) which, added to the dietary medium (Chunchukov and Yancheva, 2014), whereas single nodes, leaves or roots are usually used in the Micropropagation (Ozaslan et al., 2005). In fact there are attempts to adapt Paulownia tree in Libya in order to spread the idea of planting the tree within the country due to economic benefits of Paulownia tree which may contribute the national economy situation. The aim of this study was obtaining a suitable method to propagate Paulownia tree and obtain large quantities in order to obtain a successful procedure for culture Paulownia tree.

Furthermore Paulownia tree has the potential to grow in sandy and clay soils and grows under different climatic conditions such as high temperatures with low rainfall (Md. Atiqur et al., 2013). The process of settling the tree in Libya and obtaining success cultivation inside the country through use of plant tissue culture technology is considered as an important task.

2 Materials and Methods

This experiment was carried out at Plant Tissue culture Laboratory of the Libyan center for biotechnology research, Tripoli, Libya in order to investigate the impact of the plant regulators BA (Benzyl adenine), Kin (Kinetin), NAA (Naphthalin acetic acid) and IBA (Indol butyric acid) on Micropropagation of *paulownia elongata* tree using Murashige and Skoog culture media.

Sources of plants

Plant samples and single-nods of *Paulownia* tree were collected from the *Paulownia* plants growing in Qasr ben Ghasheer area (Abu Aisha project) while the experiment started by using single-nod parts of *Paulownia* tree to establish tissue culture free of contamination.

Culture media

Preparation of free contamination media

The first stage of the experiment was conducted for the purpose of obtaining a primary media free of contamination to obtain sufficient number of plants for the next stages of the stud whereas the Murashige and Skoog (MS) was prepared with 3% sucrose and 0.7% agar at pH of 5.7 to 5.8. While about 200 ml of prepared MS were placed in special jars. Plant samples were sterilized by sodium hypochlorite with a concentration of 2.5%. Use of MS media supplemented with different plant regulators.

The second stage started with preparation of MS media supplemented with plant regulator for obtaining the best-cultured media to be used in Micropropagation of *Paulownia* tree. A nutrition media (MS) was prepared by using MS media supplemented with benzyl adenine growth regulator (BA) and the Kin growth regulator at concentrations of 0.5, 1, 1.5, 2 and 2.5 mg / L for both growth regulators.

Rooting stage:

Rooting stage was conducted through preparation of culture media (MS) was prepared with half the concentration of salts with addition of growth regulators (IBA and NAA) at concentrations of (0.1, 0.2, 0.5 mg / L) for NAA growth regulator and (0.1, 0.2, 0.5 and 1 mg / L) for the growth regulator IBA in order to induce the cultured plants to produce roots.

Adaptation stage:

Adaptation stage was started with transferee the obtained plants from tissue culture conditions to natural conditions by taking the plants out of the jars and washing the roots to remove the residues of the culture media then transferee the plants into pots with sterile environment of soil with a 1: 1 or 1: 2 size / volume. The pots were covered with a plastic cover with a limited number of holes to maintain humidity. The number of holes in the plastic cover was gradually increased to reduce the moisture before removing the cover completely so that

the plants were adapted to the outside. When the plants reached the appropriate size, they were transferred to the greenhouse with keeping observation time to time to monitor the plants growth.

Experimental design

The experiment was designed using full random design RCD and the results were analyzed by ANOVA system. Was used at level 0.05 and the means were compared using Duncan test.

3 Results

The results of the first stage of this experiment showed that after 60 days of cultivation the growth rate of the single nod of paulownia plants which were cultured in (MS) media free of growth regulators was 70%. A sufficient number of developing plants were obtained free of pathogens (Fig. 1) then obtained plants were transferred to MS media supplemented with different plant regulators.



Figure (1) plants in MS media free of Contamination

Number of leaves:

In the second phase of the experiment, obtained plants were cultured in MS media supplemented with different concentrations of plant regulators which are (BA) and Kin at concentrations of 0.5, 1, 1.5, 2 and 2.5 mg / L. The results in terms of number of leaves parameter (Fig2) showed that a significant differences among the used treatments were found in case of number of leaves parameter, while the treatment of 2 mg BA was the best treatment compared with other used treatments followed by 2.5 mg BA and finally treatment of 2mg Kin whereas,

the 2mg BA , 2.5BA and 2mg Kin treatments recorded average of number of leaves of 19, 18.4 and 18.4, respectively .Our results were in complete agreement with those Donia *et al.*, (2014) who found that use of modified MS media supplemented with PAB growth regulator produced vigorous and well-developed plants from paulownia tree which proved that use of plant tissue culture technology was very successful for Micropropagation of paulownia tree.

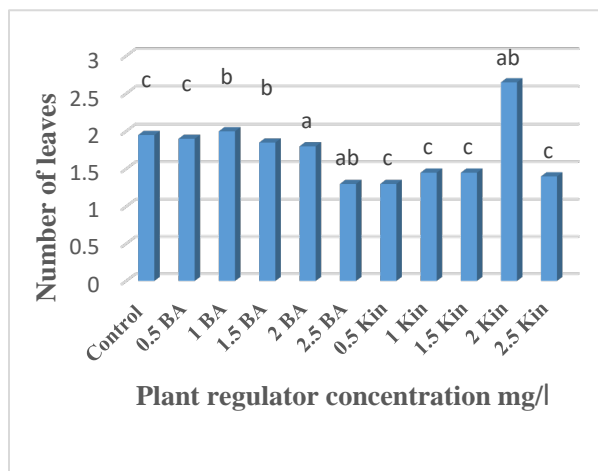


Figure (2) effect of plant regulator (BA, Kin) on plant

4 Discussion

This should explore the significance of the results of the work, not repeat them.

Plant height:

The results (Figure3) showed that in order to determine the best concentration of the growth regulator for plant growth and plant height parameters the results of this study showed that the performance of BA growth regulator in most of its coefficients was better than Kin growth regulator .The results proved that treatments of 1, 1.5, 2 mg /l BA and treatment of 2 mg/l Kin were significantly higher than other used treatments which explain that use of BA and Kin at concentration of 2 mg/l is successful for Micropropagation of paulownia tree .The result of this study proved that use of BA plant regulator is the best choice for paulownia In vitro Micropropagation. Our results agreed with Atanas and Svetla, (2015) who reported that application of the propagation medium with MS salts and addition of BAP

(0.5 mg/ l) and IBA (0.01 mg l-11) and cultivation in big vessels resulted in high proliferation and induced the development of uniform plants as a prerequisite for effective rooting and quality material production. Successful *in vitro* rooting was achieved when plants were cultivated on MS medium with IBA (0.1 mg/ l). High average efficiency of adaptation (96%) was obtained.

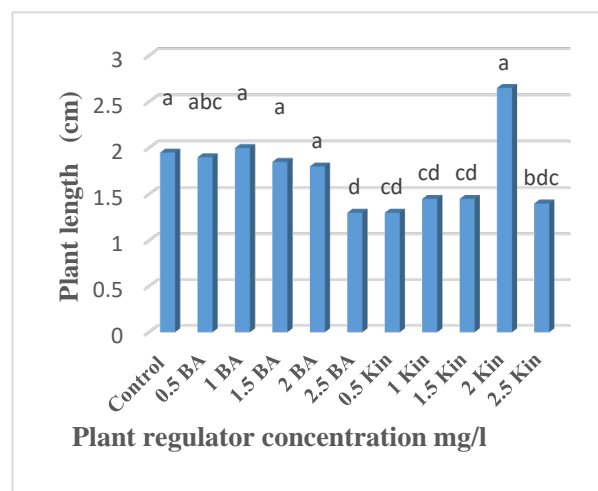


Figure (3) effect of plant regulator BA, Kin on plant height

Number of branches

In terms of number of branches parameter, the results showed that the treatment of 2mg/l Kin gave the highest average number of branches Fig (4). The concentration 2 mg / l of Kin reach the value of 2.65 branches which was the best treatment among the others in case of number of brunches factor. Although the treatment of 2mg/l gave the best results but BA treatments gave acceptable results specially treatment of 1mg/l BA which explain that BA growth regulator was able to induce the obtained plants for better growth. The results proved that (BA) is the best choice for Micropropagation of Paulownia tree .Our results were in complete agreement with Osvaldo and Jose. (2006) and Lobna, (2008) who found that the vegetative total increased with addition of (BA) at concentration of 2 mg / L.

According to our results the treatments of 2mg BA, 2.5mg BA and 2 mg Kin were significantly different among the other treatments even control treatment in case of number of leaves factor whereas, the treatments 2mg

BA gave the highest number of leaves followed by 2.5mg BA and 2mg Kin treatments.

The treatments of 1, 1.5 and 2 mg BA gave the best results compared with other treatments in case of plant height parameter but in number of branches factor treatment of 2mg Kin was significantly higher than the others followed by 1 and 2mg BA treatments, In general plant growth regulator BA and Kin have positive effect on paulownia elongate plant specially treatments of 2mg BA and 2mg Kin . Our results clearly proved that use of plant growth regulators

BA and Kin at concentrations 2mg/l were successful for in vitro Micropropagation of paulownia through use of plant tissue culture technology

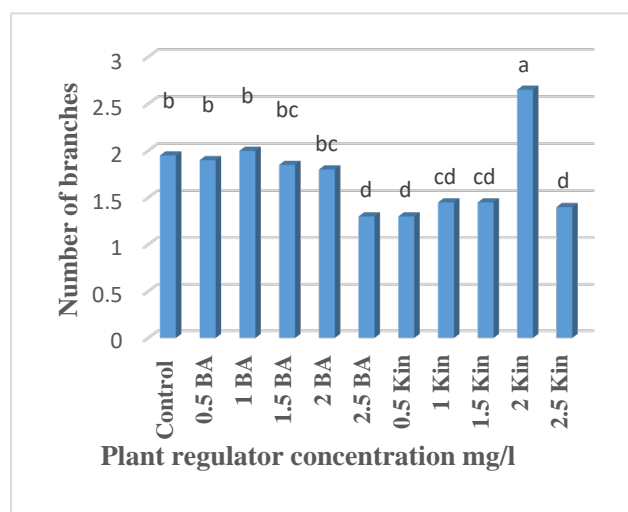


Figure (4) effect of plan growth regulators on number of brunches of *paulownia elongata*.

Number of roots:

The results of root induction stage in case of number of root parameter fig (5) the results showed that all NAA (0.1, 0.2 and 0.5mg/l) treatments were significantly higher than the other used treatments except treatment of 0.5mg/l IBA ,while the NAA growth regulator treatments reached average of 3.2, 3.9 and 3.4 respectively whereas the treatment of 0.5mg/l IBA reached average of 3.5 number of leaves. Our results proved that addition of NAA hormone was successfully induced the paulownia plants to produce roots which extremely needed for successful micro propagation of paulownia tree .Moreover control treatment (MS) gave acceptable average of number of roots this treatment seems to be

successful but not compared with NAA treatments which mean that the plants were able to produce roots in MS media without addition of hormones even in low numbers. Our results were agreed with Atanas and Svetla,(2015) who reported that application of the propagation medium with MS salts

and addition of BAP (0.5 mg/ l) and IBA (0.01 mg l-1) and cultivation in big vessels resulted in high proliferation and induced the development of uniform plants as a prerequisite for effective rooting. Our results were agreed with Fahmy and Gendy, (2018) who reported that the rooting percentage was highly improved by addition of NAA to the medium without significant differences among different concentrations since all concentrations gave 100% rooting percentage.

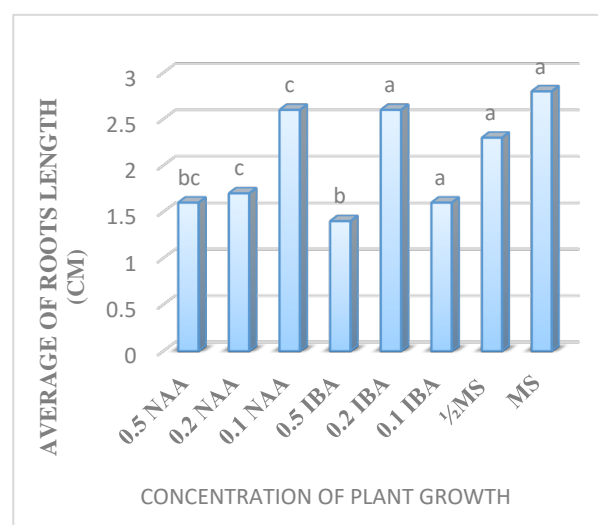


Figure (5) effect of plant regulator (NAA, BA) on number of roots

Root length:

In terms of root length Fig (6), the results showed that the best results were achieved in the control treatment (MS) free of growth regulators with an average value of 2.8 cm .Our results proved that (MS) free of growth regulators treatment seems to be the most effective dietary media followed by the treatment of IBA 0.2 mg / L which recorded 2.6 cm and finally treatment of 0.1 mg/l NAA which reached 2.6 cm. Our results were in agreement with those Al-Tinawi et al., (2009) who reported that the effect of growth regulators (IBA and NAA) is not dissimilar in promoting root lengths and this is almost consistent with the results obtained. . In the same line Zayova et al., (2014) reported that the highest rooting

percentage (100%) and the maximum number of roots per plant were recorded on a $\frac{1}{2}$ MS medium supplemented with 0.5 mg/l IBA.

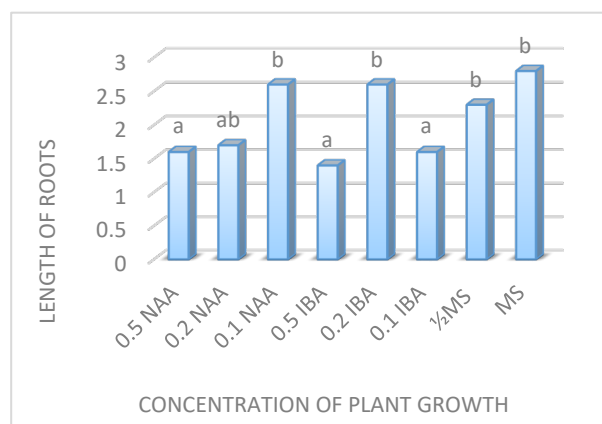


Figure (6) effect of plant regulator on average of roots length of *paulownia elongate* plant

Acclimatization stage:

The results of adaptation stage (Fig8) showed that 85% of the plants were able to reach the state of complete adaptation stage in the sterile environment of soil with peat moss in average of (1: 2, 1: 1 size / volume). After 6 weeks of adaptation some adapted plants were not able to resist and grow well due to that the number of their roots was not enough for growing normally. However the rest of adapted plants continued growing well and have good resistance to natural conditions. In general our result in this stage proved that adaptation of *paulownia* plants which obtained through plant tissue culture technology was successful. This was in the seam line with what has been found by Ozaşlanetal (2005). Our obtained results were agreed also with Atanas and Svetla, (2015) who reported that Ex Vitro adaptation of the rooted plants was performed in a growth chamber with a gradual decrease of the atmospheric humidity and the average survival rate 96% was achieved. Our results were in same lineas Crisan and Petrus. (2016) who found an excellent adaptation for propagated rooted plants.

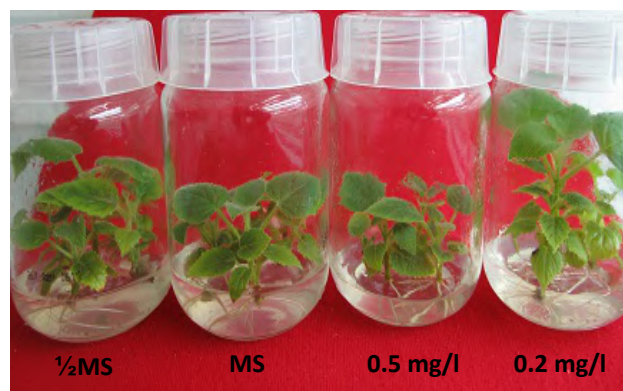


Figure (7) *paulownia elongate* plants at age of seven weeks grown in MS, $\frac{1}{2}$ MS media and MS media supplemented with IBA and NAA



Figure (8) adaptation of plants *paulownia elongate*

5 Conclusions

Recently *paulownia* tree considered as one of the most important trees in commercial side due to its high quality wood. Thereby obtaining large numbers of this tree is extremely needed, whereas plant tissue technology is one the propagation methods helps to obtain an sufficient numbers of this tree. The result of proved that Micropropagation of *paulownia* tree was really successful and large numbers of this tree might be obtained. However, the results reported that use of MS media supplemented with BA and Kin growth regulator at concentration of 2mg/l was clearly successful for Micropropagation of *paulownia* tree even without use of rooting hormones such as IBA and NAA. The results showed that present of an acceptable ability of obtained plants to adaptation conditions.

Conflict of interest: The authors declare that there are no conflicts of interest.

References

- Akyildize M H ,Kol H S .(2010). some technological propagation and use of paulownia *Tomentosa* wood . Journal of environmental biology . pp 351-355
- Al-Tiawni, E., Ali Bacha, N., Al-Rihani, K. and Abdulkader, A. 2009. *In vitro* Micropropagation of apple cv. golden delicious using tissue culture technique. *Bassel Al-Assad Journal for Engineering Sciences, Agricultural, Food, Chemical and Biotechnology*. 26:47-64. Ministry of Higher Education, Syria.
- AtanasC ., Svetla Y.(2015) Micro propagation of Paulownia species and hybrids . First national conference of biotechnology ,volume 100, 4,pp,223-230.
- AyanS ., V. Gercek ., A. Sahin(2003). Performance of Nursery Stage of *Paulownia* Sieb.&Zucc. Species and Origins, Review of Faculty of Forestry University of Suleyman Demirel, Seri. A, ISSN.1302-7085, No.2: 41-56, Isparta, Turkey.
- Chunchukov A., Yancheva S., (2014), Micropropagation of *Paulownia* species and hybrids. *Annuaire de l'University de Sofia*, 100, pp.223-230.
- Crişan L R., Petruş-Vancea A,(2016) .,Paulownia *Tomentosa* L in vitro propagation ., University of Oradea, Faculty of Science, Universităţii St., no. 1, 410087, Oradea, Romania, e-mail: adrianavan@yahoo.com.
- DoniaClapa , Alexandro Fira, Manula Simle, Laura Balcuvasu and Denial Buduroi.(2014). Improved in vitro propagation of paulownia *elongata*. *Bulletin uasvm horticulture* .ISSN:1843-5254
- El-Showk S., N. El-Showk (2003). The *Paulownia* tree – An alternative for sustainable forestry. *The Farm*. <http://www.Cropdevelopment.org/paulownia/Brochure.pdf>.
- Fahmy and Gendy .(2018). In vitro propagation of paulownia hybrid tree .journalzagazig .1633-1643
- Feria .M ,Garcia.M , Zamudio .J , Gomide.J , Lcolodette and Lopez .F .(2013) . bleaching of paulownia . wood cellulose chemistry and technology. 47(7.8) :595-601
- Kaymakci A., Bektas I., Cihad-Bad B., (2013), Some mechanical properties of *Paulownia* (*Paulownia elongata*) wood. *International Caucasian forestry symposium*, pp.917-919.
- Latibari.A, POURALI.a, Froghni.A.(2011). Manufacturing high performance wood composite panel from paulownia . *Key engineering materials*.471-472
- Lobna S. Taha, M.M. Soad Ibrahim and M.M. Farahat.2008. A Micropropagation protocol of *Paulownia kowakamii* through *in vitro* culture technique.
- Lyons A., (1993). *Paulownia*. In: *Agroforestry - Trees for Productive Farming*. Ed. D. Race. Agmedia, East Melbourne.
- MdAtiqur R., Farhana R., Mohammed R.,(2013). *In vitro* regeneration of *Paulownia tomentosa* Steud .plants through the induction of adventitious shoots in explants derived from selected mature trees, by studying the effect of different plant growth regulators ,*American-Eurasian Journal of Sustainable Agriculture*, 7(4): 259-268, 2013 ISSN 1995-0748.
- Miladinova K., Markovska Y., Tzvetkova N., Ivanova K., Geneva M., Georgieva T., 2014, Photosynthesis and growth response of two *Paulownia* hybrid lines to heavy metals Cd, Pb and Zn. *Silva Balcanica*, 15(1), pp.83-99.
- Murashige, T. and F. Skoog. 1962. A revise medium for rapid growth and bioassays with tobacco cultures. *Physiol. Plant*. 15: 473–497.
- Oswaldo, A. and José, M. 2006. Indirect organogenesis and *in vitro* rooting of *Paulownia elongate*. *E-Gnosis(online)*.Vol. 4 .Art 15, 1-12.México.
- Ozaslan, M., Can, C. and Aytekin, T. 2005. Effect of explant source on *in vitro* propagation of *Paulownia tomentosasteud*. *Biotechnol. and Biotechnol. Eq.*19/2005/3: 20-26.
- Thomas M.little and .F. Jackson Hills .1978. Agricultural experimentation , Design and analysis. USA 30 29 28 27 2.
- Wang Q., J.F. Shogren, (1992). Characteristics of the crop - *Paulownia* system in China. *Agriculture, Ecosystems and Environment*, 39: 145-152.
- Zayova, Petrova, Dimitrova, Vasilevska and Stoeva.(2014). Effect of different auxins on in vitro rooting of paulownia *elongate* propagated plants .genetics and plant physiology. pp 155-162
- Zhu Z.H., Chao C.J., Lu X.Y., Xiong Y.G., (1986) *Paulownia* in China: Cultivation and utilization. Singapore: Asian Network for Biological Science and International Development Research Centre of Canada.



Mycoflora Associated with Barely Grains (*Hordeum vulgare* L.) in the Eastern Parts of Libya

Marei M. Abdullah

Department of Plant Production, Faculty of Agriculture, University of Benghazi, Benghazi, Libya.

DOI: <https://doi.org/10.37375/sjfssu.v2i2.295>

A B S T R A C T

ARTICLE INFO:

Received 12 April 2022

Accepted 24 September 2022

Published 27 October 2022

Keywords: barley; seed mycoflora, fungal frequency; fungal relative abundance, and isolation frequency.

During the harvest season (2019-2020), local variety of barley seeds (*Hordeum vulgare* L.) were collected from three different locations, Almerj, Gerdina, and Sultan; situated in the eastern part of Libya. The present experiment was performed to identify, and compare natural mycoflora associated with barley seeds among these locations, also to evaluate sodium hypochlorite's application, as seed disinfectants against fungal contaminants. Barley seeds were surface disinfected with a 4% sodium hypochlorite for two minutes or washed only with deionized water (control) before plating on potato dextrose agar (PDA) medium. The following parameters were recorded and calculated: seed survival (G %), fungal frequency (F), isolation frequency (IF) and fungal relative abundance (RD). Four fungal species were identified as *Aspergillus niger* van Tiegh, *A. flavus* Link (ascomycetes), *Rhizopus stolonifera* (Ehrenb. :Fr.) Vuill (zygomycetes), and *Bipolaris australiensis* (Bugnicourt) (ascomycetes). The most predominant recovered species was *A. niger* followed by *B. australiensis*, *R. stolonifera*, and *A. flavus*, (18.5%), (9.67%) (2.84%), (4.65%), respectively. Results also showed Sultan had the highest seed germination, followed by Almerj and Gerdina, 64.5 %, 44.5%, and 20.5 %, respectively. Moreover, seed's pretreatment with sodium hypochlorite and seed's origin had no significant effect on frequency and relative abundance of fungi.

1 Introduction

Barley (*Hordeum vulgare* L.) has been a central and staple commodity crop in Libya. Barley usages include its grinded flour for making Bazine, a famous traditional Libyan cuisines, and bread. Furthermore, barley grains and hay are used extensively for feeding livestock, and malting. Libya's production of barley was significantly low compared with other neighboring countries' yields, 260 thousand tons in 2005, therefore, the country relies completely on importing barley seeds from foreign market (Elbeydi *et al.*, 2007).

Barley seed quality and nutritional reduction can be substantially deteriorated by the presence of

mycotoxins which are produced by filamentous fungi. In a study conducted on stored barley grains in Spain,

Aspergillus niger was reported to produce a list of toxins, for example, aflatoxin B1 (AFB1), B2 (AFB2), and ochratoxin A (OTA) (Mateo *et al.*, 2011). Aflatoxin is considered the most studied fungal toxin that affect human health and livestock alike. Prolonged human consumptions of aflatoxin result in adverse implications on human wellbeing including liver damage and digestion difficulty (Sarma *et al.*, 2017 & Williams *et al.*, 2004). Therefore, the current study aimed to isolate and identify natural barley seed mycoflora in three different locations; and whether or not presoaking seeds with sodium hypochlorite can reduce fungal contamination.

2 Materials and Methods

2.1 Site description:

Three locations were selected to conduct the present study namely, Almerj, Gerdina, and Sultan, which were chosen based on their high yield per hectare.

2.2 Sampling:

Barley seeds were collected after the harvesting season (2019-2020), transported in plastic bags, and kept at laboratory temperature. From each site, we randomly collected 1.0 kg of seeds. Of 1.0 kg, four-hundred seeds were randomly chosen and divided equally into two groups (i.e., each group had 200 seeds) for further analysis. The first seed group rinsed thrice with only deionized water (untreated), while the second group was disinfected externally with 4% sodium hypochlorite , for a period of two minutes(treated). Seeds were dried out with paper towel prior to placing them on an artificial growth medium. Each seed treatment had ten plates, therefore, the total number of plates was 60 plates. The total number of barley seeds was 600 seeds. Following the rules of International Seed Testing Association(ISTA) on seed health, ten barley seeds were picked with sterilized forceps and transferred to sterilized Petri dish (90 mm,16 mm, Bibby Sterilin Ltd, UK) equidistantly containing potato dextrose agar (PDA) medium (Oxoid Ltd, UK), amended with amoxicillin (0.5 g/ L) to eliminate bacterial growth . The plates were incubated for one week at 25°C with 12 hours photoperiod cycle, and screened for their fungal compositions.

Seed germination percentage, fungal frequency, and relative abundance of fungi were calculated by the following formulas described by Marasas (1988):

Germination percentage

$$(G\%) = \frac{\text{Numebr of seeds germinated}}{\text{Total number of seeds}} \times 100$$

Fungal frequency

$$(F\%) = \frac{\text{Number of seeds containing a particular fungi}}{\text{Total number of seeds}} \times 100$$

Relative abundance

$$(RF\%) = \frac{\text{Total number of a fungus on seed}}{\text{Total number of colonies of all fungi}} \times 100$$

2.4 Fungal identification:

A sterilized needle was used to obtain fungal fragment from Petri dish. Fungal tissues were placed on clean microscopic slide (90 mm,16 mm, Bibby Sterilin Ltd, UK) and stained with the commonly used lactophenol cotton blue stain. Fungal spores were photographed with a fixed camera attached to a compound microscope at 200 x magnification (Olympus microscope camera, Japan).

Fungal key identification texts such as(Dugan, 2006, Navi et al., 1999, & Robinson, 2011)were consulted for aiding in accurate identification.

2.3 Statistical analysis:

Complete randomized block design (CRBD) was used in the experiment. The investigated parameters were normally distributed with *Shapiro-Wilk* test. Differences in means and standard deviations were calculated with two-factorial ANOVA (P values <0.05). Means were compared using Fisher's protected LSD test. Data analyses were performed using R statistical software (R Core Team, 2019). Graphics illustrated here were done with ggplot – a package in R (Wickham, 2016).

3 Results

3.1 Barley seeds fungal compositions:

In this study, we identified four fungal species based on colony color, and conidial shape on growth medium. The species were *Aspergillus niger* (Fig.2.1), *A. Flavus* (Fig.2.2), *Biboplaris australiensis* (Fig.1.3), and *Rhizophus stolonifera* (Fig.2.4). *A. niger* was morphologically identified based on the presence of black colony color, and microscopic characters such as conidia and conidiophore (fig.2.1).

3.2 Effect of seed treatment and locations on seed germination (G%):

Sultan had the highest seed germination in comparison with Almerj and Gerdina. Moreover, seed germination was significantly higher in Almerj than in Gerdina ($P < 0.05$) as illustrated in Fig 1. Treated seeds with sodium hypochlorite had no effect on seed germination ($P = 0.7781$).

3.3 Effect of seed treatment and locations on fungal frequency (F%), and relative abundance (RD%):

In contrary to the seed germination, both treatment and location had no significant impact on F, and RD (Fig.3,

4.). It has been noted that *A. niger* was the predominant recovered species in the unsterilized treatment, but the species was not dominant in sterilized treatment.

Moreover, *R. stolonifera* was higher in sterilized seeds than unsterilized seeds (Fig.3,4).

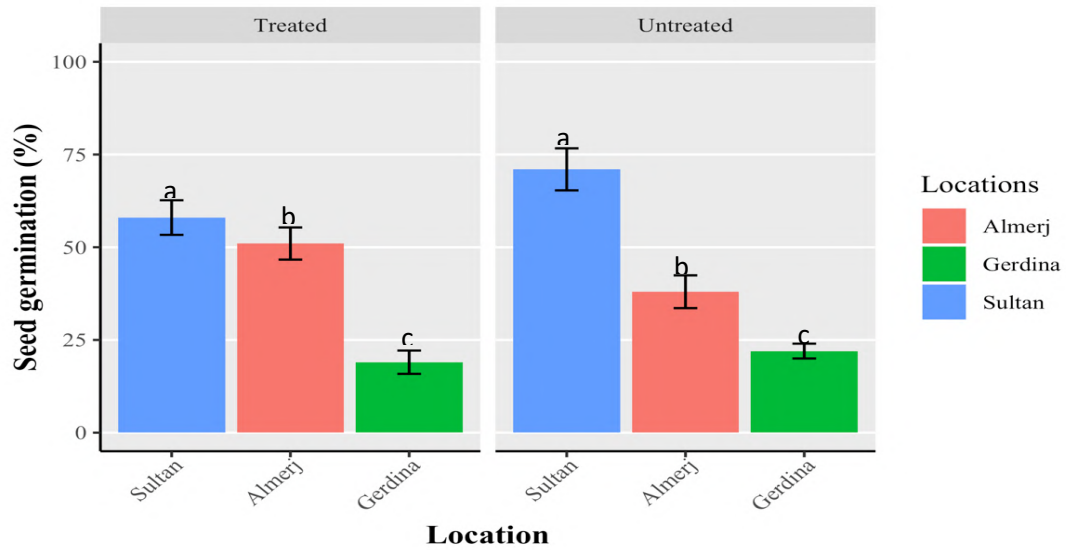


Fig.1. Effect of location and seed treatment on barley seed germination. Barley seeds were collected from three locations, Almerj, Gerdina, and Sultan. Seed treatments were barley seeds disinfected with 4 % NaClO, whereas untreated seeds were only rinsed with deionized water. Bars with the same or without letters are not statistically different according to a F-protected LSD ($P=0.000002$)

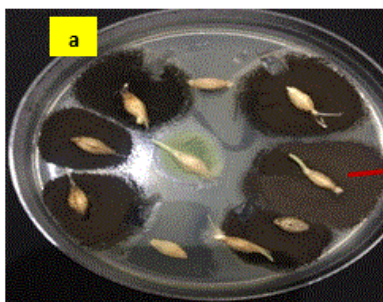


Fig.2.1 a) *A. niger* colony on PDA, b) microscopic photo of *A. niger*. Scale bar=200x C: conidia, CP: conidiophore.

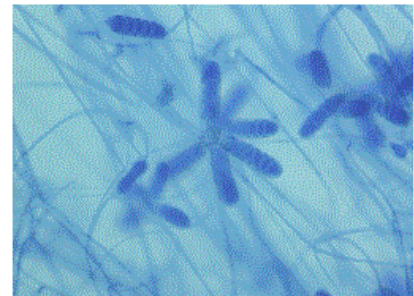
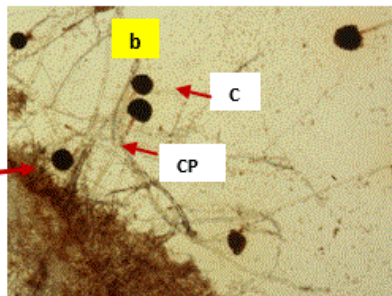


Fig.2.3 Microscopic photo of *B. australiensis* morphology.

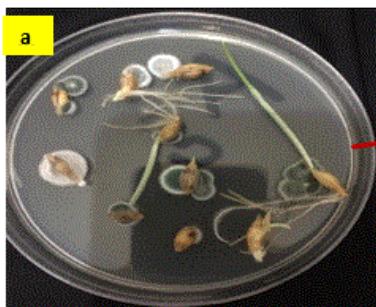


Fig.2.2 a) *A. flavus* colony on PDA, b) microscopic photo of *A. flavus*. Scale bar=200x C: conidia, Ph: phialides, S: stipe, V: vesicle.

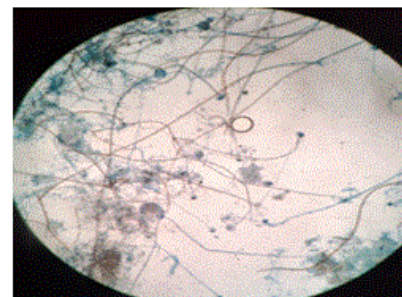
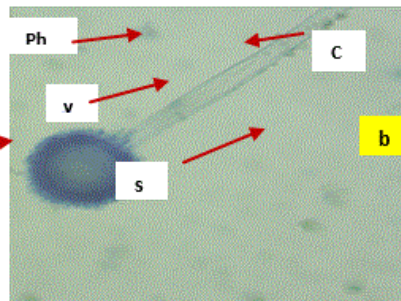
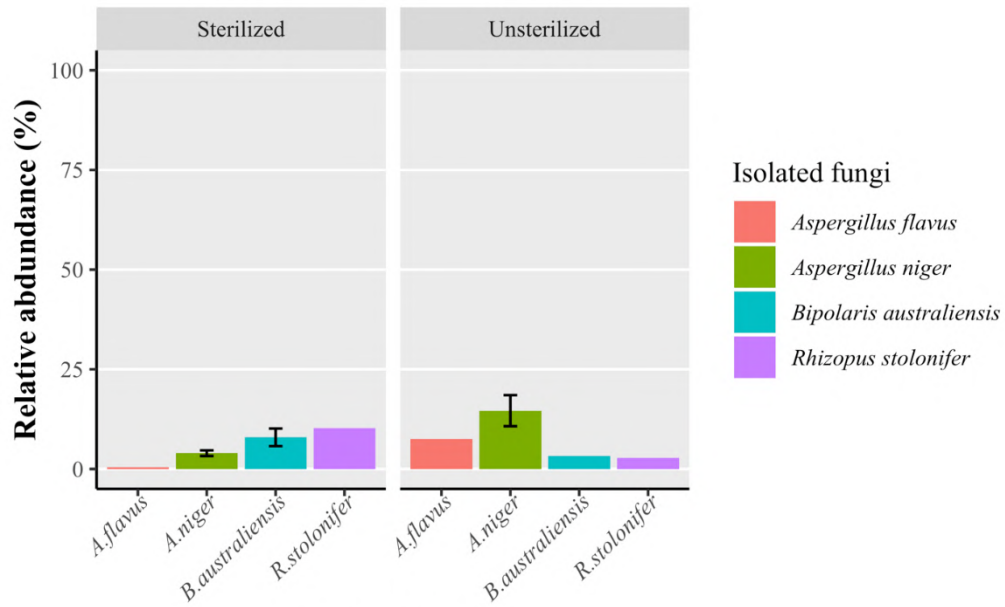
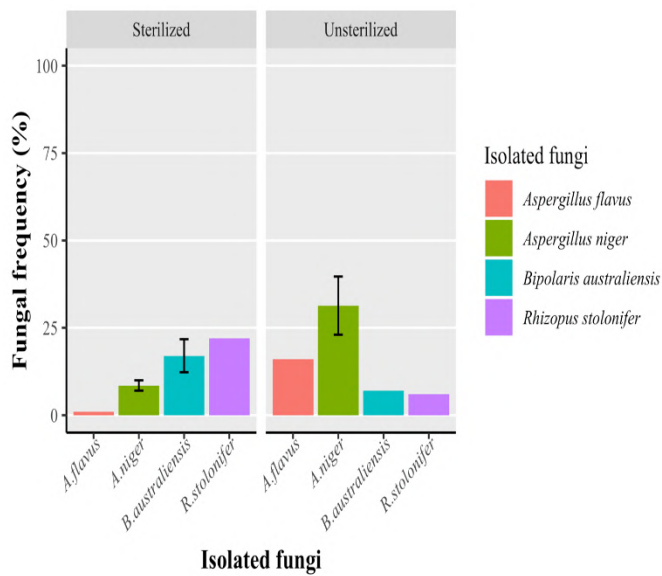


Fig.2.4 Microscopic photo of *R. stolonifera* morphology.



Isolated fungi

Fig. 3. Effect of location and seed treatment on relative abundance (RD). Barley seeds were collected from three locations, Almerj, Gerdina, and Sultan. Seed treatments were barley seeds disinfected with 4 % NaClO, whereas untreated seeds were only rinsed with deionized water. Bars with the same or without letters are not statistically different according to a F-protected LSD ($P= 0.637$).



Isolated fungi

Fig. 4. Effect of location and seed treatment on fungal frequency (F%). Barley seeds were collected from three locations, Almerj, Gerdina, and Sultan. Seed treatments were barley seeds disinfected with 4 % NaClO, whereas untreated seeds were only rinsed with deionized water. Bars with the same or without letters are not statistically different according to a F-protected LSD ($P= 0.637$)

4 Discussion

The current experiment was carried out to determine mycoflora compositions of barley seeds collected from three locations in the eastern part of Libya. The present study revealed that local barley seeds are contaminated with *A. niger*, *A. flavus*, *R. stolonifera*, and *B. australiensis*. Secondary fungal metabolite secreted by species of *Aspergillus* can lead to aflatoxicosis syndrome on human health (Sarma et al., 2017 & Williams et al., 2004). Toxins produced by these fungi varies according to the surrounding environment and the isolate type that secretes them (Blumenthal, 2004). Further studies are needed to identify the fungal toxins types being produced under the Libyan conditions, and to measure toxin's quantity for food safety consumptions.

Our findings were in line with Abubakr findings, in which *A. niger*, *A. flavus* were successfully isolated from barley seeds in the western part of Libya (Maryam, 2017). In Tunisia, *Aspergillus* was the most prevalent recovered species from barley seeds (Jedidi et al, 2018). Similarly, our finding matched Elham, and Modhi (2015) who stated that both *A. niger*, and *A. flavus* are the prevalent isolated species on external barley seeds in different areas of Saudi Arabia. Likewise, Hashem (1990) reported the presence of *A. niger*, *A. flavus* and *B. australiensis* on barley seeds in Saudi Arabia. Likewise the fungal species isolated in this study, *A. niger*, *A. flavus*, *Bipolaris* and *Rhizopus stolonifera* have been recovered from *Triticum aestivum* seeds (wheat) (Adhikari et al., 2016). Moreover, all isolated fungal species, except *B. australiensis*, reported in this study were also found on barley grains in Pakistan (Fakhrunnisa, and Ghaffar, 2006). In contrast to our finding, Ramadan et al (2013) isolated and identified different fungal genera on barley seeds, and these fungi were *Alternaria*, *Aureobasidium*, *Cladosporium*, *Drechslera*, *Penicillium*, *Rhizoctonia* and *Stemphylium*. We speculate that this discrepancy in results could be due to cultivar's type, agronomic practices or meteorological conditions.

In reference to seed germination, seeds collected from Sultan surprisingly exhibited the highest germination rate compared with the other locations, Almerj and Gerdina.

Disinfecting seeds with sodium hypochlorite, in the present study, had no effect on fungal frequency or

fungal relative abundance compared with unsterilized seeds, irrespective of the place where seeds had been collected. Our results were contradictory to Abduhu et al., 2018 who found presoaked okra seeds (*Abelmoschus esculentus* L.) with sodium hypochlorite decreased the incidence of fungi, yet increased okra seed germination.

5 Conclusions

The present study confirmed the presence of four fungal species *Aspergillus niger*, *A. flavus*, *Rhizopus stolonifera*, and *Bipolaris australiensis* that were isolated externally from barley grains. The results support previous studies' findings documenting the presence of these fungi on barley seeds. Seed germination was statistically higher in Sultan compared with the other locations. Barley seeds disinfected with sodium hypochlorite did not affect fungal frequency or fungal relative abundance compared with non-disinfected seeds. For better identification and accuracy, future research should apply molecular approaches to determine barley seed biomes.

Conflict of interest: The author declares that there are no conflicts of interest

References

- Abduhu, M., Khan, A.A., Mian, I.H., Mian, M.A.K., & Alam, M.Z. (2018). Effect of seed treatment with sodium hypochlorite and hot water on seed-borne fungi and germination of okra seed. *Annals of Bangladesh Agriculture*, 22(2). 41-50.
- Adhikari, P., Khatri-Chhetri, G.B & Shrestha, S. M. (2016). Study of prevalence of mycoflora in wheat seeds. *Turkish Journal of Agriculture – Food Science and Technology*;4(1):31–35.
- Blumenthal, C.Z. (2004). Production of toxic metabolites in *Aspergillus niger*, *Aspergillus oryzae*, and *Trichoderma reesei*: justification of mycotoxin testing in food grade enzyme preparations derived from the three fungi. *Regulatory toxicology and pharmacology: RTP*, 39(2), 214–228.
- Dugan, M.F. (2006). *The Identification of Fungi: An Illustrated Introduction With key, Glossary and Guide to Literature*. The American Phytopathological Society.
- Elham, S.D., & Modhi, K.E.(2015). Mycoflora Of Barley (*Hordeum Vulgare* L.) At Different Locations In Hail Area- Saudi Arabia. *International Journal of Scientific and Technology Research*, volume 4, issue 05.
- Elbeydi, K.R., Aljdi, A.A., & Yousef, A.A. (2007). Measuring the Supply Response Function of Barley in Libya.

- African Crop Science Conference Proceedings*, 80, 1277-1280.
- Fakhrunnisa, M.H.& Ghaffar, A.(2006). Seed-borne mycoflora of wheat, sorghum and barley. *Pakistan Journal of Botany*, 38(1), pp.185-192.
- Hashem, A.R. (1990). Fungal Flora of Barley Seeds in Saudi Arabia and Its Control. *Journal of Food Protection*, Vol. 53, No. 9, Pages 786-789.
- Jedidi, I., Soldevilla, C., Lahouar, A., Marín, P., González-Jaén, M. T., & Said, S. (2018). Mycoflora isolation and molecular characterization of *Aspergillus* and *Fusarium* species in Tunisian cereals. *Saudi journal of biological sciences*, 25(5), 868–874.
- ISTA.(2010). International Rules for Seed Testing. International Seed Testing Association. Annexe to Chapter,7Seed Health Testing Methods.
- Marasas, W.F.O., Burgess, L.W., Anelich, R.Y., Lamprecht, S.C., & van Schalkwyk, D.J. (1988). Survey of *Fusarium* species associated with plant debris in South African soils. *South African Journal of Botany*, 54, pp. 63-71,;
- Maryam, A.S.A.(2017). Isolation and Identification of Fungi from Cereal Grains in Libya. *International Journal of Photochemistry and Photobiology*, Vol. 1, No. 1, pp. 9-12.
- Mateo, E.M., Gil-Serna, J., Patiño, B., & Jiménez, M. (2011). Aflatoxins and ochratoxin A in stored barley grain in Spain and impact of PCR-based strategies to assess the occurrence of aflatoxigenic and ochratoxigenic *Aspergillus* spp. *International Journal of Food Microbiology*, 149(2), 118–126.
- Navi, S.S., Bandyopadhyay, R., Hall A.J., & Bramel-Cox, P.J. (1999). *Pictorial Guide for the Identification of Mold Fungi on Sorghum Grain*. Information Bulletin no. 59 (In En. Summaries in En, Fr). Patancheru, Andhra Pradesh, India: International Crops Research Institute for the Semi-Arid Tropics. 118 pp.
- Ramadan, Nadeem & Zrary, Taha. (2013). Isolation, Identification and Pathogenicity of Seed borne fungi of some barley cultivars. *Journal of Zankoy Sulaimani*, Part A. 16. 55-64.
- R Core Team. (2019). R: A language and environment for statistical computing. R Foundation for Statistical Computing, Vienna, Austria. URL <https://www.R-project.org>.
- Robinson, M. (2011). *Pictorial Atlas of Soil and Seed fungi: Morphologies of Cultured Fungi and Key to Species* (3rd ed.), Reference Review, Vol. 25 No. 4, pp. 43-44.
- Sarma, U.P., Bhetaria, P.J., Devi, P., &Varma, A.(2017). Aflatoxins: Implications on Health. *Indian Journal of Clinical Biochemistry* : IJCB, 32(2), 124–133.
- Wickham, H. (2016). *Ggplot2: Elegant Graphics for Data Analysis*. Springer-Verlag New York.
- Williams, J.H., Phillips, T.D., Jolly, P.E., Stiles J.K., Jolly, C.M.,& Aggarwal, D. (2004). Human aflatoxicosis in developing countries: A review of toxicology, exposure, potential health consequences, and interventions. *American Journal of Clinical Nutrition*, 80 (5):1106-1122.



Generating Matrices of Rotations in Minkowski Spaces using the Lie Derivative

Anis I. Saad¹, Muneera Muhmoud² and Attia A. Mostafa²

¹ *Mathematics Department, Omar Al-Mukhtar University, Albayda, Libya.*

² *Mathematics Department, Derna University, Derna, Libya.*

DOI: <https://doi.org/10.37375/sjfssu.v2i2.317>

A B S T R A C T

ARTICLE INFO:

Received 17 May 2022.

Accepted 15 October 2022.

Published 27 October 2022.

Keywords:

Keywords: Lie derivative, Lorentz groups, isometry, Minkowski spaces, system of ODE

This paper aims to generate matrices of rotations in Minkowski using the Lie Derivative. The calculus on manifolds in Lorentzian spaces are used to generate matrices of rotation in three-dimensional Lorentz-Minkowski space which includes one axis in timelike and the other two are spacelike axes. The findings showed that the manifolds and their calculus dramatically increased the use of Lie derivative in many branches of mathematics and physics, The findings also revealed that matrices (of rotation) leave one line (axis) fixed and these matrices of rotation are used widely in differential geometry in physics. Furthermore, the findings demonstrated that any surfaces of revolution inside this space must be invariant under one of these matrices. The main result of this paper is a new procedure of creating rotational matrices explicitly using the Lie derivative and deriving it into a linear system of ordinary differential equations. Solving this system leads to matrices of rotation that leaves one axis fixed in Minkowski space.

1 Introduction

Manifolds and their applications combine many critical areas of mathematics; they generalize concepts such as curves, surfaces, and ideas from linear algebra and topology.

In differential geometry, Lie (1842, 1899) evaluates the change of a tensor field (including scalar functions, vector fields, and one-forms) along the flow defined by another vector field. This change is invariant coordination. Therefore, the Lie derivative is defined by any differentiable manifolds. The Lie derivative is the early beginning of calculus on manifolds.

On the other hand, the rotational surfaces in Euclidean space have been studied for a long time. Many examples of curves on these surfaces have been discovered. These surfaces are called rotating a plane curve on an axis (called the axis of rotation). This rotation is done using a matrix of rotation, which is called a one-parameter group of isometry and orthogonal matrix $SO(3)$ (For

more information, see Pressley's differential geometry textbook written by Pressly, 2010).

However, in the last three decades, the vision of geometry has been developed to other spaces including the time axis. While in Euclidean space all axis are spacelike vectors $(+,+,+)$, in (Minkowski) space there is a one-time axis $(+,+,-)$. This different sign changes all theorems of inner and outer products of vectors to another field (See Hall, 2004; Hilgert and Neeb, 2011; Lopez, 2014; Saad, 2016).

Minkowski's space is more complicated compared to Euclidean's. We can distinguish other types of matrices of rotation which are later called space,time, and null rotation.

Thus, there are three types of one-parameter groups of isometries. By considering the rigid motion of ambient space that keeps a line fixed, we will solve these types of rotation to generate these different types explicitly. Firstly, similar to each axis of rotation, there is a matrix of rotation that leaves a (type) of axis fixed.

Furthermore, we use the definition of Lie derivative and Killing (1847-1923). Killing fields are the infinitesimal generator of isometries; that is, flows generated by Killing fields are continuous isometries of the manifold and matrices of rotation generate in three-dimensional Minkowskian spaces.

This work is located between differential geometry and physics. This paper also tries to show explicitly the relationship between differential geometry and Lorentz groups, i.e. Lorentzian Manifolds.

Rotation in E^3 preserves all distance. As a consequence, they preserve all inner products. Also, the map transfers the orthonormal basis to another orthonormal basis with a linear transformation of finite dimensional vector space. Rotation can be represented by a matrix once a basis is chosen.

In 3D Euclidean space, restricting the attention to the proper rotation, we find that the set of all 3×3 matrices satisfies the orthogonal-unit matrix which is known by $SO(3)$.

The group of $SO(3)$ is a group with an identity element of unit matrix I and the matrix multiplication as the group operation, then $SO(3)$ defines a rotation group of E^3 .

Any matrix $R \in SO(3)$ has been taken into account an eigenvector with an eigenvalue of 1. It gives the axis of rotation.

In this paper, as previously mentioned, we go forward to another space which is the 3D Minkowski space. While the three dimensional in Euclidean space are all positive definite in the self-inner product, in Minkowski space there is a one-time axis giving the possibility of minus singe of self-inner product. Therefore, not all axis of rotation is the same, and then we go through all possibility of the axis of rotation upon the Minkowski space criteria.

Accordingly, using the Lie derivative of diffeomorphisom functions gives a system of ODE. Therefore, three different types of matrices simulate the matrix $R \in SO(3)$, but now for Minkowski spaces i.e. $R \in SO(2,1)$. (two spacelike and one timelike vectors). Matrices of rotations generate in Minkowski space which is the beginning of the geometry of surfaces in Minkowski space.

In sections two and three, we define the isometry in Lorentz groups, rotation, and the transformation of Lorentz groups.

Section four includes the main definition of calculus on the manifold which describes the Lie derivative, its properties, and the generators of rotation in Lorentz space seeking to Killing vector fields.

Finally, section five, presenting the main results of this paper, covers in detail all the computation parts of

generating rotational matrices in three-dimensional Minkowskian spaces using systems of ordinary differential equations.

2 The Isometry

In this section, we review the isometry in E^3 and consider that for E_1^3 (three dimensional Minkowskian space). An isometry is defined as a function that preserves the matric (Carrol,1997; Torres, 2012).

2.1 Introduction

Definition: A diffeomorphism between two Riemannian manifold $\varphi: (M, g) \rightarrow (N, h)$ is an isometry if $\varphi^*h = g$ which means for every point $x, d_x\varphi$.

Linear map isometry is between T_xM and $T_{\varphi(x)}N$ that leaves a line (length) fixed .

A particular consequence of this definition is that:

Definition: $f: (M, g) \rightarrow (M, g)$ is a diffeomorphism from a manifold onto itself, with the property that is for all $p \in M$ and all $V, W \in T_pM$

$$g_{f(p)}(f_p^*V, f_p^*W) = g_p(V, W) \quad (1)$$

Then f is an isometry of (M, g) .

2.2 Isometry Group

The isometry group of the Riemannian manifold (M, g) is the set of diffeomorphism of M that is g -isometric, e.g. the Lorentz group.

2.3 Rotation

Rotation in three dimensional Euclidean space E^3 preserves all distance .i.e. they are isometries. A rotation can be represented by a matrix . All rotational matrices are special orthogonal matrices ,which in $\det R = 1$ and $R^T = R^{-1}$.

In this section we define the rotation as well as mention standard rotations in three dimensional Euclidean space E^3 (For more detail, see Hall,2004; Hilgert & Neeb, 201; Lopez, 2014).

3 The Lorentz groups and Transformation

In this section, we define the Lorentz group, Lorentz transformation and types of Lorentz transformation in three dimensional Lorentz Minkowski space E_1^3 .

- The Lorentz Group

Lorentz group is the group of isometries of Lorentz Minkowski space which preserve the origin.

- The Lorentz Transformation

The Lorentz transformation for any position (point) in Lorentz Minkowski space is defined by

$$\tilde{\Sigma} = \Lambda S \quad \text{where } g = \Lambda^T g \Lambda \quad (2)$$

Where Λ^T is the transposed matrix to the matrix Λ and

$$g = \begin{bmatrix} 1 & 0 & 0 \\ 0 & 1 & 0 \\ 0 & 0 & -1 \end{bmatrix} \quad (3)$$

is the Lorentz Minkowski metric .

4 Lie Derivative

Let v be a vector field on a smooth manifold M and ϕ_v is a local flow generated for each $t \in \mathbb{R}$. The map ϕ_v is diffeomorphism of M and so it induces the movement functions such as push-forward and pull back.

Definition: The Lie derivative of the function f with respect to v is defined by:

$$L_v f = \lim_{t \rightarrow 0} \left(\frac{\phi_t^* f - f}{t} \right) = \frac{d}{dt} \phi_t^* f |_{t=0} \quad (4)$$

Lemma: since $\phi_t^* = f \circ \phi_t$, then

$$\begin{aligned} \frac{d}{dt} \phi_t^* f |_{t=0} (p) &= \frac{d}{dt} f(\phi_t(p)) |_{t=0} = \\ \frac{d}{dt} f(\gamma_p(t)) |_{t=0} &= v(p) \cdot f, \quad \forall p \in M \end{aligned} \quad (5)$$

Where the tangent vector to γ_p at p is $X(p)$ concludes that $L_v f = v f$.

Although, if U, V be two vector fields on M . The Lie derivative of V with respect to U is given by:

$$L_U V = \lim_{t \rightarrow 0} \left(\frac{\phi_t^* V - V}{t} \right) = \frac{d}{dt} \phi_t^* V |_{t=0} \quad (6)$$

Where ϕ_t is generated by U .



On the other hand, the Lie derivative is a *linear operator* which satisfies *Leibniz identity* and always linearly dependents.

In this paper, however, the following special cases are needed to achieve the main goal.

Lie derivative of the Lorentzian metric

Definition : Let g_{ij} be the metric of Minkowski spacetime defined above (3), we find

$$L_v g_{ij} = g_{ab, c} V^c + g_{ac} V^c, b + g_{cb} V^c, a \quad (7)$$

The first term of (7) seems to be normal derivative of a constant (the metric), so the equation (7) becomes

$$L_v g_{ij} = g_{ac} V^c, b + g_{cb} V^c, a \quad (8)$$

If we rotate or boost to save isometric of this change, we always have:

$$L_v g_{ij} = 0 \quad (9)$$

The Lie derivative of the metric plays a key role in the theory of Killing fields (For a review, see Carroll, 1997.p120), which are generators of continuous isometries. A vector field is a Killing field if the Lie derivative of the metric with respect to this field vanishes. I.e the vector v in (8) is so called Killing vector fields.

Furthermore, on solution (8) to be equal zero and according to Saad , in three dimensional Minkowskian space, the generators of matrices of rotations under this space are given by :

$x \frac{d}{dy} - y \frac{d}{dx}$, is called generator of rotation , and $x \frac{\partial}{\partial t} + t \frac{\partial}{\partial x}$ and $y \frac{\partial}{\partial t} + t \frac{\partial}{\partial y}$ are called generator of boost .

However, for the null (lightlike) generator we can use $(t - y) \frac{\partial}{\partial x} + x(\frac{\partial}{\partial y} + \frac{d}{dt})$. This suggestion is found in (Hall,2004; Saad,2016).

As a result, we use only rotation, one boost and the null generator for the null case. In the following section we solve the above generators as a system of ordinary differential equations to create matrices of rotation explicitly.

5 Results

The main conclusion of this paper is that matrices of rotation generate explicitly. Now we divide the discussion into three cases of study, i.e. rotation , boost and null case.

5.1 Spatial Rotation

It is important to begin with the most obvious analogue of rotation. The infinitesimal generator of this case is

$$x d/dy - y d/dx \quad (10)$$

Therefore the Killing vector field becomes :

$$V = (-y \quad x \quad 0)^T \quad (11)$$

This defines the 3×3 matrix in Minkowski spacetime corresponding to the generator in (10), which is in (x, y, t) coordination by

$$L_k = \begin{bmatrix} 0 & -1 & 0 \\ 1 & 0 & 0 \\ 0 & 0 & 0 \end{bmatrix} \quad (12)$$

This matrix L_k is the matrix corresponding to infinitesimal generator about t-axis.

Now we have one parameter group of homomorphism $\psi_s = L_k \psi_s$, so, $\psi_s(x) = e^{sL} x$. As x is a vector in E_1^3 .

Our job now is to solve the system of ordinary differential equation of the form of :

$$\dot{\psi}_s = L_k \psi_s.$$

Then, to find eigenvalues let $\begin{vmatrix} -\lambda & -1 & 0 \\ 1 & -\lambda & 0 \\ 0 & 0 & -\lambda \end{vmatrix} = 0$

therefore $\Rightarrow \lambda_1 = 0, \lambda_2 = i, \lambda_3 = -i$

Calculating the matrix exponential gives:

$$X(\theta) = \begin{bmatrix} \cos(\theta) & -\sin(\theta) & 0 \\ \sin(\theta) & \cos(\theta) & 0 \\ 0 & 0 & 1 \end{bmatrix} \quad (13)$$

This means any point $(0,0,t)$ is fixed. Also the axis of rotation is t-axis. Additionally, the orbit of any point of a spacelike curve with t-constant in this case is a circle centered with the origin.

5.2 Boost in direction of spacelike axis.

In this section the one parameter group of transformation which fixes each point in space-like is sought. Let Y- axis is the axis of rotation, and use

$$x \partial/\partial t + t \partial/\partial x \quad (14)$$

Therefore the Killing vector field becomes :

$$V = (t \ 0 \ x)^T \quad (15)$$

This defines the 3×3 matrix in Minkowski spacetime which is similar to the generator in (14), which is in (x, y, t) coordination by

$$L_k = \begin{bmatrix} 0 & 0 & 1 \\ 0 & 0 & 0 \\ 1 & 0 & 0 \end{bmatrix} \quad (16)$$

With the same calculation and discussion above, the matrix exponential gives:

$$X(\theta) = \begin{bmatrix} \cosh(\theta) & 0 & \sinh(\theta) \\ 0 & 1 & 0 \\ \sinh(\theta) & 0 & \cosh(\theta) \end{bmatrix} \quad (17)$$

In this case the orbit of any point has fixed y-coordinate, discussion of the orbit is hyperbola-timelike. (lift for future work).

5.3 Null (lightlike) rotation in Minkowski spacetime.

Finally, we consider the situation where the axis of rotation is a null line. It is located in yt- plane i.e.(y=t) as given above before this section, so the generator of this case is:

$$(t - y)\partial/\partial x + x(\partial/\partial y + d/dt) \quad (18)$$

Therefore the Killing vector field becomes :

$$V = (t - y \ x \ x)^T \quad (19)$$

This defines the 3×3 matrix in Minkowski spacetime corresponding to the generator in (10), which is in (x, y, t) coordination by

$$L_k = \begin{bmatrix} 0 & -1 & 1 \\ 1 & 0 & 0 \\ 1 & 0 & 0 \end{bmatrix} \quad (20)$$

Same procedure, as before, of solving system of ODE.

Let

$$\begin{vmatrix} -\lambda & -1 & 1 \\ 1 & -\lambda & 0 \\ 1 & 0 & -\lambda \end{vmatrix} = 0,$$

this gives $\lambda_{1,2,3} = 0$ "multiple eigenvalues "

At this time, with mansion to Perko, the general solution to the linear system is given by

$$X(\theta) = e^{\lambda\theta} \left[I + N\theta + \dots + \frac{N^k \theta^k}{k!} \right] \quad (21)$$

Where $N = L - S$ is an $n \times n$ matrix is said to be nilpotent of order k if $N^{k-1} \neq 0$ and $N^k = 0, k \leq n$, $S = \text{diag}(\lambda)$, L is a matrix called Lorentz transformation .

$$S = \begin{bmatrix} 0 & 0 & 0 \\ 0 & 0 & 0 \\ 0 & 0 & 0 \end{bmatrix}, N = \begin{bmatrix} 0 & -1 & 1 \\ 1 & 0 & 0 \\ 1 & 0 & 0 \end{bmatrix},$$

$$N^2 = \begin{bmatrix} 0 & 0 & 0 \\ 0 & -1 & 1 \\ 0 & -1 & 1 \end{bmatrix}, N^3 = 0 \quad (22)$$

$$X(\theta) = e^{\lambda\theta} \left[I + N\theta + \frac{1}{2} N^2\theta^2 \right] \quad (23)$$

$$= \begin{bmatrix} 1 & 0 & 0 \\ 0 & 1 & 0 \\ 0 & 0 & 1 \end{bmatrix} + \begin{bmatrix} 0 & -\theta & \theta \\ \theta & 0 & 0 \\ \theta & 0 & 0 \end{bmatrix} + \frac{1}{2} \begin{bmatrix} 0 & 0 & 0 \\ 0 & -\theta^2 & \theta^2 \\ 0 & -\theta^2 & \theta^2 \end{bmatrix}$$

Therefore, the one parameter subgroups of rotation matrices is

$$X(\theta) = \begin{bmatrix} 1 & -\theta & \theta \\ \theta & 1 - \frac{\theta^2}{2} & \frac{\theta^2}{2} \\ \theta & -\frac{\theta^2}{2} & 1 + \frac{\theta^2}{2} \end{bmatrix} \quad (24)$$

This one parameter group fixes line $y = t$ in yt - plane

Therefore, the axis of rotation is given by $l = (0,1,1)$. And the orbit seems to be a parabola-time, but the discussion on is out of our scope at the moment.

In summary, the aforementioned three cases of matrices of rotation are called in physics as one parameter groups of isometry that leaves line fixed. These are the main results of this paper.

6 Conclusions

This research shows that the Lie derivative and Killing vector field are used explicitly to generate three rotational matrices (space, boost, and null). The main findings revealed that computational generators find the matrices of rotation assuming the axis of rotation is dependent on a vector field space, time, or null.

Further studies are in need to examine the geometry of surfaces in Minkowskian spaces. All geometrical aspects of curvatures, Gaussian maps, and mean curvatures are in parallel with these matrices.

Acknowledgements

Muneera Muhmoud would like to thank Derna University for the financial support.

Conflict of interest: The authors declare that there are no conflicts of interest

References

- Pressley, A. N. (2010). Elementary differential geometry. Springer Science & Business Media.
Hall, G. S. (2004). Symmetries and curvature structure in general relativity (Vol. 46). world scientific.

Hilgert, J., & Neeb, K. H. (2011). Structure and geometry of Lie groups. Springer Science & Business Media.

Lopez ,R . (2014) Differential Geometry of Curves and Surfaces in Lorentz - Minkowski space, International Electronic Journal of Geometry, 7(2014), 44-107 7 (1) , 44-107 . DOI: 10.36890/iejg.594497

Saad ,A . (2016) On Calculus of Manifolds with Special Emphasis of 3D Minkowski Space $M^{2,1}$ International Journal of Engineering and Applied Sciences, 3(1), 257742.

Carroll, S. M. (1997). Lecture notes on general relativity. arXiv preprint gr-qc/9712019.

Perko ,L . (2000) " Differential Equations and Dynamical Systems", third edition , Springer-Verlag New York Berlin Heidelberg , Germany.

Torres del Castillo G.F. (2012)" Lie Derivatives In Differentiable Manifolds", Springer, Birkhäuser, Boston,USA.

Duggal ,K and Sharma ,R. (1999) "Symmetries of Spacetimes and Riemannian Manifolds " (Vol.487) , Springer Science Business Media

Saad, A. I., Muhammed, S. A. E., & Elmabrouk, T. S (2016) On Geodesics of 3D Surfaces of Rotations in Euclidean and Minkowskian Spaces." International Journal of Engineering and Applied Sciences, 3(1), 257742.



The Fundamental Role of Neuroinflammation at the Beginning and Progression of Alzheimer's Disease

Yousef Sawikr¹, Youssef F. Lawgali^{2,3}, Abdelkarem Elgazali^{3,4} and Ibrahim S. Ibrahim⁵

¹Pharmacology and Toxicology Department, Medicine Faculty, Ajdabiya University, Libya.

²Biomedical Medical Sciences Faculty, Benghazi University.

³The Environmental and Biological Chemical Research Center, Tokara, Libya.

⁴Chemistry Department, Arts and Sciences Faculty, Benghazi University, Tokara, Libya.

⁵Zoology Department, Sciences Faculty, Ajdabiya University, Libya.

DOI: <https://doi.org/10.37375/sjfsu.v2i2.557>

A B S T R A C T

ARTICLE INFO:

Received 30 August 2022

Accepted 21 October 2022

Published 27 October 2022

Keywords:

Alzheimer disease,

S100B,

cytokines,

RAGE.

The majority of astrocytes are responsible for the expression and release of S100B, a 21-kDa calcium-binding protein of the EFhand type (helix E-loop-helix F). It is mostly present in the neurological system and, depending on concentration, has different (beneficial, detrimental) effects on neurons, astrocytes, and microglia. an effect on the survival and development of both glia and neuronal cells. Patients with Down Syndrome and Alzheimer's Disease (AD) have brains that are overexpressed with the S100 protein Down Syndrome (DS). Increased S100B concentrations are linked to brain trauma and ischemia, most likely due to astrocyte destruction. As S100B appears to influence multiple neuropathological mechanisms in (AD), a pivotal role for S100B as a significant contributor to (AD) pathology has emerged.

Studies of S100B overexpression, S100B localization, multiple relationships between S100B and increase amyloid precursor protein, the interaction between S100B and dystrophic neuritis plaques, and change in a neurofibrillary tangle in Alzheimer's disease focus on providing evidence for the involvement of S100B in Alzheimer's disease pathology and neuronal loss. The significance of S100B in head trauma and degenerative brain disease is the central subject of this review. Overexpressing s100B, which also causes more astrogliosis and microgliosis, speeds up the pathogenesis of Alzheimer's disease. Numerous clinical problems have been associated with an increase in S100B, a neurotropic signaling protein.

1 Introduction

The AD is a chronic, progressive loss of basal forebrain cholinergic neurons, and irreversible neurodegenerative disease with clinical characteristics of memory loss, dementia and impairment in memory, visuospatial skills, complex cognition, language, emotion and personality. Prominent neuropathologic features of AD are senile plaques, neurofibrillary lesions, synaptic and neuronal loss, and gliosis, destroys the higher structures of the brain. The formation of amyloid plaques and

neurofibrillary lesions are thought to contribute to the neurodegeneration in the brain of Alzheimer's disease sufferers play an important role in the inflammatory response in the central nervous system (CNS) and in AD pathogenesis. cognitive dysfunction concomitant with the accumulation of senile plaques (SP) is consist of Beta-amyloid (A β) plaques (extracellular A β deposition) and neurofibrillary tangles (NFT, intracellular deposits of hyper-phosphorylated tau

protein) have been identified as two classical pathological hallmarks of AD. Accordingly, numerous studies have focused on A β generation and deposition as well as on NFT formation as the triggering factors for AD occurrence. Gliosis is also seen in AD: activated astrocytes and microglia are characteristically found in abundance near neurons and plaques, and this can be seen even in a case described by Alzheimer in 1911. This suggests that inflammation may be involved in AD, because glial cells mediate the innate immune response in the central nervous system. When activated, astrocytes and microglia produce several proinflammatory signal molecules, including cytokines, growth factors, complement molecules, and adhesion molecules. Of particular interest in AD are the cytokines S100B, which is mainly produced by astrocytes, and interleukin1 (IL-1), which is mainly produced by activated microglia.

Role of Astrocytes in Alzheimer's Disease:

Histo-pathological features of AD include large extracellular senile plaques (SPs) composed of the amyloid- β (A β) plaques and neurofibrillary tangles, which (Wyss-Coray and Rogers, 2012) are intracellular inclusions of hyperphosphorylated tau protein in selective regions of the brain (Xiao *et al*, 2014) (Wyss-Coray and Rogers, 2012) β -amyloid is a peptide of 42 amino acid residues produced by the selective photolytic cleavage of transmembrane amyloid precursor proteins (APP) by β and γ -secretases. A β can directly induce (Sidoryk-Wegrzynowicz *et al* 2011) neuronal cytotoxicity, but the relevance of such toxicity to the disease is controversial [1]. Morphological characterization of GFAP-positive astroglial cells performed on AD mouse model at different ages showed an age-dependent reduction in GFAP expression. These authors suggested that in an AD transgenic, reactive hypertrophic astrocytes surround the neuritic plaques whereas astroglial cells in other brain regions undergo atrophy, which may account for early changes in synaptic plasticity and cognitive impairments inherent to AD. In the AD human tissue, prominent astrogliosis occurs in the cells surrounding amyloid plaques, and these activated astrocytes accumulate large amounts of Ab42, which are derived from neuronal debris and associated with plaques (Andrea *et al*, 2004). Moreover, astrocytes from patients with dementia show significantly decreased complexity compared to the healthy brain (Sidoryk-Wegrzynowicz *et al* 2011). It

is widely recognized that age is the most important risk factor for AD and that the innate immune system plays a role in the development of neurodegeneration. Very little information is available on how aging affects the innate immune system. However, there are clear indications that the development of AD is due to age-related changes that modulate innate immunity. It is interesting that A β and other proteins found in the senile plaques of AD patients are potent activators of the innate immune response because chronic stimulation of the innate immune system may lead to alterations of astrocytes. When the brain is injured, astrocytes are believed to react by putting down glial scar tissue as part of the healing process. Recently, it has been shown that astrocytes themselves actively contribute to the inflammatory response (Sidoryk-Wegrzynowicz and Aschner 2014). It has been shown that the neurotransmitter glutamate is released in neuroinflammatory conditions and to some degree under normal circumstances, which on the long term is proved to be toxic to neurons. The neuroprotective action of astrocytes has also been attributed to their capacity to take up the neurotransmitter glutamate, convert it to glutamine, and recycle it to neurons (Vesce *et al*, 2007).

Neuroinflammation and immune system crosstalk in Alzheimer disease:

Neuroinflammation is the mechanism of CNS inflammation that occurs in response to trauma, infections, and/or neurodegenerative diseases. In neuroinflammation, cellular and molecular immune components such as specialised macrophages (microglia), cytokines, chemokines, complement, tumor necrosis factor (TNF) (Allen *et al*, 1999) recruited from the peripheral system following disruption of the blood-brain barrier. Alterations in the permeability of the BBB and chemotaxis may permit the recruitment and passage of peripheral cells into the brain parenchyma. Determining the detailed mechanism of this process is an active area of research. Investigators are exploring the processes involved in both the passage of inflammation into, and the effect of cytokines on, the central nervous system (CNS) (Fung, *et al* 2012). This in turn leads to the activation of the glial cells, such as microglia and astrocytes. The effect of neuroinflammation is considered neuroprotective when the inflammatory activity is for a shorter period of time whereas chronic neuroinflammation is associated with harmful consequences for the CNS. (Allen *et al*, 1999) (Boulanger *et al*, 2001). In the brain, inflammation is

mediated largely by glial cells, the support cells of the nervous system. Glial cells include astrocytes, which support neuronal metabolism, oligodendrocytes which produce myelin insulation for nerve cells (allowing more efficient conduction of nerve impulses), and microglia, which serve as a kind of immune system. Glial cell activation is a key feature of brain inflammation. When activated, microglia produce inflammatory mediators that activate more cells to produce additional inflammatory mediators. These mediators can thus create positive feedback loops, thereby amplifying inflammation. Brain inflammation, including increased microglia and astrocyte (Joseph *et al*, 2005) activation, generally increases as part of the aging process and brain inflammation is a key feature of neurodegenerative diseases, including AD. The immune system comprises a complex interrelated network of cellular, molecular, and chemical mediators that function to protect the body against environmental stress factors. These stressors can be as diverse as microorganisms (viral, bacterial, fungal agents), physical damage (burns, lacerations), or environmental toxins (snake venoms, nonessential metals, chemicals). To combat all these stressors, the first line of defense is innate or natural immunity. The inflammatory component of this response is important in recruiting cells of the immune system to the compromised area, and cytokines and chemokines mediate this function. Cytokines orchestrate a specific response that is appropriate based on the type of foreign antigen that has penetrated the tissue, and chemokines are important in allowing cells of the immune system to reach the area under attack (Campbell, 2004), some endogenous factors are response by inhibition proinflammatory gene expression via negative feedback inhibition (Nadeau and Rivest, 2003) however, over activation of innate immunity can lead to neurodegenerative disorders which is accompanied by enhanced expression level of S100B and S100B receptor, RAGE in neural and inflammatory and cytokines and chemokines e.g. TNF, IL-1, S100B. have been implicated as etiological factors in a variety of neurological disease states including AD (Huell *et al*, 1995).

Relationship between S100, Interleukin 1, and Alzheimer Disease:

S100B in Alzheimer Disease:

S-100B proteins, named for their solubility in a 100% saturated solution of ammonium sulphate at neutral pH (Sindic *et al*, 1982). It is belong to a group of closely

related, small, acidic, water-soluble, Ca²⁺-binding proteins (Mata *et al*, 1990) (Zimmer *et al*, 1995). A great body of evidence suggests that S-100 could be viewed as a multifunctional subfamily of Ca²⁺-binding proteins of the EF-hand type. A large number of diverse functions is attributed to S-100 proteins, ranging from calcium-buffering through intracellular (e.g., modulation of enzyme activities, energy metabolism, motility, and secretion cell proliferation and differentiation, cytoskeletal assembly and disassembly) and nuclear (e.g., transcription and apoptosis) functions to extracellular activities (e.g., secretion, neurite extension, calcium homeostasis and chemotaxis) (Donato 1999). S100B, one of the originally described S100 proteins, is abundantly expressed by central and peripheral nervous system glia, and to a much lesser extent, by some populations of neurons (Ichikawa *et al*, 1997) (Yang *et al*, 1995) S100B is detected in varying abundance in a limited number of brain cells including astrocytes, maturing oligodendrocytes, neuronal progenitor cells, pituitary cells, ependymocytes, and certain neural populations. Although the majority of astrocytic S100B localizes within the cytoplasm, 5%–7% is membrane bound. S100B is also expressed by non-neural cells, including melanocytes, chondrocytes, and adipocyte (Donato 1999). increased S100B levels are also found in the cerebral spinal fluid of A.D patients (Peskind *et al*, 2001) Astrocytic S100B is considered to be the major factor contributing to the formation of dystrophic neurites, which are pathologically transformed neurites concentrated around amyloid plaques (Mrak *et al*, 2005) (Cairns *et al*, 1992) AD neuropathological hallmarks include brain deposition of amyloid- β (A β) peptide as senile plaques, accumulation of abnormal tau protein filaments as intracellular neurofibrillary tangles, extensive neuronal degeneration and loss, profound synaptic loss, and β -amyloid plaque associated astrogliosis and microgliosis (Zhang and Song 2013) (Selkoe, 2001) S100B release is driven by the developmental stage of the astrocytes (Van Eldik and Zimmer, 1987) and metabolic stress (oxygen, serum, or glucose deprivation) (Gerlach *et al*, 2006) S100B can also be released in response to external stimuli such as glutamate (Cicarelli *et al*, 1999) serotonin (Whitaker-Azmitia *et al*, 1990), the pro-inflammatory cytokines TNF- α (Edwards and Robinson, 2006) and IL-1 β (de-Souza *et al*, 2009), β -amyloid peptides (Peña *et al*, 1995), 1-methyl-4-phenyl 1,2,3, and 6 tetrahydropyridine (MPTP) (Iuvone *et al*, 2007), forskolin, lysophosphatidic acid (Pinto *et*

al, 2000) .Local synaptic responses with local overexpression of the A β precursor protein and local astrocyte activation with over expression of S100B might then be responsible in part for the progression of pathology across brain regions in Alzheimer's disease.

Interleukin-1:

Interleukin-1 was first described in 1972 as a lymphocyte activating factor (Gery and Waksman 1972) and later was shown to exert a variety of effects including induction of inflammation, body temperature increase, proliferation of T and B cells, induction of acute phase proteins and prostaglandins and regulation of hematopoiesis. Its activities are not restricted to the immune system. Interleukin-1 is also involved in the regulation of blood calcium levels, stimulation of proliferation of various cells, regulation of blood pressure or modulation of sleep. However, IL-1 represents one of the most important mediators of the inflammatory response that induces a cascade of proinflammatory effector molecules (Sharma 2011). Interleukin-1 (IL-1) has been implicated in a number of neurodegenerative conditions and is generally believed to have neurotoxic actions, although the mechanisms of these effects are unclear (Zilka 2006). There are two molecular forms (IL-1 α and IL-1 β), that is secreted by microglia and astrocytes. IL-1 produced by activated microglia may trigger production of other cytokines, such as IL-6, TNF- α by astrocytes and other cells.

Furthermore, IL-1 induces astrocytes and neurons to produce more B-amyloid which leads to deposition of amyloid fibrils (Zilka 2006). Through various pathways, IL-1 causes neuronal death, which activates more microglia, which in turn releases more IL-1 in a self-sustaining and self-amplifying fashion. Interleukin-6 (IL-6) is a multifunctional cytokine that stimulates the acute-phase reaction, which enhances the innate immune system and protects against tissue damage. IL-6 is synthesised by microglia, astrocytes, neuronal and endothelial cells. In certain condition, IL-6 may have inflammatory or immunosuppressive effects (Klegeris and McGeer 2005) IL-6 seems to act as a secondary process amplifying the inflammatory response initiated by IL-1 β (Lee *et al*, 1993). Elevated levels of IL-6 mRNA were demonstrated in the entorhinal cortex and the superior temporal gyrus of AD patients (Y.-W. GE and LAHIRI 2002) IL-1 is markedly overexpressed by activated microglia in Alzheimer's disease (Shaftel *et al*, 2008) and, like activated

astrocytes, these activated microglia show characteristic patterns of association with different stages of A β neuritic plaques. and enhances production and processing of (β -amyloid precursor protein (β -APP). A major inducer of astrocyte activation and S100B expression is the immunomodulatory cytokine IL-1 (Giulian *et al*, 1988) (Sheng *et al*, 1996). Activated Microglia overexpressing IL-1, like activated astrocytes overexpressing S100B, are frequently found in the early nonfibrillar amyloid deposits of Alzheimer's disease (Griffin *et al*, 1995) (Mackenzie *et al*, 1995). These proposed pathogenic mechanisms elevated levels of the inflammatory cytokine IL-1 drive S100 β and β -APP overexpression and dystrophic neurite formation in Alzheimer's disease. interact with other cellular and molecular factors to form a cytokine cycle of molecular cascades with feedback amplification of glial activation and with progressive neuronal injury (Griffin and Mrak 2002) (Mrak and Griffin 2000). In moreover to the previously mentioned, S100B-mediated effects on free calcium levels and on dystrophic neurite formation within neuritic A plaques, there are other consequences of cytokine cycle activation. IL-1 expression (Mrak 2001). Astrocytic S100 β , in turn, i) increases intracellular free calcium concentrations, ii) promotes growth of neuronal processes that, coincidentally, necessitate further neuronal expression of β -APP favoring release of neurotoxic β -amyloid; and iii) induces astrocytic nitric oxide synthase activity with release of potentially neurotoxic nitric oxide. The resultant neuronal cell dysfunction and death, together with β -amyloid activation of the classical complement pathway microglial IL-1 overexpression i) promotes astrocyte activation and upregulates astrocytic expression of S100 β , ApoE, α 1-antichymotrypsin and the complement protein C3; ii) stimulates neuronal synthesis and processing of β -APP; and iii) has autocrine effects to activate microglia and to further promote IL-1 expression (Hu and Van Eldik 1999).

RAGE in Alzheimer disease:

Non-enzymatic glycosylation theory of aging' proposed that the AGE-mediated crosslinking of long-lived proteins contributes to the age-related decline in the function of cells and tissues in normal aging (Monnier and Cerami, 1981), AGEs and S100B are also abundant in the nervous system, therefore their interaction with RAGE appears to be implicated not only to the pathology of amyloid-type disorders, but with other neurodegenerative disorders such as Huntington's

disease (HD) Parkinson's disease (PD) and amyotrophic lateral sclerosis (ALS) (Ma and Nicholson 2004). RAGE expression, apart from neurons, microglial cells astrocytes in the healthy human brain (Brett *et al.*, 1993). The involvement of AGEs in brain aging and – in an accelerated fashion – in AD was first proposed in the mid-1990s (Takeda *et al.*, 2014) The stability of proteins that constitute the long-lived intracellular (neurofibrillary tangles and Hirano Bodies) and extracellular protein deposits (senile plaques) suggests that they would be ideal substrates for glycation, a process that occurs over a long time, even at normal levels of glucose, ultimately resulting in the formation of AGEs. establishing a link between the expression of RAGE and the pathophysiological changes in AD, showed that extracellular deposition of A β and its interaction with the brain vasculature or directly with neurons and microglia, lead to neuronal dysfunction. The latter dysfunction was mediated by RAGE in a dose dependent manner and moreover, binding of A β to RAGE generated oxidative stress, activation of NF-kB and induced expression of macrophage-colony stimulating factor (M-CSF) (Onyango *et al.*, 2005). AGE harmless post-translational protein modification; various pathophysiological effects have been found at the cellular and molecular level. One of the proposed mechanisms of AGE-induced damage are reactive oxygen species (ROS), particularly superoxide and hydrogen peroxide released by AGEs (Guglielmotto *et al.*, 2010). The activation of microglial RAGE by many of its ligands, including AGEs and A β , results in the release of proinflammatory mediators such as free radicals and cytokines (Guglielmotto *et al.*, 2005). Additionally, in astrocytes of AD brain, epitopes of A β , AGEs and RAGE were found to co-localize, suggesting a potential participation in the pathogenesis of the disease (Sasaki *et al.*, 2001), microglia had increased expression levels of IL-1 and TNF- α , suggesting an inverse correlation between cytokine production and A β clearance. These data indicate that, although early microglial recruitment promotes A β clearance and is neuroprotective in AD, as the disease progresses, proinflammatory cytokines are produced in response to A β deposition (with RAGE as the A β -binding receptor), which then downregulate genes involved in A β clearance and promote A β accumulation. Microglia may thus contribute to plaque formation, accumulation of AGEs on plaques over time, more intense crosslinking, inflammation and chronic neurodegeneration. As S100 proteins and especially

S100B are abundantly expressed in the nervous system, Huttunen and his coworkers initially suggested that RAGE, already known to interact with A β , can also mediate neurotoxicity due to elevated levels of S100B, shedding new light on studies of the molecular pathophysiology of AD (Sindic *et al.*, 1982). S100B stimulated NF-kB transcriptional activity in microglia in a manner that was strictly dependent on RAGE, therefore pointing to additional RAGE-mediated effects on microglia activation with impact in AD and other neurodegenerative disorders (Adami *et al.*, 2004).

Conclusion and perspective:

In order for the human nervous system to operate normally, astrocytes are essential. They also play a crucial role in neurodegenerative illnesses and coordinate many of the first and ongoing astrocyte responses to injury. Certain neurological illnesses primarily involve astroglial cells, Astrocytes control synaptic transmission and plasticity, safeguard neurons from harmful substances, and provide metabolic support for neurons to guarantee their proper operation. By providing growth factors and cytokines chemokines and IL-1 α astrocytes are involved in all types of neurodegenerative processes, and display prominent remodelling in the AD; early dystrophic changes in astroglia can represent an important step in initiation and progression of Alzheimer's disease. Targeting of astroglia may provide a new principle for treatment of AD at the early stages of the disease.

Conflict of interest: The authors declare that there are no conflicts of interest.

References

- Wyss-Coray T and Rogers J (2012) "Inflammation in Alzheimer disease-a brief review of the basic science and clinical literature.," *Cold Spring Harb. Perspect. Med.*, vol. 2, no. 1, p. a006346.
- Xiao Q, Yan P, Ma X, Liu H, Perez R, Zhu A, Gonzales E, Burchett J, Schuler D, Cirrito J, Diwan A, and Lee J (2014) "Enhancing Astrocytic Lysosome Biogenesis Facilitates A β Clearance and Attenuates Amyloid Plaque Pathogenesis," *J. Neurosci.*, vol. 34, no. 29, pp. 9607–9620
- Sidoryk-Wegrzynowicz M, Wegrzynowicz M, Lee E, Bowman A, and Aschner M (2011) "Role of astrocytes in brain function and disease.," *Toxicol. Pathol.*, vol. 39, no. 1, pp. 115–23,

- D'Andrea M, Cole G, Ard M (2004) "The microglial phagocytic role with specific plaque types in the Alzheimer disease brain.," *Neurobiol. Aging*, vol. 25, no. 5, pp. 675–83.
- Sidoryk-Wegrzynowicz M and Aschner M (2013) "Role of astrocytes in manganese mediated neurotoxicity.," *BMC Pharmacol. Toxicol.*, vol. 14, p. 23.
- Vesce S, Rossi D, Brambilla L, Volterra A (2007) "Glutamate release from astrocytes in physiological conditions and in neurodegenerative disorders characterized by neuroinflammation.," *Int Rev Neurobiol.* 2007;82:57-71. doi: 10.1016/S0074-7742(07)82003-4.
- Allen, P. M., Murphy, K. M., Schreiber, R. D., & Unanue, E. R. (1999). Immunology at 2000. *Immunity*, 11(6), 649-651
- Fung A, Vizcaychipi M, Lloyd D, Wan Y, and Ma D (2012) "Central nervous system inflammation in disease related conditions: mechanistic prospects.," *Brain Res.*, vol. 1446, pp. 144–55.
- Boulanger L, Huh G, and Shatz C (2001) "Neuronal plasticity and cellular immunity: shared molecular mechanisms.," *Curr. Opin. Neurobiol.*, vol. 11, no. 5, pp. 568–78.
- Joseph, J. A., Shukitt-Hale, B., Casadesus, G. E. M. M. A., & Fisher, D. (2005). Oxidative stress and inflammation in brain aging: nutritional considerations. *Neurochemical research*, 30(6), 927-935.
- Campbell A (2004) "Inflammation, neurodegenerative diseases, and environmental exposures.," *Ann. N. Y. Acad. Sci.*, vol. 1035, pp. 117–32.
- Nadeau S and Rivest S (2003) "Glucocorticoids play a fundamental role in protecting the brain during innate immune response," *J. Neurosci.* 2; 23(13): 5536–5544. doi: 10.1523/JNEUROSCI.23-13-05536.2003
- Huell M, Strauss S, Volk B, Berger M, Bauer J (1995) "Interleukin-6 is present in early stages of plaque formation and is restricted to the brains of Alzheimer's disease patients," *Acta Neuropathol.*, vol. 89, no. 6, pp. 544–551.
- Sindic C, Chalon M, Cambiaso C, Laterre E, Masson P (1982) "Assessment of damage to the central nervous system by determination of S-100 protein in the cerebrospinal fluid.," *J. Neurol. Neurosurg. Psychiatry*, vol. 45, no. 12, pp. 1130–1135.
- Mata M, Alessi D, Fink D (1990) "S100 is preferentially distributed in myelin-forming Schwann cells," *J. Neurocytol.*, vol. 19, no. 3, pp. 432–442.
- Zimmer D, Cornwall E, Landar A, Song W (1995) "The S100 protein family: History, function, and expression," *Brain Res. Bull.*, vol. 37, no. 4, pp. 417–429.
- Donato R (1999) "Functional roles of S100 proteins, calcium-binding proteins of the EF-hand type," *Biochim. Biophys. Acta - Mol. Cell Res.*, vol. 1450, no. 3, pp. 191–231.
- Ichikawa H, Jacobowitz D, Sugimoto T (1997) "S100 protein-immunoreactive primary sensory neurons in the trigeminal and dorsal root ganglia of the rat," *Brain Res.* 14;748(1-2):253-7. doi: 10.1016/s0006-8993(96)01364-9.
- Yang Q, A. Hamberger, Hyden H, Wang S, Stigbrand T, Haglid K (1995) "S-100β has a neuronal localisation in the rat hindbrain revealed by an antigen retrieval method," *Brain Res.*, vol. 696, no. 1–2, pp. 49–61.
- Peskind E, Griffin W, Akama K, Raskind M, Van Eldik L (2001) "Cerebrospinal fluid S100B is elevated in the earlier stages of Alzheimer's disease," *Neurochem. Int.*, vol. 39, no. 5–6, pp. 409–413.
- Mrak R and Griffin W (2005) "Glia and their cytokines in progression of neurodegeneration.," *Neurobiol. Aging*, vol. 26, no. 3, pp. 349–54.
- Cairns N, Chadwick A, Luthert P, Lantos P (1992) "Astrocytosis, βA4-protein deposition and paired helical filament formation in Alzheimer's disease," *J. Neurol. Sci.*, vol. 112, no. 1–2, pp. 68–75.
- Zhang X and Song W (2013) "The role of APP and BACE1 trafficking in APP processing and amyloid-β generation.," *Alzheimers. Res. Ther.*, vol. 5, no. 5, p. 46.
- Selkoe D (2001) "Alzheimer's disease: genes, proteins, and therapy.," *Physiol. Rev.*, vol. 81, no. 2, pp. 741–66.
- Van Eldik L and Zimmer D (1987) "Secretion of S-100 from rat C6 glioma cells," *Brain Res.*, vol. 436, no. 2, pp. 367–370.
- Gerlach R, Demel G, König H, Gross U, Prehn J, Raabe A, Seifert V, Kögel D (2006) "Active secretion of S100B from astrocytes during metabolic stress.," *Neuroscience*, vol. 141, no. 4, pp. 1697–701.
- Ciccarelli R, Di Iorio P, Bruno V, Battaglia G, D'Alimonte I, D'Onofrio M, Nicoletti F, Caciagli F (1999) Activation of A(1) adenosine or mGlu3 metabotropic glutamate receptors enhances the release of nerve growth factor and S-100beta protein from cultured astrocyte. *Glia Sep*;27(3):275-81
- Whitaker-Azmitia P, Murphy R, Azmitia E (1990) "Stimulation of astroglial 5-HT1A receptors releases the serotonergic growth factor, protein S-100, and alters astroglial morphology.," *Brain Res.*, vol. 528, no. 1, pp. 155–8.
- Edwards M and Robinson, S (2006) "TNF alpha affects the expression of GFAP and S100B: implications for Alzheimer's disease.," *J. Neural Transm.*, vol. 113, no. 11, pp. 1709–15..
- Souza D, Leite M, Quincozes-Santos A, Nardin P, Tortorelli L, Rigo M, C. Gottfried C, Leal R, Gonçalves C (2009) "S100B secretion is stimulated by IL-1beta in glial cultures and hippocampal slices of rats:

- Likely involvement of MAPK pathway.," *J. Neuroimmunol.*, vol. 206, no. 1–2, pp. 52–7.
- Peña L, C. Brecher, and Marshak D (1995) "β-amyloid regulates gene expression of glial trophic substance S100β in C6 glioma and primary astrocyte cultures," *Mol. brain Res.* 1;34(1):118-26.doi:10.1016/0169 328x(95)00145-i.
- Iuvone T, Esposito G, De Filippis D, Bisogno T, Petrosino S, Scuderi C, Di Marzo V, Steardo L (2007) "Cannabinoid CB1 receptor stimulation affords neuroprotection in MPTP-induced neurotoxicity by attenuating S100B up-regulation in vitro.," *J. Mol. Med. (Berl.)*, vol. 85, no. 12, pp. 1379–92.
- Pinto S, Gottfried C, Mendez A, Gonçalves D, Karl J, Gonçalves C, Wofchuk S, Rodnight R (2000) "Immunocontent and secretion of S100B in astrocyte cultures from different brain regions in relation to morphology.," *FEBS Lett.*, vol. 486, no. 3, pp. 203–7.
- Gery I and Waksman B (1972) "Potentiation of the T-lymphocyte response to mitogens II. The cellular source of potentiating mediator (s).," *J. Exp. Med.*, vol. 136, no. 1, pp. 143–155.
- Sharma V, (2011) "Neuroinflammation in Alzheimer's disease and Involvement of Interleukin-1: A Mechanistic View," *Int. J. Pharm. Sci.*
- Zilka N, Ferencik M, Hulin I (2006) "Neuroinflammation in Alzheimer's disease : protector or promoter?," vol. 107, no. 2, pp. 374–383..
- Klegeris A and McGeer P (2005) "Non-Steroidal Anti-Inflammatory Drugs (NSAIDs) and Other Anti-Inflammatory Agents in the Treatment of Neurodegenerative Disease," *Curr. Alzheimer Res.*, vol. 2, no. 3, pp. 355–365.
- Lee S, Liu W, Dickson D, Brosnan C, Berman J (1993) "Cytokine production by human fetal microglia and astrocytes. Differential induction by lipopolysaccharide and IL-1 beta.," *J. Immunol.*, vol. 150, no. 7, pp. 2659–67.
- GE Y and LAHIRI D (2002) "Regulation of Promoter Activity of the APP Gene by Cytokines and Growth Factors," *Ann. N. Y. Acad. Sci.*, vol. 973, no. 1, pp. 463–467.
- Shaftel S, Griffin W, O'Banion M (2008) "The role of interleukin-1 in neuroinflammation and Alzheimer disease: an evolving perspective.," *J. Neuroinflammation*, vol. 5, p. 7.
- Giulian D, Woodward J, Young D, Krebs J, Lachman L (1988) "Interleukin-1 injected into mammalian brain stimulates astrogliosis and neovascularization.," *J. Neurosci.*, vol. 8, no. 7, pp. 2485–90.
- Sheng j, Ito K, Skinner R, Mrak R, Rovnaghi C, Van Eldik L, Griffin W (1996) "In vivo and in vitro evidence supporting a role for the inflammatory cytokine interleukin-1 as a driving force in Alzheimer pathogenesis.," *Neurobiol. Aging*, vol. 17, no. 5, pp. 761–6.
- Griffin W, Sheng J, Roberts G, Mrak R (1995) "Interleukin-1 expression in different plaque types in Alzheimer's disease: significance in plaque evolution.," *J. Neuropathol. Exp. Neurol.*, vol. 54, no. 2, pp. 276–81.
- Mackenzie I, Hao C, Munoz D (1995) "Role of microglia in senile plaque formation," *Neurobiol. Aging*, vol. 16, no. 5, pp. 797–804.
- Griffin W and Mrak R (2002) "Interleukin-1 in the genesis and progression of and risk for development of neuronal degeneration in Alzheimer's disease.," *J. Leukoc. Biol.*, vol. 72, no. 2, pp. 233–8.
- Mrak R and Griffin W (2000) "Interleukin-1 and the immunogenetics of Alzheimer disease.," *J. Neuropathol. Exp. Neurol.* vol. 59, no. 6, pp.471–6.
- Mrak R (2001) "The role of activated astrocytes and of the neurotrophic cytokine S100B in the pathogenesis of Alzheimer's disease," *Neurobiol. Aging*, vol. 22, no. 6, pp. 915–922..
- Hu J and Van Eldik L (1999) "Glial-derived proteins activate cultured astrocytes and enhance beta amyloid-induced glial activation," *Brain Res.*, vol. 842, no. 1, pp. 46–54, Sep. 1999.
- Monnier V and Cerami A (1981) "Nonenzymatic browning in vivo: possible process for aging of long-lived proteins," *Science (80-)*, vol. 211, no. 4481, pp. 491–493.
- Ma L and Nicholson L (2004) "Expression of the receptor for advanced glycation end products in Huntington's disease caudate nucleus," *Brain Res.*, vol. 1018, no. 1, pp. 10–17.
- Brett J, Schmidt A, Yan S, Zou Y, Weidman E, Pinsky D, Nowygrod R, Neeper M, Przysiecki C, Shaw A (1993) "Survey of the distribution of a newly characterized receptor for advanced glycation end products in tissues.," *Am. J. Pathol.*, vol. 143, no. 6, pp. 1699–712.
- Takeda S, Sato N, Morishita R (2014) "Systemic inflammation, blood-brain barrier vulnerability and cognitive/non-cognitive symptoms in Alzheimer disease: relevance to pathogenesis and therapy.," *Front. Aging Neurosci.*, vol. 6, p. 171.
- Onyango I, Tuttle J, Bennett J (2005) "Altered intracellular signaling and reduced viability of Alzheimer's disease neuronal cybrids is reproduced by beta-amyloid peptide acting through receptor for advanced glycation end products (RAGE).," *Mol. Cell. Neurosci.*, vol. 29, no. 2, pp. 333–43,
- Guglielmotto M, Giliberto L, Tamagno E, and Tabaton , "Oxidative stress mediates the pathogenic effect of different Alzheimer's disease risk factors.," *Front. Aging Neurosci.*, vol. 2, p. 3, Jan. 2010.

- Schmidt B, Braun H, Narlawar R, (2005) "Drug development and PET-diagnostics for Alzheimer's disease.," *Curr. Med. Chem.*, vol. 12, no. 14, pp. 1677–95.
- Sasaki N, Toki S, Chowei H, Saito T (2001) "Immunohistochemical distribution of the receptor for advanced glycation end products in neurons and astrocytes in Alzheimer's disease," *Brain Res.*
- Adami C, Bianchi R, Pula G, Donato R (2004) "S100B-stimulated NO production by BV-2 microglia is independent of RAGE transducing activity but dependent on RAGE extracellular domain.," *Biochim. Biophys. Acta*, vol. 1742, no. 1–3, pp. 169–77.

Scientific Journal for the Faculty of Science-Sirte University - SJFSSU



sjsfsu@su.edu.ly



journal.su.edu.ly/index.php/JSFSU



Crossref
Content
Registration

CC BY 4.0:



ROAD
REPOSITORY OF OPEN ACCESS
SCALABLE
RESOURCES

